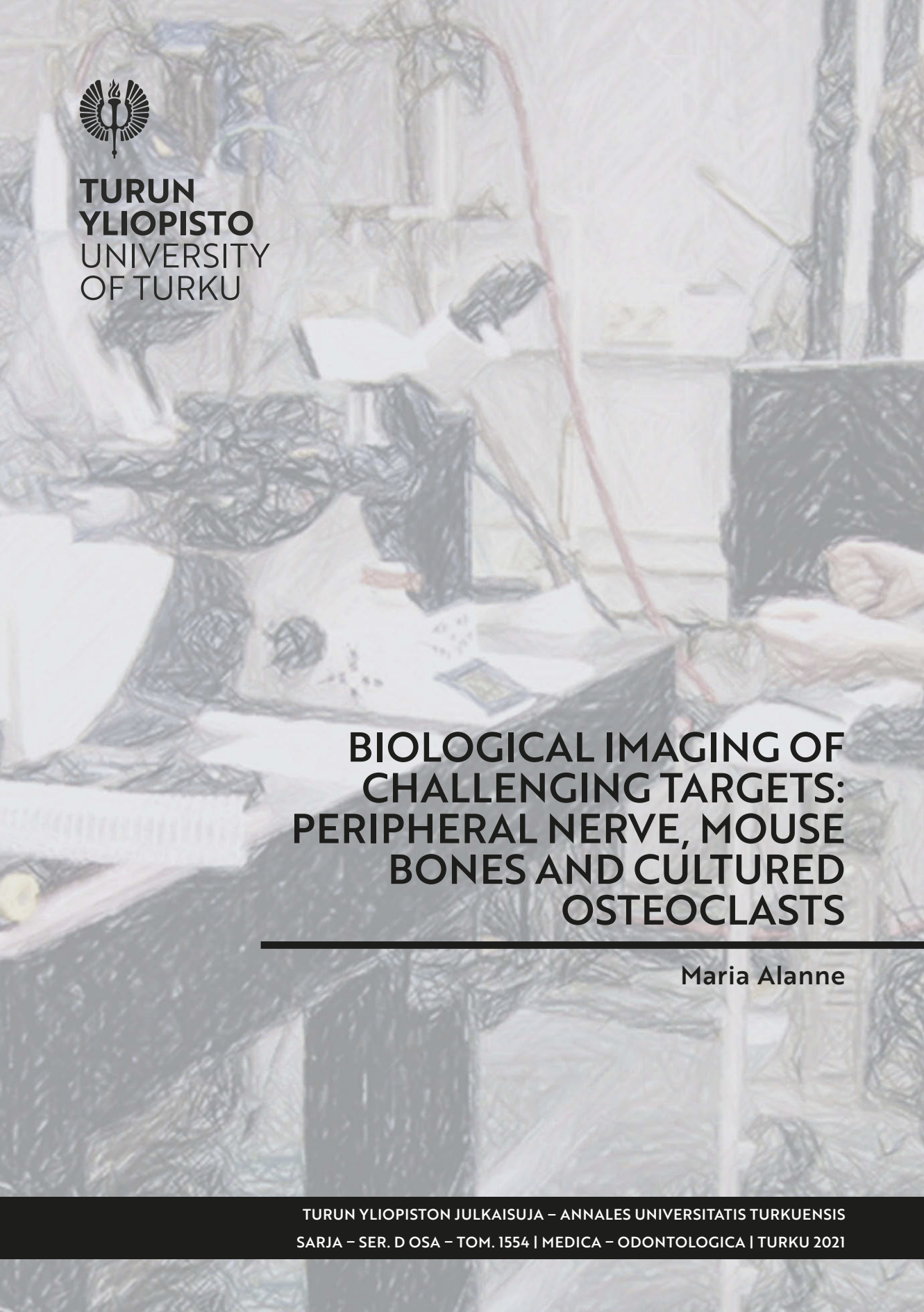

TURUN YLIOPISTO
UNIVERSITY OF TURKU

BIOLOGICAL IMAGING OF CHALLENGING TARGETS: PERIPHERAL NERVE, MOUSE BONES AND CULTURED OSTEOCLASTS

Maria Alanne

TURUN YLIOPISTON JULKAISUJA – ANNALES UNIVERSITATIS TURKUENSIS
SARJA – SER. D OSA – TOM. 1554 | MEDICA – ODONTOLOGICA | TURKU 2021

TURUN
YLIOPISTO
UNIVERSITY
OF TURKU

BIOLOGICAL IMAGING OF CHALLENGING TARGETS: PERIPHERAL NERVE, MOUSE BONES AND CULTURED OSTEOCLASTS

Maria Alanne

TURUN YLIOPISTON JULKAISUJA – ANNALES UNIVERSITATIS TURKUENSIS
SARJA – SER. D OSA – TOM. 1554 | MEDICA – ODONTOLOGICA | TURKU 2021

University of Turku

Faculty of Medicine
Institute of Biomedicine
Cell Biology and Anatomy and Department of Dermatology and Venereology
Doctoral Programme in Clinical Research

Supervised by

Professor Juha Peltonen, MD, PhD
Institute of Biomedicine
University of Turku
Turku, Finland

Docent Sirkku Peltonen, MD, PhD
Department of Dermatology
University of Turku
Turku, Finland
Professor, Department of Dermatology and Venereology
University of Gothenburg
Gothenburg, Sweden

Reviewed by

Professor Mikko Lammi, PhD
Department of Integrative Medical Biology
Umeå University
Umeå, Sweden

Docent Kirsi Rilla, PhD
Institute of Biomedicine
University of Eastern Finland
Kuopio, Finland

Opponent

Professor Juha Tuukkanen, DDS, PhD
Department of Cell Biology and Anatomy
University of Oulu
Oulu, Finland

The originality of this publication has been checked in accordance with the University of Turku quality assurance system using the Turnitin OriginalityCheck service.

Cover Image: Maria Alanne

ISBN 978-951-29-8461-9 (PRINT)
ISBN 978-951-29-8462-6 (PDF)
ISSN 0355-9483 (Print)
ISSN 2343-3213 (Online)
Painosalama, Turku, Finland 2021

To my family

UNIVERSITY OF TURKU
Faculty of Medicine
Institute of Biomedicine
Cell Biology and Anatomy
Department of Dermatology and Venereology
MARIA ALANNE: Biological imaging of challenging targets: Peripheral nerve, mouse bones and cultured osteoclasts
Doctoral Dissertation, 131 pp.
Programme in Clinical Research
May 2021

ABSTRACT

During this study, advances in bioimaging have affected the biomedical research field. In this thesis, traditional microscopy and selected new techniques, namely microcomputed tomography (μCT), STED microscopy and laser-capture microdissection have been combined to study complex tissues in human adults such as developing peripheral nerves, bones and osteoclasts to reveal previously unseen features of these tissues and cells.

Confocal microscopy was used to analyze the adult and developing human peripheral nerves. Tight junction proteins were localized to subcellular structures of myelinating Schwann cells. The combination of tight junction proteins differed from that of rodents. Furthermore, claudin expression was weak in fetal endoneurium during the second trimester, and the junctions were not fully maturated by the end of the third trimester. The results suggest that the maturation of Schwann cell autotypic junctions continues after birth.

Various imaging modalities were combined in order to analyze the phenotype of the Nf1Ocl mouse model. μCT revealed narrowed growth plates and slight differences in trabecular and cortical bone in $NfOcl^{-/-}$ mice, but not in the osteoporotic bone phenotype. However, *in vitro* studies showed accelerated bone resorption capacity and a hyperactivated Ras signaling pathway in $Nf1^{-/-}$ osteoclasts.

STED microscopy uncovered new features of actin, as bending and branching filaments were demonstrated in human osteoclasts. New features of actin filaments were detected also in macrophages and keratinocytes. The results emphasize the importance of bioimaging techniques in studying challenging tissues.

KEYWORDS: Super-resolution, NF1, osteoclast, tight junction, Schwann cell, actin cytoskeleton,

TURUN YLIOPISTO
Lääketieteellinen tiedekunta
Biolääketieteen laitos
Solubiologian ja anatomian oppiaine
Iho- ja sukupuolitautioppi
Maria Alanne: Biokuvantamisen haastavat kohteet: Perifeerinen hermo, luu ja osteoklastiviljelmät
Väitöskirja, 131 s.
Turun kliininen tohtoriohjelma
Toukokuu 2021

TIIVISTELMÄ

Väitöskirjassa tutkittiin vaikeasti kuvannettavia kudoksia, aikuisen ja kehittyvän sikiön perifeerista hermoa, luuta sekä osteklasteja yhdistämällä tavanomaisia kuvantamismenetelmiä valikoitujen mikroskopian erityismenetelmien kanssa.

Aikuisen ja kehittyvän sikiön perifeerinen hermo kuvannettiin konfokaalimikroskopialla. Tiiviit liitokset sijaitsivat solunsisäisissä rakenteissa myeliiniä tuottavissa soluissa. Tulokset eroavat aiemmin jyrsijöillä tehtyihin havaintoihin nähden. Tiivisliitosproteiini klaudiinin ilmentyminen oli vähäistä toisen raskauskolmanneksen aikana, eivätkä tiiviit liitokset ehtineet kehittyä loppuun asti viimeisen kolmanneksen loppuun mennessä. Todennäköisesti tiiviit liitokset kehittyvät vielä syntymän jälkeen.

Ehdollisesti poistogeenisen Nf1Ocl -hiirimallin ilmiasua tutkittiin yhdistämällä useita kuvausmodaliteetteja. Mikrotietokonetomografian avulla havaittiin sääriluussa kasvulevyn madaltuneen sekä kuoriluussa että hohkaluussa havaittiin useita pieniä muutoksia, mutta vastoin olettamusta kudoksessa ei todettu luukatoon viittaavaa. Soluviljelyolosuhteissa Nf-/- osteoklastit hajoittivat aggressiivisesti luuta sekä niiden Ras-signaalireitti oli aktivoitunut.

STED mikroskoopin avulla paljastui uusia aktiinin ominaisuuksia. Aktiinin havaittiin taipuvan ja haarautuvan ihmisen osteoklasteissa sekä muissa solutyypeissä, makrofageissa ja keratinosyyteissä. Nämä tulokset korostavat biokuvantamisen tekniikan tärkeyttä varsinkin, kun kohteena on haastava kudos.

AVAINSANAT: Superresoluutio, NF1, osteoklasti, tiivis liitos, Schwannin solu, aktiinitukiranka

Table of Contents

Abbreviations

γ-TuC	Gamma-tubulin complex
λ	wavelenght
Ad-Cre	Adenovirus
ADAM	A disintegrin and metalloprotease
Akt	Serine/threonine-specific protein kinase
ATP	Adenosine triphosphate
CAR	Coxsackie and adenovirus-associated receptor
c-Fms	Receptor for colony stimulating factor-1
cAMP	Cyclic adenosine monophosphate
CT	Computed tomography
CPT	Congenital pseudarthrosis of the tibia
DAAM	Disheveled-associated activator of morphogenesis
DC-STAMP	Dendritic cell-specific transmembrane protein
DFR	Diaphanous-related formin
dSTORM	Direct stochastic optical reconstruction microscopy
ECM	Extracellular matrix
ERK	Extracellular-signal-regulated kinase
FAK	Focal adhesion kinase
FH	Formin homology protein
FRL	Formin-like protein
GFAP	Glial fibrillary acidic protein
GIST	Gastrointestinal stromal tumor
GTPase	Guanosine triphospatase
IBS	Irritable bowel syndrome
IFN-γ	Interferon gamma
IL-6	Interleukin 6
ILK	Intergrin-linked kinase
IP3	Inositol trisphosphate
JAM	Junctional adhesion molecules
JNK	C-Jun N-terminal kinase
LCM	Laser-capture microdissection

LOH	Loss of heterozygosity
M-CSF	Macrophage colony stimulation factor
MAGI	Membrane-associated guanylate kinate inverted
MAP	Microtubule-associated protein
MAPK	Mitogen-activated protein kinase
MPNST	Malignant peripheral nerve sheath tumors
MTOC	Microtubule-organizing center
MUPP1	Multi-PDZ domain protein 1
NFATc1	Nuclear factor of activated T-cells
µCT	Micro-computed tomography
mTOR	Mammalian target of rapamycin
NA	Numerical aperture
NFATc1	Nuclear factor of activated T cells c1
NF1	Neurofibromatosis type 1
NIH	National Institutes of Health
OSCAR	Osteoclast-associated immunoglobulin-like receptor
PKC	Protein kinase C
PSF	Point spread function
RANKL	Receptor activator of nuclear factor kappa-B ligand
SAM	Scanning acoustic microscopy
SAXS	Small-angle X-ray scattering
SH3	SRC Homology 3
SIM	Structured illumination microscope
STED	Stimulated emission depletion microscopy
STORM	Stochastic Optical Reconstruction Microscopy
TGF-β	Transforming growth factor beta
TUBB1	Tubulin beta 1 class VI
VEGFR-2	Vascular endothelial growth factor receptor 2
WASP	Wiskott-Aldrich syndrome protein
ZO	Zona occludens

List of Original Publications

This dissertation is based on the following original publications, which are referred to in the text by their Roman numerals:

I Maria H Alanne, Kati Pummi, Anthony M Heape, Reidar Grènman, Juha Peltonen, Sirkku Peltonen. Tight junction proteins in human Schwann cell autotypic junctions. *Journal of Histochemistry and Cytochemistry,* 2009; 57(6): 523–529.

II Maria H Alanne, Elina Siljamäki, Sirkku Peltonen, Kalervo Väänänen, Jolene J Windle, Luis F Parada, Jorma A Määttä, Juha Peltonen. Phenotypic characterization of transgenic mice harboring $Nf1^{+/-}$ or $Nf1^{-/-}$ osteoclasts in otherwise $Nf1^{+/+}$ background. *Journal of Cellular Biochemistry*, 2012; 113(6): 2136–2146.

III Paula Pennanen*, Maria H Alanne*, Elnaz Fazeli, Takahiro Deguchi, Tuomas Näreoja, Sirkku Peltonen, Juha Peltonen. Diversity of actin architecture in human osteoclasts: network of curved and branched actin supporting cell shape and intercellular micrometer-level tubes. *Molecular and Cellular Biochemistry*, 2017; 432(1–2): 131–139.

* equal contribution

1 Introduction

This dissertation is composed of three original studies that were initiated to investigate tissues and cell types affected in neurofibromatosis type 1 (NF1) syndrome being specifically peripheral nerves and bones. Bioimaging with various techniques play a major role in forming this dissertation. Visualization of immunofluorescence labeling developed during this study was started using traditional florescence microscopy and confocal laser scanning microscopy and completed with images taken with a super-resolved stimulated emission depletion (STED) microscope. Micro-computed tomography (μCT) is an X-ray imaging method downscaled from clinical use to study small targets such as the microarchitecture of mouse trabecular bone. In certain objects, μCT can replace laborious histomorphometry. Laser-capture microdissection allows for the selection of the region of interest in a tissue under the microscope and the cutting of the cells with a laser for further analyses using various methods of biochemistry or molecular biology.

The connective tissue of peripheral nerves contains three layers being the epineurium, perineurium and endoneurium. Neurofibromas are the most characteristic feature of NF1. They are benign tumors that originate from peripheral nerves and contain all the elements of the nerve connective tissue. The perineurium forms a barrier that regulates diffusion and maintains the homeostasis of the endoneurium (Peltonen. et al., 2013). The cell extensions of neurons from the central nervous system, the axons, are surrounded by Schwann cells. Schwann cells can either wrap the axons with a myelin sheath, or one Schwann cell may invaginate the axons without forming myelin. Tight junctions form a selective diffusion barrier in all types of epithelia. In addition, tight junctions exist in certain other specific locations such as perineurium. Neighboring perineurial cells are sealed with tight junctions to form a protective diffusion barrier between the epineurium and the endoneurium (Pummi et al., 2004). Prior to this study, tight junction components had been described in mouse nerves and were shown to be present between the lamellae of myelinating Schwann cells thus forming so called autotypic junctions (Poliak et al., 2002).

Patients with NF1, both men and women, have an increased risk for osteoporosis and bone fractures (Heervä et al., 2010; Kuorilehto et al., 2005). NF1 is caused by pathogenic variants of the *NF1* gene, which encodes the neurofibromin protein. Neurofibromin is a negative regulator of the Ras signaling pathway, which in turn, regulates various cellular functions such as proliferation and differentiation (Jouhilahti et al., 2011). Osteoclasts are cells that continuously resorb bone tissue, while osteoblasts synthesize new bone. If the resorption exceeds synthesis, the bone becomes osteopenic, which can further proceed to osteoporosis. Over-activation of resorption capacity has been noted in osteoclasts cultured from patients with NF1 (Heervä et al., 2010).

Osteoclasts are multinucleated cells that originate from bone marrow monocytes. Osteoclast cultures can be initiated by isolating monocytes from peripheral blood, and the cells can be differentiated into bone resorbing multinucleated cells in the presence of the receptor activator of nuclear factor kappa-B ligand (RANKL). Typical structures of osteoclasts include the actin-rich podosome belt and actin ring in addition to a common actin cytoskeleton and cell protrusions. These cellular structures are associated with osteoclast-specific functions such as bone resorption, cell fusion and cell motility that require rapid remodeling of the actin network. The appropriate architecture of the actin network is formed when actin-binding proteins branch, elongate, bundle, form cross-links and eventually accelerate by severing the actin filaments in a coordinated manner (Pollard, 2016).

2 Review of the Literature

2.1 Imaging

2.1.1 The roots and principles of modern imaging

Imaging has contributed to the development of bioscience and modern medicine. The roots of modern imaging extend to the 17th century, when a primitive compound/light microscope was invented, and bacteria were observed for the first time in 1672 (Hooke, 1665). Initially, the histology of various tissues was described concurrently with the development of the light microscope and histochemical staining solutions in the early 1900s. Histological details at the nanoscale, such as microscopic cellular junction plaques, were identified using the electron microscope. However, the molecular composition of these subcellular structures remained unclear until fluorescence microscopy and fluorescent probes, such as fluorescent-conjugated antibodies began to increase in use slowly since 1980 (Geisse, 2009).

Bioimaging is based on several basic imaging techniques such as light and fluorescence microscopy, electron microscopy and computed tomography. Light microscopy is useful to recognize the histological details up to a resolution of 200 nm. The electron microscopy technique exceeds the resolution of light microscopy. A method was published in 1931 by Ruska and Knoll (Ruska & Knoll, 1931).During the 1940s, commercial electron microscopes were manufactured and enabled the first observations of viruses. The methodology of electron microscopy become more commonly available in the 1970s, and the number of publications increased markedly (Harris, 2015). There are two types of electron microscopy being transmission electron microscopy and scanning electron microscopy. Transmission electron microscopy is based on an accelerated electron beam that is directed through a thin specimen to generate an image. Scanning electron microscopy uses electron beams, which by reflecting, allows for visualization of the topography of a coated specimen. Electron microscopy can detect much smaller details than light microscopy, for instance, it can detect the plasma membrane and cellular junction plaques at the nanoscale. However, electron microscopy reveals structural details only from fixed specimens and thus cannot be used to image live biological objects,

because the method requires the vacuum system (Arana-Chavez & Castro-Filice, 2019; Geissinger & Abandowitz, 1976).

Each of the basic imaging methods has expanded to a large group of various applications, such as atomic force microscopy, scanning electron microscopy, nano-computed tomography, stochastic optical reconstruction microscopy (STORM) to mention a few applications. Especially in recent years, imaging has been focused on detecting subjects at the nanoscale (Galbraith & Galbraith, 2011) A major development of technical applications, equipment and reagents allows for three-dimensional (3D) and four-dimensional, (4D) bioimaging, and five-dimensional (5D) bioimaging (Chu et al., 2020). All these advancements have required and benefited from the simultaneous advances in computing technologies. This thesis work has focused on selected imaging methods, which are mostly based on fluorescence and X-ray methods.

2.1.2 Principles of microscopy

Physical quantities determine the requirements and limits of all types of imaging. Light or photons behave like energy-containing particles and have features of waves. Therefore, according to wave-particle duality, a wave can be reflected, refracted, diffracted as well as be absorbed and emitted. The imaging is based on these qualities of a wave, and the utilization of the waves is the cornerstone of imaging.

Principles of bioimaging are based on the physical properties of electromagnetic radiation in visible and non-visible wavelengths and magnification. The imaging process produces and detects wavelengths of electromagnetic radiation. The electromagnetic spectrum contains all the wavelengths of photons being visible light, ultraviolet, infrared, micro- and radio waves as well as ionizing radiation such as gamma- and X-radiation. Different wavelengths can be used to image objects of various properties and sizes. The wavelength of visible light is from 400–700 nm and the wavelength of X-rays is less than 10 nm. Therefore, each wavelength of photons requires special imaging and detector equipment. Furthermore, white light is a mixture of wavelengths of visible spectrum which is detected by widefield microscopy whereas each color of visible spectrum is separated with fluorescence microscopy. (Ryan et al., 2017). Basic principles of widefield and confocal microscopy are summarized in **Figure 1**.

Optical imaging is based on biophysical properties such as magnification, resolution and contrast. Magnification involves the idea to enlarge a target specimen. Magnification is a physical quantity that is proportional to the distance between the specimen, lenses and image. Magnification is also proportional to the field of view and amount of refracting light in order that greater magnification reduces the amount of refracted light, and the visible area is smaller compared to the original field of

view. Due to the reduction of light, an additional light source is needed (Abbe, 1873; Rayleigh, 1903).

In addition to magnification, the resolution strongly affects the imaging process. Resolution can be defined as the shortest distance at which two adjacent spots can be distinguished as a separate structure. The optical resolution of microscopy (d) (formula: $d=\lambda/2NA$) is proportional to wavelength (λ) and the numerical aperture (NA) (Rayleigh, 1903). The numerical aperture is classified as a value of lens capacity, which gathers the light from a feasible angle ($NA=N\sin\theta$). The resolution of light microscopy is limited to 200 nanometers (Goodwin, P. C., 2015). The point spread function (PSF) is the experimental or theoretical concept which reduce excessive fluorescence thus to improve the resolution of scanning confocal microscopy images.

Contrast indicates the difference in luminance or color, which makes an object distinguishable from the other object or background. Contrast can be adjusted in many ways.

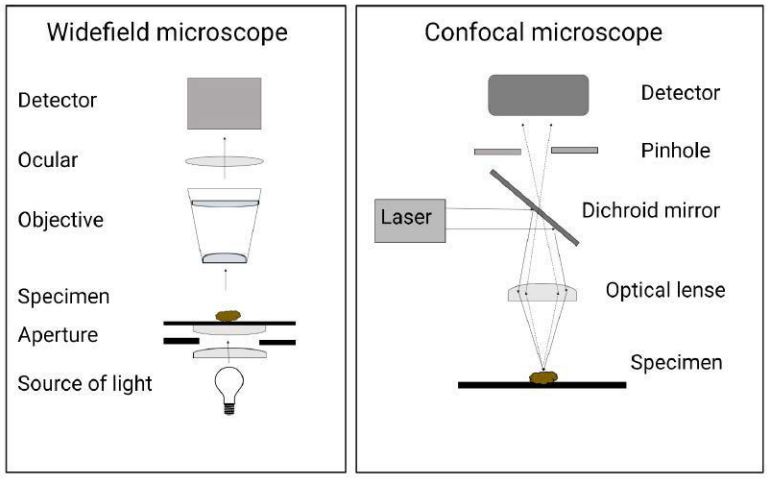

Figure 1. Principles of widefield microscopy and confocal microscopy.

Applications of the light microscopy at the present include basic screening and histology, automated virtual microscopy and fluorescence microscopy. The benefits of confocal laser microscopy include the possibility of using thicker samples and production of clearer images compared to fluorescence. Fluorescence microscopy was routinely used in the 1970s and, since the 1980s, more fluorescent probes have become available (Bayguinov et al., 2018).

Limitations of traditional fluorescent microscopy include inaccurate localization of a fluorescent spot compared to confocal and STED imaging. In general, phototoxicity and photobleaching during the long-term imaging process have been a

problem of conventional fluorescence microscopy. On the other hand, these features, such as photobleaching, can be utilized as a critical step of the certain imaging method such as fluorescence recovery after photobleaching.

2.1.3 Super-resolution microscopy

Super-resolution refers to the ability to detect a specimen at nanoscale resolution. Super-resolution microscopy is based on principles of light and confocal microscopy and fluorophores. In practice, the super-resolution is achieved, when an excess of the emitting light wave is excluded by optical- or mechanical modifications. Benefits of super-resolution imaging are particularly noticed in studies where the focus is on structural and dynamical details of biomolecular components such as subcellular structures.

Super-resolution microscopy is categorized into three major microscope techniques being stimulated emission depletion microscopy (STED), structured illumination microscopy (SIM) and localization microscopy. These three techniques share the same property of reducing the interfering fluorescence (Feng et al., 2018).

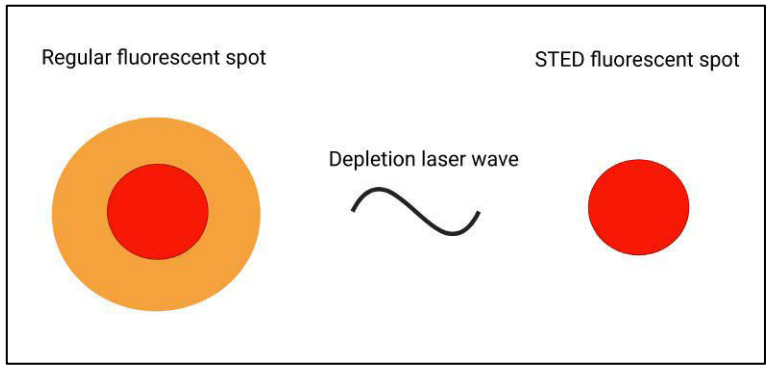

Figure 2. Principle of STED super-resolution.

STED microscopy was invented by Hell and Wichmann. They proposed a theory, where a higher resolution can be achieved by depleting the original emission wave, which in the end, increases the resolution through a reduction of the PSF (Hell & Wichmann, 1994). The theory of depletion and reduction of emission can be demonstrated as a doughnut-shaped emission wave. Coherent waves switch off circumferential emission (the yellow doughnut shape in **Figure 2**), and the remaining emission wave (**Figure 2**, red spot) is detected and processed into an image (Klar et al., 2000). In practice, an additional laser beam, which generated the coherent waves, is incorporated into ordinary confocal microscopy equipment. Resolution of STED

microscopy varies depending on the sample, fluorophore and other technical details of the protocol, the laser beam and the equipment system. Axial resolution varies from 100 to 30 nm. Computed tomography at the micro-scale

X-rays are one type of high-energy, electromagnetic radiation, and they have been used for decades as a scientific tool. All the applications of the computed tomography equipment include an X-ray tube, a radiation filter and a collimator, a detector and a camera (Boerckel et al., 2014). The principle of X-ray imaging is based on detecting the X-rays that are transmitted through the specimen. Briefly, the X-rays are produced in an X-ray tube and are directed through the radiation filter and a beam-narrowing collimator. Attenuated X-rays then penetrate the specimen, when a part of the X-rays is absorbed into the specimen in a tissue-specific manner. Finally, the transmitted X-rays are captured by a detector and camera for further digital processing (du Plessis et al., 2017).

The intensity of transmitted X-rays in the formation of the computed tomography image is based on the tissue-specific ability to absorb X-rays, the intensity of the X-ray beam and the distance between the X-ray tube and the detector. Each tissue has a unique density or radiological resolution, and the image is a spatial summary of transmitted X-rays. A higher contrast is formed into an image when the dense tissues absorb most of the X-rays. For instance, bone is a radiologically denser tissue than muscle or nerves. Thus, when X-ray imaging is adjusted optimally for bone tissue, nerves are barely distinguished from surrounding soft tissues.

Several advanced methods of X-ray imaging have been used as tools for basic science and modern medicine. A well-known method is computed tomography (CT) which produce cross-sectional images. Micro-computed tomography, μCT, which is an application used by basic researchers, was designed for small objects such as murine or other tissue samples (Elliott & Dover, 1982). The first micro-scanners were established in 1982 but were not commercially available until the mid-nineties (Rüegsegger et al., 1996). The spatial resolution of *in vivo* μCT is 50–200 μm, *ex vivo* μCT is 5–100 μm and nano-CT is 50–600 nm. A major advantage of computed tomography imaging is that it is a non-destructive method with high spatial resolution due to the cross-sectional imaging process. Therefore, the ability to reconstruct 3-dimensional images favors naturally multidimensional objects such as bone. One advantage of the non-destructive method of μCT is that the structural modalities are measured directly from three-dimensional specimens, while traditional histomorphometric analyses require production of histological slices and therefore produces 2-dimensional data (Bouxsein et al., 2010). μCT can be used, for example, to study the metabolism of bone, to follow the healing of fractures, to monitor pharmacological treatments and to study genetic bone diseases. Nowadays μCT has become a standardized method for murine imaging and has partly replaced laborious histomorphometry.

2.1.4 Laser microdissection

Improvements in microscopy technology include a laser-assistant method, laser-capture microdissection (LCM), where the target is identified with light or fluorescence microscopy and extracted by an infrared or ultraviolet laser technique. Resolution, in this context, is referred to as the ability to select specimens and to discard an interfering biological substance. LCM is based on identification and isolating a target specimen such as cell populations, single cells, DNA and RNA (Mahalingam, 2018). After isolating, additional procedures such as sequencing and amplification of DNA, analyzing RNA or protein expression profiles can be commenced (Cummings et al., 2018; MacDonald et al., 2019). With this methodology, specific gene mutations, gene expression profiling, proteomics, epigenetic alterations and metabolic profiling can be studied in health and disease (Cheng et al., 2013). For example, in medical conditions such as cancer, LCM provides opportunities to analyze alterations of specific cell populations at the molecular lever in the original environment (Ong et al., 2020). Furthermore, laser-capture microdissection is applicable for forensic investigation (Costa et al., 2017).

Two major implementations, which are based on infrared or ultraviolet laser techniques, are commercially available (Hunt et al., 2020; Vandewoestyne et al., 2013). One application of laser microdissection, laser-pressure catapulting technology, is based on two strategies being with an ultraviolet laser detachment of a target specimen that falls due to gravity into the collection tube or by a catapulting pressure of laser that lifts the target specimen to the adhesive collection tube (Brasko et al., 2018). One of the major benefits of laser microdissection is to avoid physical contact between the sample and the microdissection system, which thus prevents contamination of the specimen with a non-target tissue or having chemical modification of the target molecules. A second application of microdissection is operated by infrared beams. Infrared beams melt the target specimen into a thermoplastic ethylene vinyl acetate polymer film that contacts the tissue section. After lasering, the target specimen is attached to thermoplastic films, and the whole complex is lifted up to further analysis (Gallagher et al., 2012). Ultraviolet and infrared laser microdissection methods can also be combined.

Specific identification of the target specimen can be increased by using several labeling methods such as common histological procedures, indirect immunolabeling and *in situ* hybridization prior to laser capturing. Advantages of LCM are its rapid procedure, increased tissue sensitivity, avoidance of contamination and delineation of the target specimen (Baldelli et al., 2015; Brasko et al., 2018; Lutz & Peng, 2018).

2.1.5 Post-processing of images

Nowadays, digital post-processing includes much more than adjustment of brightness and contrast. The post-processing could be described as a laborious part of bioimaging protocols. The aim of the post-processing is to modify raw imaging data into a more feasible format. For example, single plain sections are combined to a 3-dimensional image. The imaging resolution can be improved with additional post-processing software provided by microscope manufacturers. In addition, imaging data can be converted to numeric data for further statistical analysis.

The resolution can be enhanced with computational processes. Particularly, in an optical imaging process such as confocal microscopy, deconvolution has become as standard method during the last years. Deconvolution includes a group of mathematic algorithms. These algorithms determinates the original focus of the emitting (light) source and eventually decreases scattered light emission thus to improve the resolution (Laasmaa et al., 2011; Sage et al., 2017).

Even though the super-resolution imaging method has taken a place in the field of bioimaging, a need for image post-processing has not decreased. Instead, the super-resolution technique has increased the amount of raw imaging data. These processes are time-consuming, and computing power is limited. Various research has been focused on to improve post processing techniques in order to reduce time and effort. Perhaps the most powerful method is an artificial intelligence, specifically a deep learning (Gong et al., 2020; Wang, Hongda et al., 2019). Advanced deconvolution algorithms learn to recognize the factors that increase the image resolution. Therefore, only some of raw images are selected for further analysis instead of all raw images. As an end result, the process is accelerated tenfold to several thousandfold (Guo et al., 2020).

Post-processing is already a valuable method to increase the quality of bioimaging. Perhaps in the future, a researcher should pay more attention to advanced post-processing techniques in order to save time and data processing capacity and to obtain higher quality data.

2.2 Specific tissues, bone and nerves

2.2.1 Bone

2.2.1.1 Bone tissue

The skeleton provides the structural strength and protection for the body. Long bones and cartilaginous synovial joints make locomotion possible. In addition, hematopoietic and mesenchymal cells are produced in the bone marrow cavity in flat

(e.g., hipbone) and short (e.g., vertebral bodies) bones. The skeleton is a reservoir for calcium and minerals that enable homeostasis. Bone tissue is composed of a calcified collagenous matrix and cellular components such as osteoclasts, osteoblasts and osteocytes. Cartilage is associated with bone, although cartilage is a distinct and specialized type of connective tissue. Chondrocytes are organized into stratified layers of cartilaginous tissue especially at the growth plate and joint surface. Type II collagen and aggrecan are characteristics for the extracellular matrix of cartilage.

Bone tissue contains 20 to 40% of organic components, 50 to 70% of inorganic components such as hydroxyapatite and phosphate carbonate, 5 to 10% water and less than 3% lipids. Approximately up to 90% of organic components contains type I collagen. Other organic components such as types III, V and X collagen, hyaluronan, albumin, bone sialoprotein, proteoglycans, non-collagenous glycoproteins, osteonectin; osteopontin and osteocalcin have been recognized (Clarke, 2008; Feng, 2009).

The human adult skeleton consists of 80% cortical bone and 20% trabecular bone. However, approximately 80% of active bone remodeling takes place in trabecular bone (Langdahl et al., 2016). During aging, bone remodeling increases in cortical bone and decreases in trabecular bone.

Bone is a dynamic tissue and displays continuous remodeling. Bone turnover studies show that human adult bone tissue is renewed in ten-year cycles. In this remodeling process, osteoclasts are recruited in order to degrade the old bone tissue. After bone resorption, osteoclasts are programmed to go into apoptosis. Osteoblasts initiate new bone formation and mineralization. An imbalance between the catabolic and anabolic state promotes the development of medical conditions such as osteopenia or osteopetrosis (Novack & Mbalaviele, 2016).

2.2.1.2 Regulation and differentiation of osteoclasts

Osteoclasts are multinuclear bone resorbing cells that originate from a hematopoietic cell lineage. Granulocyte-macrophage precursors can differentiate into dendritic cells, monocytes, macrophages and osteoclasts (Boyce et al., 2009; Georgess et al., 2014) Circulating hematopoietic stem cells or monocytes are recruited from the blood. M-CSF and RANKL are essential for normal osteoclast differentiation, and both cytokines are secreted by osteoblasts (Hodge et al., 2007; Xing & Boyce, 2014; Yasuda et al., 1998). Macrophage colony-stimulation factor (M-CSF) drives monocytes to form colonies and further stimulates monocytes to differentiate into osteoclast precursor cells. M-CSF binds to the c-Fms receptor in the cell membrane of the osteoclast precursor, and M-CSF has an effect on signaling pathways such as MAPK, ERK, Jun N-terminal kinase (JNK), which in turn, activate the transcription factor called the nuclear factor of activated T-cells, cytoplasmic 1 (NFATc1). NFAT

regulates the transcription of osteoclast-specific genes such as tartrate resistant acid phosphatase (TRACP), OSCAR and cathepsin K. The receptor activator of nuclear factor kappa-B ligand (RANKL), a member of tumor necrosis factor family, promotes osteoclast precursor cells to fuse into multinuclear osteoclasts. In addition, several cytokines, such as the vascular endothelial growth factor receptor 2 (VEGFR-2), growth differentiating factor-15, insulin-like growth factor 2, interleukin-6 (IL-6), IL-17 and transforming growth factor-β (TGF-β) have been described to promote osteoclast differentiation (Hayashida et al., 2014). Osteoclastogenesis is inhibited by osteoprotegerin (OPG), which is a decoy receptor for RANKL. Osteoprotegerin is secreted by osteoblasts (Lacey et al., 1998; Simonet et al., 1997). Other inhibitory cytokines are interferon gamma (IFN-γ) and IFN-β, IL-4, IL-10, IL-12, IL-13 and IL-18 (Hayashida et al., 2014).

Cells can be recognized according to their differentiation state during osteoclastogenesis using certain cell surface markers. The surface antigen CD34 is a marker for hematopoietic stem cells. Monocytes express RANK, αVβ3 integrin and the surface antigen CD14. Osteoclast precursors express DC-STAMP, E-cadherin, protocadherin-7, a disintergrin and the metalloporeinase (ADAM). Fully differentiated osteoclasts express αVβ3 integrin, cathepsin K, the calcitonin receptor, the IgG-like receptor and the osteoclast-associated receptor (OSCAR), which is a member of the leukocyte receptor complex protein family (Miron et al., 2016; Pereira et al., 2018).

2.2.1.3 Bone resorption

Bone resorption includes a cascade of cytoskeletal rearrangements, secretion and degradation. Prior to initiation of bone resorption, multinucleated osteoclasts have to become polarized, which includes the forming of four distinct structures being a sealing zone, a dense membranous ruffled border, a basolateral domain and a functionally secretory domain (**Figure 3**).

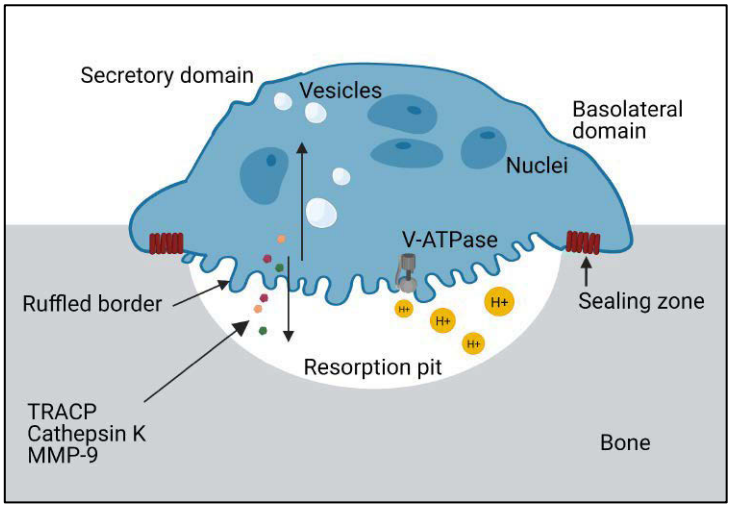

Figure 3. Resorbing osteoclast.

Osteoclasts adhere on the bone matrix via a special focal adhesion type called a podosome (Destaing et al., 2003). The protein composition of a podosome includes intracellular proteins such as actin, talin, vinculin and paxillin and the transmemebrane protein called αVβ3 integrin (Chabadel et al., 2007; Chellaiah & Hruska, 2003). αVβ3 integrin recognizes the Arg-Gly-Asp motif and is a receptor for vitronectin, osteopontin, type I collagen and bone sialoprotein. At the basolateral side of osteoclast, clusters of podosomes are reorganized into podosome belts, which precedes the formation of an actin ring (Teitelbaum, 2011). Bone resorbing osteoclasts feature a sealing zone, which is an osteoclast-specific actin containing structure. The sealing zone encloses a space between the ruffled border of an osteoclast and the bone matrix to form resorption lacuna. The degradation of bone is carried out by carbonic anhydrase II, which produces protons (H^+), while V-ATPases at the ruffled border deliver H^+ to the resorption lacuna. In addition, a chloride channel selects Cl^- ions to the resorption lacuna. Other proteolytic agents such as TRACP, cathepsin K and matrix metalloproteinase-9 are excreted to the resorption lacuna. The degraded bone matrix is transported via a transcytotic route and are excreted in a functionally secretory domain. Transcytotic vesicles are transported via microtubules and small GTPases to a functionally secretory domain to be discharged. The degraded bone matrix contains TGF-β and IGF-1 that are considered to induce osteoblast recruitment and the production of a new bone matrix. The degraded bone matrix also contains c-terminal telopeptides and soluble calcium.

2.2.2 Peripheral nerves

2.2.2.1 Structure of peripheral nerves

Human peripheral nerves have a triple layer system to form a protecting barrier for axons, for review see (Peltonen et al., 2013). **Figure 4** summarizes the structural details of peripheral nerve. The nerve trunk is covered with the epineurium, which is the outermost layer with embedded nerve fascicles and blood vessels. The epineurium provides mechanical strength and is mainly composed of fibrillar collagens, fibronectin and elastin fibers. The cell types of epineurium include fibroblasts, adipocytes and lymphocytes. The structure of the epineurium is not known to contribute to diffusion barrier properties.

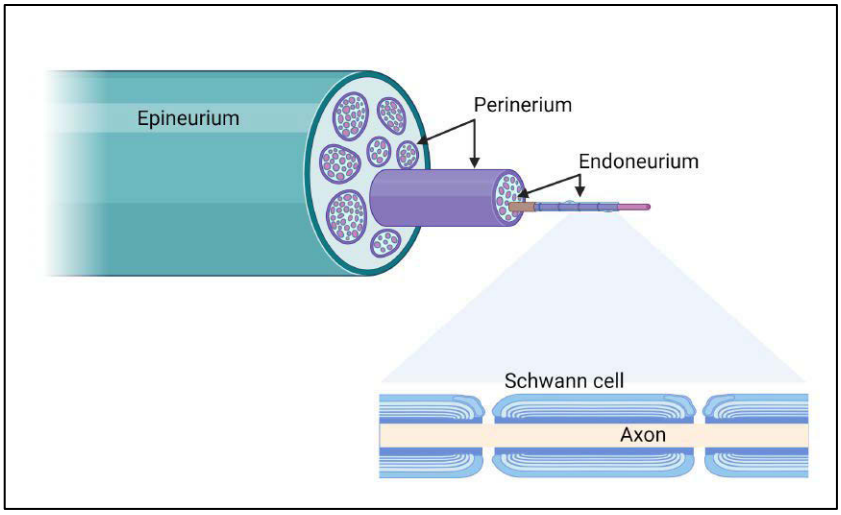

Figure 4. The structural features of peripheral nerve, epineurium, perineurium and endoneurium.

The perineurium surrounds groups of axon-Schwann cell units. The perineurium is composed of concentric layers of flat, polygonal perineurial cells. The number of perineurial cell layers is related to the size of the nerve fascicle with larger fascicles in the more perineurial cell layers (Thomas, 1963). The perineurium functions as a selective nerve-tissue barrier to maintain the strictly regulated homeostasis of the endoneurial space. The perineurial diffusion barrier is partly formed by the exceptionally thick basement membranes on both sides of each perineurial cell (Gamble & Eames, 1964). The main component of the diffusion barrier is the tight junctions between overlapping cell membranes of adjacent perineurial cells (Reale et al., 1975). The perineurial tight junctions are composed of claudins-1 and -3,

occludin and zona occludens (ZO-1). In the adult perineurium, continuous strands of tight junctions encircle the perineurial cells and seal the contacts between the neighboring cells. The meeting points of several perineurial cells are most tightly sealed Schwann cells surrounding axons are embedded in the endoneurium, which is the innermost connective tissue structure of peripheral nerve Schwann cells and myelination (Pummi et al., 2004)

Schwann cells can be divided into myelinating and non-myelinating cells (**Figure 5**). Myelinating Schwann cells wrap around a single axon, while a variable number of axons and also collagen fibrils can become invaginated into non-myelinating Schwann cells. The main function of Schwann cells is to isolate the axon and to enhance the velocity of electrical impulses.

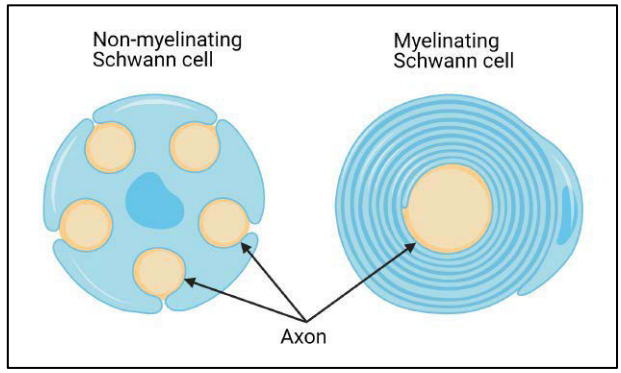

Figure 5. The schematic illustration of a myelinating and non-myelinating Schwann cells.

During the myelination, the cell membrane of the Schwann cell wraps several times around the axon. Membrane sheets are organized into compact and non-compact structures such as the Schmidt-Lanterman incisure, the paranodal region, the nodal region and the inner- and outer mesaxon. The structural details have been summarized in **Figure 3**. These structures have distinct roles to support metabolism and to serve in the transcellular and radial pathway to maintain ion and molecular trafficking (Arroyo & Scherer, 2000).

Even though the structural details of the endoneurium have been characterized with light and electron microscopy decades ago (Gamble & Eames, 1964; Thomas, 1963), the molecular composition has been investigated during the recent decades. The studies carried out in animal models have revealed autotypic cell junctions, i.e., cell junctions that adhere to cell membrane sheaths of a single Schwann cell. The tight junction, gap junction and adherens junction components have been localized to the adjacent membrane lamellae of myelinating Schwann cells of mouse nerves. Tight junction complexes lineate into compact and non-compact myelin structures.

In addition, adherens and gap junctions have been localized to Schmidt-Lanterman incisures (Poliak et al., 2002).

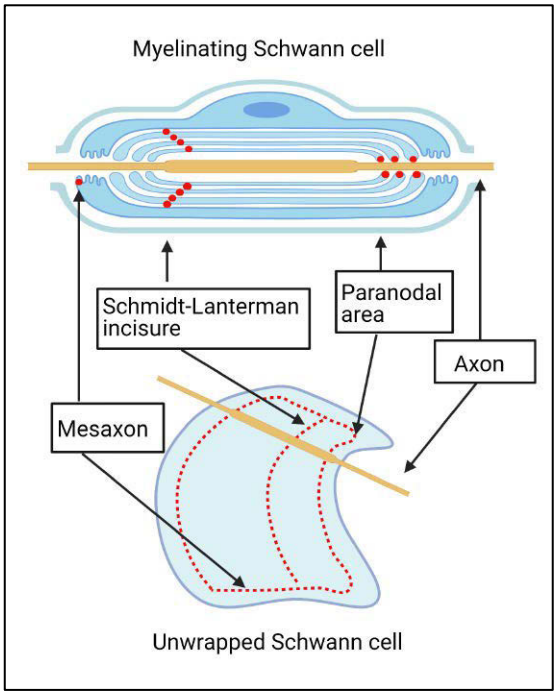

Figure 6. Specific subcellular structures of Schwann cell: Schmidt-Lanterman incisure, paranodal area, and mesaxon.

Schwann cells surrounding axons are embedded in the endoneurium, which is the innermost connective tissue structure of a peripheral nerve. Schwann cells can be divided into myelinating and non-myelinating cells. Myelinating Schwann cells wrap around a single axon, while a variable number of axons and also collagen fibrils can become invaginated into non-myelinating Schwann cells. The main function of Schwann cells is to isolate axon and to enhance the velocity of electrical impulses.

During the myelination, the cell membrane of a Schwann cell wraps around the axon. Membrane sheets are organized into compact and non-compact structures such as the Schmidt-Lanterman incisure, the paranodal region, the nodal region and the inner- and outer mesaxon (**Figure 6)**. These structures have a distinct role to support metabolism and to serve in the transcellular and radial pathway to maintain ion and molecular trafficking (Spiegel & Peles, 2002).

Even though the structural details of the endoneurium have been characterized with light and electron microscopy decades ago, the molecular composition has been studied rather late. The studies revealed that Schwann cells have autotypic cell

junctions, i.e., cell junction proteins that adhere to adjacent cell membrane sheets of the single cell (Fannon et al., 1995; Kikuchi et al., 2010; Poliak et al., 2002). These unique autotypic tight junctions lineate compact and non-compact myelin structures. In addition, adherens and gap junctions have been localized to Schmidt-Lanterman incisures.

2.3 Neurofibromatosis

2.3.1 Neurofibromatosis syndrome

Neurofibromatosis type 1 (NF1), called von Recklinghausen syndrome, is an autosomal dominant disease that is caused by mutations in the NF1 gene. NF1 is one of the most common genetic syndromes with an incidence of 1:2000 (Huson et al., 1988; Uusitalo et al., 2015). A tumor suppressor protein, neurofibromin, is encoded by the NF1 gene, and it is a negative regulator of the Ras signaling pathway (Martin et al., 1990). NF1 syndrome is caused by a mutation in one NF1 allele, but the pathological mechanism of severe clinical manifestations such as malignant peripheral nerve sheath tumor (MPNST) and congenital pseudarthrosis are considered to result from two distinct mutations leading to loss of heterozygosity (LOH) (Fang et al., 2009; Lee et al., 2012; Skuse et al., 1989; Upadhyaya et al., 2008). Approximately 50% of mutations in NF1 patients are sporadic, and the remaining mutations are considered to be inherited. Furthermore, the penetrance of the clinical syndrome is 100%.

NF1 disease affects mainly the peripheral and central nervous system, the skeleton and the skin. The most common clinical features of NF1 disease are benign cutaneous neurofibromas, café-au-lait macules, Lisch nodules, multiple bone defects, learning disabilities and a higher risk for malignancies such as MPNSTs and intracranial gliomas, breast cancer, gastrointestinal stromal tumors (GIST) and pheochromocytoma (Peltonen et al., 2017; Tabata et al., 2020; Uusitalo et al., 2017) NF1-patients have a two-fold increased life-time risk for malignancies (59.6% vs. 30.8%) (Uusitalo et al., 2016). Furthermore, NF1 patients die 16 or 26 years in men and women, respectively, earlier than the general Finnish population (Uusitalo et al., 2015).

A NF1 diagnosis is based on clinical symptoms according to National Institutes of Health (NIH) criteria. The NF1 disease belongs to RASopathies sharing some clinical features such as abnormal skin pigmentation and defects in skeletal, vascular and nervous system with Noonan, Leopard and Costello syndromes (Bezniakow et al., 2014). In fact, modern applications of gene sequencing provide diagnostic tools to distinguish similar diseases, if a clinical diagnosis needs to be verified. However,

medical support is mostly restricted to symptom-related therapy, surgical operations and medical counseling due to a lack of curative treatments.

2.4 Clinical features

2.4.1 Defects in the nervous system

Benign cutaneous neurofibromas are visible hallmarks of NF1 disease affecting at least 80% of adult NF1 patients (Anderson & Gutmann, 2015; Plotkin et al., 2012). Neurofibromas arise from a single peripheral nerve or bundles of nerve plexus and are composed of a mixed-cell population of peripheral nerve such as Schwann cells, fibroblasts, perineurial cells, mast cells, axonal components and a collagenous extracellular matrix (Peltonen et al., 1988). Cutaneous neurofibromas cause a generally aesthetic disadvantage but may be painful and cause itch. Approximately 5-10% of plexiform neurofibromas transform into malignant tumors. The majority of MPNSTs are histopathologically classified as high-grade sarcomas. These tumors have a poor prognosis due to a high probability of recurrence and metastasis (James et al., 2016). MPNST affects 8-13% of NF1 patients (Evans et al., 2002). Most of the brain tumors are benign pilocytic astrocytomas or optic gliomas. These optic gliomas are particularly diagnosed in pediatric NF1 patients. Instead, glioblastomas resulting in a fatal outcome are rare. However, the mean overall survival of glioblastoma is rather high at 9.25 years in pediatric NF1 patients, while patients without NF1 survive 1.08 years on average (Huttner et al., 2010). Non-tumor neurological manifestations, for instance, learning disabilities and attention defects, are common in NF1 patients, while seizures and mental retardation have been considered to be uncommon features of the NF1 disease (Anderson & Gutmann, 2015).

2.4.2 Skeletal defects

Skeletal abnormalities in NF1 disease can be classified as impaired bone metabolism, abnormal bone growth, remodeling and bone healing. Skeletal abnormalities affect more than 50% of NF1 patients and are categorized into general and focal abnormalities. General abnormalities include osteopenia/osteoporosis, a short stature and macrocephaly, which are classified as mild abnormalities. Focal abnormalities are sphenoid wing dysplasia, dystrophic scoliosis, tibial dysplasia, cystic lesions, enlarged mandibular canal particularly in women, and chest wall deformities (Elefteriou et al., 2009; Visnapuu et al., 2018). The quality of life and medical condition varies according to the severity of bone manifestations. For

instance, macrocephaly does not restrict daily activities, while severe dystrophic scoliosis increases morbidity.

Osteoporosis was the first bone abnormality that was associated with the NF1 disease in the 1950s (Gordan, 1951; Ortuzar et al., 1956). Current osteoporosis research started at the beginning of the 2000s (Illés et al., 2001). NF1-related osteoporosis displays specific features. One of the exceptional features of bone manifestations is the decreased bone mineral density at a young age beginning at 37 year old equally in males and females (Heervä et al., 2010; Kuorilehto et al., 2005). In addition, osteoporotic bone is localized to load-carrying parts of the body affecting 20–50% of NF1 patients (Kuorilehto et al., 2005; Tucker et al., 2009). Osteopenia often progresses to osteoporosis within 12 years (Heervä, E. et al., 2013). The fragile bone phenotype increases fracture risk. Adult NF1 patients have an approximately 5-fold fracture risk and pediatric NF1 patients display a 3.5-fold fracture risk compared to a healthy population (Heervä, E. et al., 2012; Tucker et al., 2009). Several studies have shown that bone metabolism is increased in NF1 patients. Many metabolic markers such as the C-terminal cross-linking beta-telopeptide of type I collagen, alkaline phosphatase, osteocalsin, TRACP5b and the N-terminal propeptide of procollagen type I have revealed similar results (Heervä et al., 2012; Petramala et al., 2012). Low levels of 25-OH vitamin D and high levels of serum parathyroid hormone have been associated with abnormal bone metabolism in adult and pediatric NF1 patients as well (Riccardi et al., 2020). A constant catabolic state of bone tissue, decreased bone mineral density and increased fracture risk encourage pharmacological treatments. NF1 patients suffering from osteoporosis were treated with bisphosphonate alendronate for 23 months. After alendronate treatment, bone metabolic markers were normalized, but bone mineral density was recovered less than expected (Heervä et al., 2014).

Bone softening and anterolateral bowing of the tibia precede congenital pseudarthrosis of the tibia (CPT), which is usually observed before the age of 3 years and affects 1–4% of NF1 patients. Histological analysis showed atypical fibrous tissue formation, increased cartilage formation and impaired bone recovery at the pseudarthrosis site (Sakamoto et al., 2007). Studies suggest that the loss of two NF1 alleles in mesenchymal stem cells precedes the formation of pseudarthrosis even though experiments are not replicative in all cases (Lee et al., 2012; Leskelä et al., 2009; Sakamoto et al., 2007; Sant et al., 2015; Stevenson, D. A. et al., 2006). It is interesting to note that common treatments of CPT are ineffective to induce bone healing (Tikkanen et al., 2010). Details of current operative and pharmaceutical treatments are discussed in the reviews by Stevenson and Eisenberg (Eisenberg & Vuillermin, 2019; Stevenson et al., 2013).

Dystrophic scoliosis is diagnosed in 2% of pediatric NF1 patients, and it may progress rapidly. Loss of heterozygosity has been associated as a one

pathomechanisms of dystrophic scoliosis in NF1 patients (Margraf et al., 2019).Like CTP, dystrophic scoliosis is often difficult to treat. New approaches to surgical and pharmaceutical management are under investigation (Tauchi et al., 2020; Yao et al., 2019).

2.4.3 The NF1 gene

The NF1 gene was mapped to chromosome 17 band q11.2 for the first time in 1990 (Wallace et al., 1990). The NF1 gene is one of the largest genes in humans spanning 287-kilobases (kb) of chromosome 17, including 57 constitutive and 4 alternatively spliced exons (exons: 9br, 10a2, 23a, 48a) (Danglot et al., 1995; Gutman et al., 1993; Kaufmann et al., 2002; Trovó-Marqui & Tajara, 2006). In addition, the three other genes OMGP (oligodendrocyte-myelin glycoprotein), EVI2A (ecotropic viral integration site) and EVI2B are embedded in intron 27 of the NF1 gene. These genes are transcribed in opposite direction on the NF1 gene (Cawthon et al., 1990; Cawthon et al., 1991; Viskochil et al., 1991).

The NF1 gene displays a rather high mutation rate with approximately $1x10^{-4}$ per gamete per generation (Huson et al., 1989). Nearly 2700 (2660 recorded in The Human Gene Mutation Data Base) individual mutations have been described. Approximately 80% of NF1 gene mutations are truncating, which leads to the disruption of NF1 gene expression. NF1 gene mutations are most frequent in exons 3, 5 and 27 and the structural segments of which favor a higher mutation rate. However, these gene locations cannot be considered as “hot spots.” Furthermore, most of the remaining NF1 gene mutations are classified to missense mutations, where the content of amino acid has been changed, and dysfunctional neurofibromin, in the end, is expressed (Abramowicz & Gos, 2014). Nonetheless, obvious genotype-phenotype correlations have not been demonstrated with some exceptions (Liu et al., 2020). Microdeletions are classified as short sequences in the chromosome, up to 5 mega-base pairs. 5% of all NF1 patients carry a microdeletion and feature severe abnormalities such as childhood overgrowth, a higher risk for malignancies compared to other NF1 patients, early onset of cutaneous neurofibromas, dysmorphic features in the extremities and face and cognitive abnormalities (Cawthon et al., 1990; Kehrer-Sawatzki et al., 2017; Upadhyaya et al., 1998). Conversely, a 3-bp in-frame deletion in exon 17 has been related to mild symptoms such as pigmentary lesions in skin and iris in the absence of neurofibromas (Upadhyaya et al., 2007). Furthermore, variable phenotypes are observed in patients carrying the same NF1 gene mutation. This suggests that the NF1 gene is regulated by other agents, such as modifier genes and epigenetic factors, in addition to a NF1 mutation (Szudek et al., 2002; Yapijakis et al., 2016).

Somatic mutations are present in all other cells, while mutations in germline cells are excluded. Therefore, somatic mutations do not lead to genetic syndromes and are not inherited (Martincorena & Campbell, 2015). Somatic mutations in genes, which are associated with tumor suppressing and cell signaling, give rise to variable malignant tumors. Somatic mutations in the NF1 gene have been associated with malignancies such as melanoma, non-small lung squamous cell carcinoma, ovarian adenocarcinoma, pancreatic carcinoma, gastric adenocarcinoma, glioblastoma and bladder uroepithelial carcinoma in non-NF1 patients (Kiuru & Busam, 2017). For instance, a data showed that each lung adenocarcinoma featured approximately 2–5 sporadic mutations including NF1 (Shi et al., 2016). In addition, a somatic mutation in the NF1 gene is a common finding in gastric cancer patients without NF1 syndrome (Hu et al., 2016).

2.4.4 The NF1 protein

The NF1 gene encodes neurofibromin, a tumor suppressor protein. Neurofibromin has 2818 amino acids and a molecular weight of 280 kDa. Principally, neurofibromin is a catalytic domain of guanosine triphospatase (GTPase) thus switching active RAS-GTP to inactive RAS-GDP eventually inhibiting the Ras signaling pathway (Bergoug et al., 2020). Neurofibromin is highly conserved among species. For example, mouse neurofibromin is 98% homologous to human neurofibromin (Bernards et al., 1993). A study showed that neurofibromin is ubiquitously expressed in various tissues during the early phases of embryogenesis Otherwise, neurofibromin is normally expressed in the nervous system when studied with adult rats (Daston et al., 1992; Daston & Ratner, 1992). Neurofibromin is also expressed in bone and cartilage. Neurofibromin expression is detected in hypertrophic and mature cartilage, in periosteum as well as in osteoclasts in adult rodents, and protein is also detectable in cartilage during the embryogenesis (Kuorilehto et al., 2004).

2.4.5 Nf1 mouse models

In order to elucidate the pathological mechanisms of bone manifestations, several Nf1 mouse models have been generated. Genetically modified mouse models provide an opportunity to evaluate the specific role of a certain cell population, evaluate gene inactivation in a dose-dependent manner and serve as models for bone remodeling and repairing.

A traditional knockout mouse model, where Nf1 gene inactivation was completed in both alleles ($Nf1^{-/-}$), leads to lethal phenotype due to cardiorespiratory abnormalities by embryonic day 14.5 thus emphasizing the critical role of neurofibromin during the development (Brannan et al., 1994). Instead, heterozygous

Nf1 knockout mice ($Nf1^{+/-}$) remained vital but did not feature macroscopic or histological bone- or nervous system-related abnormalities seen in NF1 patients. However, $Nf1^{+/-}$ mice displayed higher tumorigenesis, and histopathological analysis showed tumors being classified as lung adenocarcinoma, fibrosarcoma, lymphoma, lymphoid leukemia and hepatoma. Half of the tumors displayed the LOH according to the two-hit hypothesis (Jacks et al., 1994).

In vitro methods have been a remarkable tool to analyze the molecular pathological mechanisms in Nf1-related mouse models. Bone marrow mononuclear cells isolated from $Nf1^{+/-}$ mice were differentiated into osteoclasts. The results showed that $Nf1^{+/-}$ osteoclasts displayed an increased activation of the Ras signaling pathway, a higher capacity of bone resorption and an increased survival rate (Yang et al., 2006). These results correlate with human data, which showed that osteoclasts differentiated from monocytes of NF1 patients displayed similar results (Heervä et al., 2010; Stevenson, David A. et al., 2011).

Conditional knockout mouse models have been created to analyze targeted NF1 gene inactivation in a time-, tissue- or cell-specific manner. Targeted inactivation of the Nf1 gene is based on Cre/loxP technology, where the Cre recombinase enzyme is coupled to the guidance of specific gene promoter (Zhu, Y. et al., 2001). Details of the protocol are described in the Material and Methods chapter. Bone-related conditional knockout mouse models mainly focus on Nf1 gene inactivation in the mesenchymal cell lineage (i.e., osteoblasts and chondrocytes) or the myeloid cell lineage (i.e., osteoclasts).

Several Nf1 mouse models focus on evaluating the role of mesenchymal cell lineage in bone-related pathogenesis in order that gene inactivation is targeted to mesenchymal cell lineage during several phases of differentiation (Elefteriou et al., 2006; Kolanczyk et al., 2007; Wang, W. et al., 2011). The results show that Nf1 gene inactivation in the early phase of mesenchymal cell lineage leads to remarkable bone manifestations. In the $Nf1^{flox/flox}$;Prx1Cre mouse model, where Nf1 gene inactivation is programmed during early and late stages of limb bud development, macroscopic findings such as severe deformities of joints, a bowing tibia and shortened bones were detected. In addition, increased bone porosity was detected by back scattered electron microscopy. At the microscopic level, the results suggested that number of osteoclasts was increased in a consequence of abnormal osteoblast differentiation, even if the genotype of osteoclasts remained normal (Kolanczyk et al., 2007). NF1 gene inactivation restricted to osteoprogenitor ($Nf1^{Col2-/-}$) cells displayed similar features of a phenotype seen in $Nf1^{flox/flox}$;Prx1Cre mice (Wang et al., 2011). Instead, in a mouse model featuring NF1 gene inactivation in fully differentiated osteoblasts ($NF1^{ob-/-}$), no macroscopic abnormalities were detected. Histomorphometric analysis showed increased bone volume, which correlates to *in vitro* findings such as abnormal osteoblast and osteoclast differentiation and delayed bone mineralization

(Elefteriou et al., 2006). Even though structural details of $Nf1^{flox/flox}$;Prx1Cre and $NF1^{ob-/-}$ mouse models were originally analyzed using standard histomorphometry and μCT, additional imaging with high resolution μCT, small-angle X-ray scattering (SAXS) and scanning acoustic microscopy (SAM) was carried out. The results showed the fine details of Nf1-deficient bone featuring larger lacunae, decreased mineral density and softening of cortical bone, while mineral particle size and orientation remained normal (Kühnisch et al., 2014)

In bone-related Nf1 mouse models, neurofibromin deficiency in mesenchymal or hematopoietic cell lineages promote the formation of bone abnormalities. Gene inactivation during the early phases of cell differentiation contributes to severe bone abnormalities, while Nf1 gene inactivation in fully differentiated bone cell lineages leads to mild bone abnormalities seen in NF1 patients. Furthermore, cell signaling pathways such as MAPK/ERK, Serine/threonine-specific protein kinase (Akt) and mammalian target of rapamycin (mTor), which are essential for decent osteoclastogenesis, are disturbed (Rhodes & Yang, 2016).

The role of neurofibromin deficiency in hematopoietic progenitor cells and osteoclasts has been evaluated using two Nf1 mouse models, in which one Nf1 allele is inactivated in myeloid progenitor cells (LysMCre;$Nf1^{flox/+}$) or terminally differentiated osteoclasts (CtskCre;$Nf1^{flox/+}$) (Rhodes et al., 2015). The results showed that heterozygous neurofibromin expression is not sufficient to induce macroscopic bone abnormalities, even though Nf1 expression is disrupted during the early phase of hematopoietic differentiation. *In vitro* studies using LysMCre;$Nf1^{flox/+}$ mice showed that osteoclasts were larger in size, the actin structure was altered and resorption capacity was increased in osteoclasts. The results of the CtskCre;$Nf1^{flox/+}$ mouse model revealed rather a normal bone phenotype suggesting that Nf1-deficient osteoclasts are sufficient to maintain bone homeostasis.

Bone-specific mouse models have also been used to analyze the biological responses in cell signaling pathways. In general, Nf1 deficiency predisposes to hyperactivation of the Ras signaling pathway and downstream effectors in mesenchymal and hematopoietic cell lineages. Abnormal activation in serine/threonine-specific protein kinase; Akt and mTOR, signaling pathways has been reported (Ma et al., 2012; Yang et al., 2006). Hyperactivation of these signaling pathways generally predisposes to unnecessary cell growth, differentiation, proliferation and motility. Hyperresponsivity of the receptor for colony-stimulating factor-1, c-Fms, and TGF-β, results in a gain-in function in neurofibromin-deficient osteoclasts (He et al., 2012; Rhodes et al., 2015). Hyperstimulation of c-Fms increases activity in the c-Fms downstream effectors being Erk1/2 and p90RSK in Nf1-deficient osteoclasts. Increased expression of β-catenin is associated with cellular dysfunction in the absence of neurofibromin. Increased osteoclast activity

and abnormal osteoblasts have been associated with alterations in the Wnt/β-catenin signaling pathway (Ghadakzadeh et al., 2016).

Genomic engineering and phenotypic findings of bone-related Nf1 mouse models provide a model for experimental procedures such as fracture healing, pseudarthrosis and osteoporosis with surgical or pharmaceutical modifications. Several studies have been performed to rescue Nf1-related bone abnormalities to normalize aberrant cell signaling. Furthermore, experimental procedures of pseudarthrosis in healthy mice are unsatisfactory due to a high bone metabolic rate and a rapid healing process (Kuorilehto et al., 2006). A recent study showed that local administration of adenovirus (Ad-Cre) into a surgically induced tibial fracture site in $Nf1^{flox/flox}$ mice yielded pseudarthrosis, where cells showed a LOH (Ghadakzadeh et al., 2016). The healing process of pseudarthrosis was normalized by modulating the β-catenin antagonist Dickkopf-1. Similar results have been obtained with Nf1Prx1Cre and $NF1^{ob-/-}$ mouse models by administrating lovastatin locally to a surgically-induced fracture site (Kolanczyk et al., 2008; Wang et al., 2011). Even though Nf1 deficiency facilitates dysfunction of each bone cell type, most of the Nf1 mice are inadequate models for osteoporosis. However, anabolic bone metabolism can be induced with ovariectomy. $Nf1^{+/-}$ mice display a decreased bone mineral density compared to healthy control mice after ovariectomy (Yang et al., 2006). Bone loss could be prevented and treated with PLX3397, a selective c-Fms inhibitor (He et al., 2012).

2.5 Cell junctions

2.5.1 General principles about cell junctions

Cell junctions operate between the cytoskeleton and the cell microenvironment to bind individual cells to the extracellular matrix or to attach cell membranes of adjacent cells. The first observations of cell junctions were made by electron microscopy from epithelial tissue, which was easily available and simple to process. Electron microscopy studies recognized that tight junctions, adherens junctions and desmosomes are three distinct morphological structures in the junctional complex. Studies also demonstrated the relationship of these cell junctions to the microenvironment, particularly localization in the cell membrane and the association to adjacent epithelial cells (Adil et al., 2020; Farquhar & Palade, 1963; Thomas, 1963). Subsequently, gap junctions and focal adhesions were also recognized. The development of immunohistochemical techniques and advanced methods for production of specific antibodies showed the diversity of cell junctions from a biomolecular perspective. These observations revealed the molecular composition of cell junctions, which are discussed below in this context.

2.5.2 Intercellular junctions from a functional point of view

Cell junctions have been classified according to their structural and functional properties. Cell junctions increase mechanical strength, form a barrier, allow ions and small molecules to diffuse and participate in cell signaling (Hartsock & Nelson, 2008; Wehrle-Haller, 2012). These properties maintain the homeostasis of the microenvironment and participate in developmental processes at the cellular and tissue level. One of the essential functions of tight junctions is to define cell polarity, when a cell is divided into its apical and basolateral side according to the localization of tight junction strands. Furthermore, tight junctions participate to maintain intercellular homeostasis by forming a semi-selective diffusion barrier. Particularly, adherens junctions and desmosomes increase mechanical strength and stabilize cell-cell adhesion, while gap junctions provide intercellular communication to allow the ions and small molecules to diffuse freely (Goodenough & Paul, 2009). Focal adhesions are localized between the cell and extracellular matrix to adhere the cell to the substratum. Focal adhesions participate in cell migration and increase mechanical strength (Wu, C., 2007).

2.5.3 Tight junctions

Tight junctions, formerly named as zonula occludens, were identified for the first time in 1963 by electron microscopy (Farquhar & Palade, 1963). In epithelial cells, tight junction proteins are composed of strands to adjoin cells. Two tight junction proteins of adjacent cells are orientated in opposite positions in the plasma membrane (Mineta et al., 2011). A major function of tight junction is to form semi-selective barrier.

The tight junction protein complex is categorized to transmembrane proteins and intracellular scaffolding proteins. The molecular assembly of tight junction proteins is summarized in **Figure 7**. Four-pass transmembrane proteins being claudins, occludin, tricellulin and single-span transmembrane proteins junctional adhesion molecules (JAM) and coxsackie and adenovirus-associated receptor (CAR) are connected to intracellular scaffolding proteins such as the zona occludens (ZO) 1, 2, and 3; multi-PDZ domain protein 1 (MUPP1) and the membrane associated guanylyl kinase with inverted orientation (MAGI) (Steed et al., 2010). Eventually, the tight junction complex is linked to cytoskeletal components of actin and microtubules (Hartsock & Nelson, 2008).

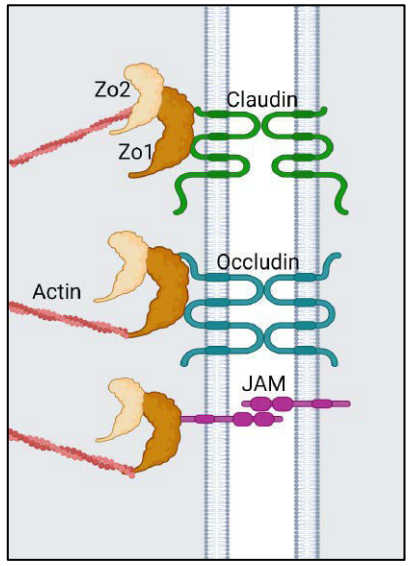

Figure 7. Molecular assembly of tight junction proteins.

Claudin, a major molecule of the tight junction complex, is encoded by 27 individual genes in the human and mouse and is highly conserved among species (Mineta et al., 2011). Claudins commonly feature homotypic interactions but occasionally claudin-3 forms heterotypic interactions with claudin-1, claudin-2, claudin-3 or claudin-5. Heterotypic claudin interactions have been suggested to participate in the fine tuning of paracellular permeability (Overgaard et al., 2011). The expression profile of claudins correlates to the functional properties in a tissue-specific manner. For instance, claudin-16 and claudin-19 are expressed in the kidney to regulate paracellular ion reabsorption (Hou et al., 2009), whereas claudin-11 is expressed in myelinating oligodendrocytes in the central nervous system (Denninger et al., 2015) and in Sertoli cells in testis (Mazaud-Guittot et al., 2010).

Claudins, specifically claudin-1, were first discovered to regulate paracellular homeostasis by forming a selective barrier. Furthermore, claudin-2, -4, -10, -16 and -17 are considered to form pores to allow selective paracellular water and ion diffusion (Liang & Weber, 2014). Claudins also participate in cell signaling with their cytoplasmic tails. Previous studies show that claudins are involved in the regulation of cell signaling pathways such as the MAPK, Akt, Protein kinase A and C and Rho (González-Mariscal et al., 2008). In addition, claudins seem to operate, in some cases, as a receptor via extracellular domains. Particularly claudin-1, -3, -4 -6, -9, occludin and the Clostridium perfringes enterotoxin function as a co-receptor for the hepatitis C virus (Freedman et al., 2016).

Occludin was the first transmembrane tight junction molecule to be recognized and found to be widely expressed in several organ tissues such as the intestine, the

liver, the kidney, the lung and the brain (Furuse et al., 1998; Hwang et al., 2013). Occludin forms tight junctions with other occludin molecules when junctions are classified to homotypic junctions. Furthermore, occludin contacts with the other claudins to form heterotypic tight junctions as well. Occludin is encoded by the occludin gene and forms a four-pass transmembrane protein including two extracellular loops, two intracellular domains and cytoplasmic N- and C-terminal domains (Saitou et al., 1997). Eventually, occludin is linked to the actin cytoskeleton via the ZO-1, ZO-2 or ZO-3 proteins (**Figure 7**).

The significance of occludin has been somewhat unclear. Occludin regulates paracellular permeability in a size-selective manner rather than maintaining barrier function (Campbell et al., 2017). Furthermore, previous studies have suggested that occludin is not a necessary molecule for decent tight junction formation. The results of the occludin knockout mouse model showed that the formation and function of normal tight junction remain even if the expression of occludin is prevented (Saitou et al., 2000; Schulzke et al., 2005). Occludin expression is transiently increased in skin epithelial cells during the wound healing (Volksdorf et al., 2017). Furthermore, occludin expression is occasionally replaced by tricellulin, a tight junction protein, which is usually binds three neighbouring epithelials cells to form tricellular junctions in epithelial cells (Ikenouchi et al., 2008).

2.5.4 Adherens junctions

Originally, adherens junctions were found concurrently with tight junctions. Adherens junctions, in general, are localized to the vicinity of tight junction strands and desmosomes. Adherens junctions anchoring adjacent cells increase stability, maintain integrity and cell polarity (Farquhar & Palade, 1963). Structural components of adherens junctions are categorized to classic transmembrane proteins cadherins and intracellular proteins such as plakoglobin, and alpha-, beta- and p-120-catenins. These intracellular proteins connect the adherens junction to the actin cytoskeleton. Assembly of adherens junction proteins is illustrated in **Figure 8**. The cadherin superfamily contains over a hundred proteins, which represent several subtypes such as classical cadherins, protocadherins, desmosomal cadherins and cadherin-related families, for instance (Hartsock & Nelson, 2008). However, this overview has focused on classical cadherins. The classical cadherin family consists of E-, P-, M-, N- and R-cadherins. The most prevalent cadherin, E-cadherin is expressed in epithelial cells widely to ensure strong intercellular adhesion (Goodwin, M. & Yap, 2004). Cadherins are single-pass transmembrane glycoproteins. The structure of classic cadherin includes five extracellular repeat domains, one transmembrane domain and two catenin-binding domains (Coopman & Djiane, 2016).

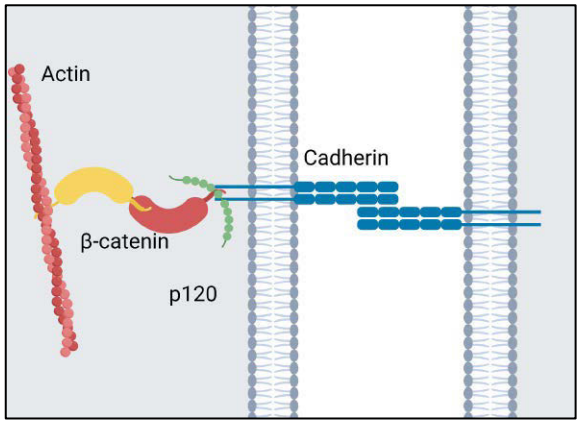

Figure 8. Schematic illustration of adherens junction proteins.

Intracellular proteins of adherens junctions, α-catenin, β-catenin and p120-catenin have their specific role to adjoin cadherins to actin cytoskeleton. In addition to their mechanical properties, catenins serve as a route for signaling pathways. For instance, β-catenin binds to transcription factors in order to regulate gene expression via Wnt signaling pathway (Alok et al., 2017). p120-catenin interacts with Rho GTPases, which in turn, regulate cell migration and cell motility (Schackmann et al., 2013).

2.5.5 Focal adhesions

Focal adhesions form a large group of adhesive structures, which can be divided according to their molecular composition, function and subcellular localization to several subtypes such as classical focal adhesions, focal complexes, fibrillary adhesions, podosomes, invadopodies and three-dimensional matrix adhesions (Wozniak et al., 2004). Here, the focus is on classical focal adhesions and podosomes. Focal adhesions mediate the cytoskeleton interactions with the extracellular matrix (ECM) and vice versa. Focal adhesions bind intracellular actin mechanically to the extracellular matrix via transmembrane proteins, integrins and a heterogenic group of cytoplasmic molecules (**Figure 9**). Focal adhesions are expressed in various cell types. Specifically, podosomes are abundantly expressed in monocyte-derived cells such as osteoclasts, macrophages and dendritic cells (Luxenburg et al., 2007). Up to sixty focal adhesion proteins have been recognized in mammalian cells (Wu, 2007; Zhu, L. et al., 2020).

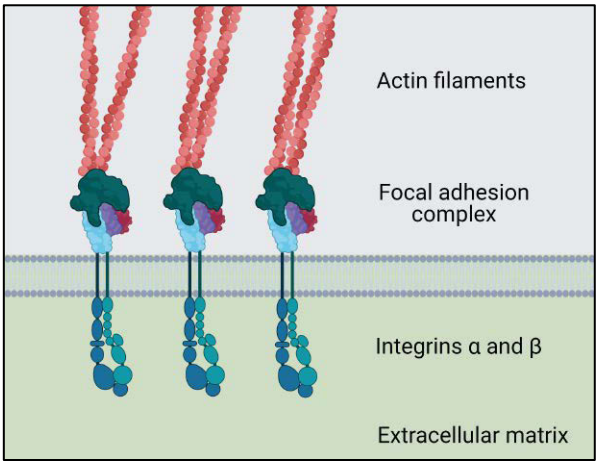

Figure 9. Schematic illustration of focal adhesion molecular assembly.

Transmembrane proteins of focal adhesion include integrins and transmembrane proteins such as the layilin glycoprotein receptor for hyaluronan and the syndecan-4 heparan sulfate proteoglycan receptor for fibronectin (Wehrle-Haller, 2012). Integrins contain alpha (α) and beta (β) subunits. At least 18 α-subunits and 8 β-subunits have been identified, and they can form 24 distinct heterodimeric compounds. Integrins act as receptors for stimuli from ECM and cytoplasmic signaling pathways (Oh et al., 2017; Renner et al., 2016). For instance, the α5β1 integrin is a receptor for fibronectin, a glycoprotein in the ECM.

The cytoplasmic group of proteins is rather large, and these proteins, for example, integrin-linked kinase (ILK), parvin, focal adhesion kinase (FAK), paxillin, talin, vinculin, tensin, vinexin, profilin and Rho participate in cell signaling and have structural or enzymatic properties. Other cytoplasmic molecules of focal adhesions feature differences according to structural and enzymatic properties. Cytoplasmic proteins can be classified as kinases, phosphatases or modulators of small GTPases, which have enzymatic properties. These proteins mediate cell signaling pathways such as FAK, protein kinase C (PKC) and Src (Wehrle-Haller, 2012).

Cytoplasmic proteins, for instance, α-actinin, talin and vinculin participate in focal adhesion formation to increase and maintain structural strength. Talin has binding sites for actin, integrin β3, vinculin and FAK and acts as a structural mediator between actin cytoskeleton, cell signaling pathways and ECM via integrin molecules. Cytoplasmic proteins of focal adhesion complex regulate the integrity and adhesive properties of focal adhesions in complicated manner.

2.5.6 Desmosomes

Desmosome junctions are hyper-adhesive intercellular structures, which maintain structural integrity and tissue homeostasis. Desmosomes are widely expressed in all vertebrate tissues and share structural and functional similarities with adherens junctions. Desmosomes consist of three molecular components, the desmosomal cadherins being desmoglein and desmocollin, armadillo proteins and desmoplakin. Four isoforms of desmoglein and three isoforms of desmocollin have been distinguished (Lowndes et al., 2014).

Desmoglein and desmocollin are single-pass transmembrane proteins that form a bond between adjacent cells in a homo- or heterophilic manner in the presence of calcium ions (Celentano et al., 2017). The cytoplasmic domain of desmoglein or desmocollin adhere to the armadillo residue of intracellular desmosomal plaque proteins such as plakoglobin or plakophilins. Eventually, the intracellular protein desmoplakin adjoins the molecular complex to intermediate filaments.

A recent study characterized desmosome structure of human primary keratinocytes in super-resolution by direct stochastic optical reconstruction microscopy (dSTROM) (Stahley et al., 2016). For the first time, dimensional features such as the length of desmosomal plaque molecules, could be measured. Furthermore, the mutual localization of these molecules was analyzed. dSTROM (microscopy) was even superior to electron microscope in showing the details. Furthermore, particularly in myocardial tissue, intercalated discs contain a special adhesive structure, called the area composita, which contains molecules from adherens junctions and desmosomes. For example, α-catenin interacts with plakophilin (Vite & Radice, 2014). It has been suggested that the hybrid junction reinforces intercellular adhesion when tissue is under a heavy mechanical burden.

2.5.7 Gap junctions

The first observations of gap junctions were detected by electron microscopy when this method became common during the 1960s (Dewey & Barr, 1962). Gap junctions are widely present in various cell types in vertebrates and invertebrates. Gap junctions are organized into clusters in the cell membrane, whereas tight junctions align in strands (Meşe et al., 2007). Gap junctions connect the intracellular spaces of the neighboring cells.

Structural studies have shown that gap junction channels are formed by two opposing hemichannels leaving a small extracellular gap, approximately 2–3 nm, between the adjacent plasma membranes. A hemichannel is a hexamere that consists of six connexin molecules (Calderón & Retamal, 2016; Revel & Karnovsky, 1967). Connexins are a large, transmembrane protein family encoded by 21 genes in humans (Söhl et al., 2005). Each connexin is a four-pass transmembrane protein

containing two extracellular loops and one intracellular loop. A heteromeric hemichannel is formed of two different connexins, while a homomeric hemichannel contains one connexin isoform. Furthermore, a pair of hemichannels can adjoin in a homo- or heterotypic manner.

Gap junctions play a significant role in intercellular communication in order to maintain tissue homeostasis. Furthermore, a single hemichannel maintains molecule diffusion between the intracellular and extracellular space. Gap junction channels enable ions and small molecules such as glucose, glutamate, adenosine triphosphate (ATP), cyclic adenosine monophosphate (cAMP), inositol 1,4,5-trisphosphate (IP_3) and small RNA molecules to diffuse passively when channels are opened. Closed gap junction channels prevent molecule diffusion (Calderón & Retamal, 2016). Several factors such as changes in pH, protein-protein interactions, phosphorylation and redox reactions regulate functional properties of gap junctions. In humans, gap junctions play a crucial role in various tissues. Several studies have mapped connexin distribution in a cell- and function-specific manner. For instance, connexin 43 is ubiquitously expressed in the skin, the heart, the eye and the brain, whereas connexin 30.3 is expressed in skin, kidney and placenta (Meşe et al., 2007).

2.5.8 Intercellular junctions from a clinical point of view

Alterations in cell junctions reflect cellular behavior and eventually to the functional properties of the organ system. The expression pattern of cell junction proteins is a dynamic process, which is regulated in a tissue-specific and developmental manner. Furthermore, inadequate function of cell junctions provides pathological mechanisms to several medical conditions such as genetic disorders, autoimmune-related diseases and cancers.

Tight junctions participate in maintaining a barrier system in the skin, the intestine, blood vessels and the nervous system (Steed et al., 2010). Dysfunctions of these barriers are considered to be one possible pathological mechanism of several diseases. For instance, altered claudin expression has been reported to increase the dysfunction of the gastrointestinal barrier. In diarrhea-predominant irritable bowel syndrome (IBS) patients, expression of the tight junction protein, claudin-2, was increased in epithelial cells in ileum, whereas expression of claudin-15 was increased in the colon when IBS patients followed a gluten-containing diet (Ishimoto et al., 2017; Wu, R. L. et al., 2017). Alterations in the blood-brain barrier have been associated with neurological diseases such as stroke, epilepsy or Parkinson disease (Sweeney et al., 2019). Furthene expression of the tight junction protein, claudin-11, is upregulated in the plasma of multiple sclerosis patients (Hassanzadeh et al., 2016). However, the precise mechanisms of this neurodegenerative disease are unclear.

Adherens junctions and desmosomes are, similarly to tight junctions, expressed in epithelial cells, for instance, in the heart, the intestine, the skin and the bladder to increase mechanical strength (Hartsock & Nelson, 2008). Alterations in cadherin expression have been associated with conditions such as uncontrollable growth in cancer tissues. Decreased E-cadherin expression has been associated with several epithelial-derived malignancies such as breast cancer, ovarian cancer, non-small cell lung cancer, bladder cancer and cancers in the gastrointestinal tract (Becker et al., 2002; Kaszak et al., 2020). Furthermore, decreased E-cadherin expression in breast cancer tissue suggests a poor prognosis (Li et al., 2017). Adherens junctions are widely expressed in the central nervous system. For instance, several psychiatric disorders such as schizophrenia, attention-deficit/hyperactivity disorder, bipolar and depression disorder as well as the spectrum of autism have been associated to abnormal cadherin expression. Particularly cadherin-7, cadherin-11 and cadherin-13 have been shown to associate with these psychiatric disorders (Hawi et al., 2018). In general, desmosome-related diseases cause visible symptoms such as skin blistering and woolly hair in addition to myocardial manifestations by genetic mutation, autoimmune-related or infectious mechanisms (Celentano et al., 2017). Pathophysiological alteration, such as abnormal expression of desmosomes, promotes carcinogenesis in epithelial-derived malignancies (Stahley et al., 2016).

Abnormal expression of integrins and focal adhesions have been associated with various malignant conditions, which emphasize the importance of controlled cell dynamics. From a pathologically mechanical point of view, integrins are a presumable target of therapeutic treatments. Previous studies have shown that the increased expression of integrin α5β3 is associated with breast, prostate and lung cancer and contributes to bone metastasis and medical complications such as bone-related pain and pathological fractures. Various clinical trials of α5β3 antagonists are currently ongoing (Karakus et al., 2020; Tang, L. et al., 2020; Zhao et al., 2020). α5β1 integrin is highly expressed in human glioblastoma cell cultures. The expression of α5β1 integrin is associated with uncontrolled adhesion, migration and proliferation. These malignant features of glioblastoma cells can be suppressed by interference of the α5β1-integrin signaling pathway with cucurbitacin B (Touihri-Barakati et al., 2017).

Gap junctions are mainly distributed in skin, nervous tissue, heart and muscles to maintain intercellular communication. A deficient function of gap junctions leads to dysfunctions of these organs (Goodenough & Paul, 2009; Skerrett & Williams, 2017). For instance, connexin gene mutations lead to several hyperproliferative skin disorders, which share similar clinical manifestations such as palmoplantar keratoderma, sensorineural deafness, nail dystrophy and hypotrichosis (Lilly et al., 2016). Furthermore, malignant features of hepatocellular carcinoma and dysfunction in lymphatic vessels, the pulmonary vasculature and pulmonary epithelium have been associated with abnormal gap junction formation (Wong et al., 2017).

2.6 The Cytoskeleton

2.6.1 General principles about the cytoskeleton

Three players of the cytoskeleton being actin microfilaments, intermediate filaments and microtubules compose highly dynamic structures that participate in nearly all cellular events including various subcellular processes, maintenance of cell shape and motility and increasing mechanical strength.

The earliest observations of actin were from 1942, when actin was detected as a separate protein from myosin, the contractile component of muscles (Risal et al., 2004). Microtubules were found within the cell during mitosis, and tubulins were found by disrupting the microtubules with colchicine (Borisy & Taylor, 1967). Intermediate filaments were recognized for the first time with electron microscopy (Ishikawa et al., 1968). The first evidence of cell dynamics was revealed with contrast microscopy. The studies showed that cells actually migrate. Details of actin filament architecture were seen with electron microscopy (Abercrombie et al., 1970). Invention of green fluorescent protein (GFP) brought advances in actin research. The connection between actin and focal adhesions was discovered in 1978, and some of the proteins of focal adhesion complexes were characterized. Combining the microscope with a video camera has enabled studies of cell movements since 1981. Connections between actin and cell signaling, for example, the modulation of cell functions by Rac and Ras via actin were found in the 1990s (Spiering & Hodgson, 2011).

2.6.2 The cytoskeleton from a functional point of view

The cytoskeleton plays a role in cell shape, cell migration and structural strength, and it also serves as a route for intracellular trafficking, for instance, in cell organelles, proteins and vesicles. Even though the cytoskeleton has been considered as a supportive and stabilizing structure, dynamics of the cytoskeleton include rapid interactions with cell junctions and signaling pathways, which in the end, lead to continuous reorganization of cytoskeletal components and cell junction molecules. Interactions of these cytoskeletal components have been studied from many perspectives (Dogterom & Koenderink, 2019).

2.6.3 Actin

Actin is widely expressed in all eukaryotic and prokaryotic cells. Actin was first detected as a contractile component of muscle and actin filaments purified from muscle. The earliest attempts to recognize actin from chicken breast muscle by

antibody labeling were performed in 1961, and imaging was proceeded with fluorescent microscopy (Tunik & Holtzer, 1961). Later, by immunohistochemical methods, actin was found also in non-muscle components, such as stress fibers.

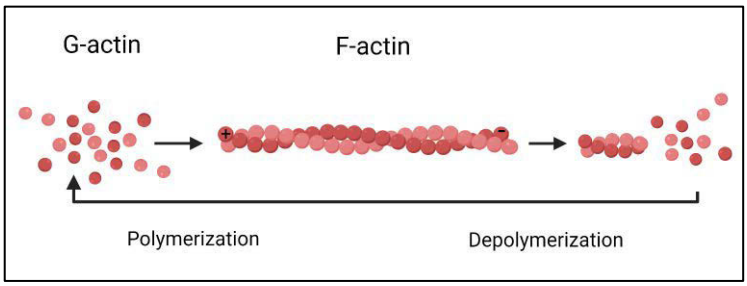

Figure 10. Equlibrium of filamentous actin formation and degradation.

Actin filaments are composed of globular actin (G-actin) monomers, which are actively polymerized to filamentous actin (F-actin). Two actin protofilaments are orientated in a parallel direction to form a single helical actin filament (Coutts & La Thangue, 2016). Filamentous actin is polarized. The barbed end is the fast-growing end, where actin turnover favors active and rapid polymerization (**Figure 10**). On the other hand, depolymerization is prevalent in the pointed end. Polymerization of actin is accelerated by ATP and ions such as magnesium and calcium (Blanchoin et al., 2014). Three main steps being nucleation, elongation and depolymerization take place continuously, and equilibrium of these three steps is coordinated with multiple regulatory proteins and interactions.

Dynamics of actin filaments at the cellular lever are regulated in a complicated manner. Various actin containing dynamic structures, such as cell protrusions and a leading edge, are actively regulated and maintained by actin-binding proteins. These actin-binding proteins are categorized according to function being nucleation, capping, crosslinking, bundling and severing (Siton-Mendelson & Bernheim-Groswasser, 2017). Numerous actin-binding proteins, at least 150, have been (Risal et al., 2004) described, and the most significant proteins are discussed in this context (Schoenenberger et al., 2011).

Actin nucleation-promoting factors include several heterogenic protein families such as Arp2/3 complex, formins and tandem-monomer-binding nucleators. Actin nucleators initiate the polymerization or increase the length of actin filament. The Arp2/3 complex is associated with the branching of actin filaments. The molecular composition of the Arp2/3 complex includes Arp2, Arp3 and five additional subunits being Arp C1-5 (Abella et al., 2016). The Arp2/3 complex is located at the branching site of actin and initiates polymerization in order to grow new actin filament in the

presence of nuclear promoting factors such as the Wiskott-Aldrich syndrome protein (WASP) and other WASP homologs, cortactin and Ena/VASP proteins.

Formins are actin nucleators *de novo*, in which case, nucleation is initiated from G-actin monomers. Formins are diaphanous-related formins (DRFs) which belong to subfamily of Rho GTPase-binding formin homology (FH) proteins. Formin proteins such as Dia, DAAM and FRL in mammalian cells are regulated by Rho GTPase (Isogai & Innocenti, 2016). Formins have strong affinity naturally, and are autoinhibited, which ensures that formation of actin filaments is not uncontrollable. The regulation of actin structures by formins has been related to cellular processes such as vesicle trafficking, membrane protrusion, migration, participating in asymmetric cell division and also in cell-cycle and apoptosis–related processes.

A common nucleation-promoting factor called cortactin is expressed in nearly all mammalian cell types and, in general, it has a major influence on cell migration by regulating the actin cytoskeleton (van Rossum, Agnes G. S. H. et al., 2005). The actin nucleation-promoting factor is encoded by the cortactin gene. Cortactin was first categorized as a substrate for the Src non-receptor tyrosine kinase. Later, studies showed that cortactin activates the Arp2/3 complex in order to initiate the actin branching. Cortactin contains numerous phosphorylation sites, binding sites for Arp2/3, actin, the SCR Homology 3 (SH3) domain, p120-catenin and ZO-1 (Kelley et al., 2010) Cortactin regulates nucleation of filamentous actin instead of globular actin. Furthermore, cortactin inhibits debranching and stabilizes the actin network (MacGrath & Koleske, 2012).

Capping proteins prevent excessive actin polymerization by blocking the barbed end of the actin filament. Capping proteins are members of the gelsolin superfamily, and proteins, such as gelsolin, villin, advillin, superfillin, adseverin, the flightless I homolog and CapG are expressed in mammalian cells (Shekhar et al., 2016). Some of these capping proteins also participate in actin severing by binding to the pointed end of an actin filament.

Actin severing proteins accelerate actin depolymerization and coordinate the disruption of actin filaments. One of the actin severing proteins, cofilin, is required for actin disassembly in the presence of proteins coronin and Aip1 (Andrianantoandro & Pollard, 2006). Furthermore, cofilin has been categorized to an actin nucleator *de novo* like formins. Cofilin induces depolymerization of the actin filament into monomers, which are recruited to the barbed end for actin polymerization and extension. Low concentrations of cofilin induce the dissociation of actin filament from the minus end, while high concentrations of cofilin inhibit the severing process. Cofilin is targeted into the nucleus during DNA damage and cell stress (Chang et al., 2015).

2.6.4 Microtubules

Microtubules participate in cell migration, maintaining several cellular processes such as cell shape, transportation of organelles, ciliary function, vesicles and positioning the cell organelles, for instance, during the mitosis. Microtubules are encoded by several genes to yield nine α- and nine β-tubulins and three γ-tubulins in mammalian cells (Gadadhar et al., 2017). A heterodimer, a subunit of microtubule, is composed of α- and β-tubulins, which are polymerized to protofilaments. 13 protofilaments form a hollow tube.

Active polymerization and hydrolyzation are required for rapid cellular processes, and the half-life of microtubules is generally 5–10 minutes. A microtubule is continuously polymerized at the plus (i.e., growing) end and depolymerized (i.e., shrinking) at the minus end. Microtubules can be extended from the plus and minus ends. Depolymerization at the minus end may occur 100-fold faster than depolymerization at the plus end. The plus and minus ends determine the polarity of microtubules similarly to actin filaments. The microtubule organization center (MTOC) is at the minus end. The γ-tubulin complex (γ-TuC) form the template to induce α- and β-tubulin nucleation (Lin et al., 2015).

Tubulin isotypes are expressed in a cell- or function-specific manner. For instance, β1-tubulin, which is encoded by TUBB1 gene, is related to hematopoietic-specific tubulin expressed in platelets and megakaryocytes. Mutation in TUBB1 gene induces thrombocytopenia and bleeding symptoms (Fiore et al., 2017). Furthermore, expression of β3-tubulin was detected in neuronal cells and neuronal malignancies, and β3-tubulin was considered to be a neuron-specific marker (Katsetos et al., 2003). However, transient expression of β3-tubulin was detected as a molecular component of the mitotic spindle in keratinocytes, two transitional cell carcinoma cell lines T24 and 5637, human fibroblasts and Schwann cells isolated from benign neurofibromas of NF1 patients (Jouhilahti et al., 2008). These findings together illustrate the diverse functional properties of tubulin isoforms. In addition, the molecular function of microtubules and microtubule-associated proteins are regulated by posttranslational modifications such as tyrosination, acetylation and glutamylation (Gadadhar et al., 2017). For instance, polyglutamylation of microtubules in neuronal cells promotes neuronal differentiation and survival (Rogowski et al., 2010).

Microtubules participate in mitosis and operate intercellular trafficking of proteins, organelles and vesicles. Microtubules are involved in cellular events such as proliferation, migration, maintaining cellular shape and secretory processes.

Microtubules also participate in signal transmitting. Specifically, microtubules guide neuronal growth and separate chromosomes during mitosis. Microtubules cooperate with actin and intermediate filaments to control, for example, cell migration and wound healing and influence T-cell-based immune responses. Actin-

microtubule interactions transmit signals to Rho GTPases, which in turn, regulate the assembly of focal adhesions, actomyosin contractility and actin dynamics (Etienne-Manneville, 2013).

2.6.5 Intermediate filaments

Intermediate filaments are categorized into six types according to their sequence, gene structure and cell-type specific expression patterns being type I: acidic keratins; type II: basic keratins; type III: desmin, vimentin, glial fibrillary acidic protein (GFAP) and peripherin; type IV: neurofilament proteins and alpha-internexin; type V: nuclear lamins and type VI: nestin and synemin.

Thus far, over 65 genes have been identified to encode intermediate filaments, which comprise one of the largest gene family in humans (Tang, D. D. & Gerlach, 2017). Intermediate filaments are expressed in a developmental- and cell-specific manner. Most of the intermediate filaments are localized in the cytoplasm (i.e., cytoplasmic) but type V intermediate filaments, being lamins, are expressed in the nucleus. Lamins are localized beneath the nuclear membrane to form a supportive network and increase the structural strength of the nucleus (Tang & Gerlach, 2017). For instance, type I and II intermediate filaments are expressed in epithelial cells, while expression of type IV intermediate filaments, neurofilaments, is restricted to neural tissue. The most ubiquitously expressed intermediate filament in various cell types is vimentin. The main intermediate filament in non-myelinating Schwann cells in peripheral nervous system is the glial fibrillary acidic protein (GFAP). GFAP is also expressed in astrocytes in the central nervous system and in enteric glial cells.

Intermediate filaments contain α-helical and non-α-helical domains. Non-α-helical domains contain numerous phosphorylation sites. The α-aminoterminal head is essential for assembly of intermediate filaments, and the carboxyterminal head of intermediate filaments is essential for the organization of intermediate filaments. Intermediate filaments contain subunits 1A, 1B, 2A and 2B. Compared to microtubules and actin filaments, intermediate filaments do not express any polar elements. Intermediate filaments are transported via microtubules with dynein and kinesin (Hookway et al., 2015).

2.6.6 A clinical point of view about the cytoskeleton

The cytoskeleton participates in nearly every intracellular and intercellular function and mechanism that is associated with, for example, intracellular molecule trafficking, tunneling nanotubes, cell migrations and invasion, cell division and cell and tissue differentiation. Mutations in cytoskeletal genes have been associated with various medical conditions, particularly with malignant tumors. Therefore, some

intriguing medical conditions related to the abnormalities in the cytoskeleton have been highlighted in this review.

Diseases in which the cytoskeleton is affected, lead to similar symptoms seen in diseases were junction protein expression is aberrant. Features of malignant cells include ability to migrate, invade, adhere and detach. In malignant diseases, all three components of the cytoskeleton being actin, microtubules and intermediate filaments display alterations in tissue in a developmental manner.

An actin binding protein, cortactin, is associated with a poor prognosis of cancer. Cortactin participates in the development and maturation of invadopodia. This feature is particularly important to invasive cancer cells. Overexpression of cortactin has been detected from invasive cancers such as glioblastoma, colorectal cancer and melanoma. Therefore, cortactin has been categorized as a biomarker of invasive cancer (Castellanos-Martínez et al., 2020; MacGrath & Koleske, 2012).

Alterations in microtubules have been associated with tumorigenesis. Microtubules participate in chromosome separation during mitosis and serve as an ideal mechanism to target in cancer treatment. In general, the expression of γ-tubulin is a mandatory component in mitotic spindle formation in human cells. Furthermore, γ-tubulin is overexpressed particularly in stage III non-small cell lung cancer (Maounis et al., 2019). Therefore, it is feasible to understand the association between γ-tubulin, uncontrollable cell proliferation and cancer. Mutations in βI-, βIIA- or βIVB-tubulin isotypes have been associated with breast cancer (Wang et al., 2017). Alterations in microtubule expression have been reported in various malignancies. These molecular pathological mechanisms provide pharmaceutical opportunities to control abnormal growth of malignancies and treat patients (Čermák et al., 2020; Federico et al., 2020).

Altered lamin expression has been associated with several cancers. For instance, in prostate cancer, laminA/C is overexpressed in prostate cancer tissue, and inhibition of the lamin synthesis decreases prostate cancer cell locomotion/migration *in vitro* (Kong et al., 2012). Alterations in lamin expression have been associated with cancers, and the modulation of lamins in cancer cells decreases the motility of cancer cells.

3 Aims

The purpose of the present study was to examine complex tissues namely peripheral nerves and bone tissues by combining specific imaging techniques. Furthermore, the study was also performed to elucidate the role of the neurofibromin-deficient osteoclasts play in the pathological mechanisms behind bone abnormalities associated with NF1 disease.

The specific aims of the study were:

1. To study Schwann cell autotypic tight junctions in human adult and developing peripheral nerves.
2. To characterize the bone phenotype of a Nf1Ocl mouse model *ex vivo* and *in vitro*.
3. To image the actin cytoskeleton of osteoclasts at super-resolution.

4 Materials and Methods

4.1 Materials

4.1.1 Human adult and fetal peripheral nerves (I)

All human tissue and blood samples were obtained with the appropriate informed consent and approval of the Joint Ethical Committee of Turku University Hospital and University of Turku, Finland.

Human adult peripheral nerve samples were obtained from healthy 16-, 21-, 39- and 40-year-old men, who had died in accidents. Sciatic nerve samples were taken during autopsies performed at the Department of Pathology, Turku University Hospital, Finland. Sciatic nerve samples of four fetuses were removed during autopsies performed at the Department of Pathology, Turku University Hospital, within 2 days of spontaneous miscarriage after premature labor at 19, 23, 26 and 37 weeks of gestation. The autopsies showed no macroscopic or chromosomal abnormalities. Samples were either used as frozen section samples or fixed with formalin and embedded in paraffin.

Great auricular nerve samples were removed from four patients (57–75 years of age) for surgical reasons encountered in the course of parotidectomies performed in the Department of Otorhinolaryngology-Head and Neck Surgery, University of Turku. Nerve samples were immediately fixed in 10% formaldehyde for 15 min. Nerve samples were cut into 2–3 mm pieces, and excess tissue was removed under a preparation microscope. Epineurium and perineurium were opened, and endoneurial tissue were transferred onto silanated glass slides. Endoneurial tissue was teased with fine needles to separate Schwann cell axon units. After air drying, the samples were postfixed and permeabilized in methyl alcohol at -20ºC for 20 min. Slides were blocked for 30 min with PBS containing 1% BSA and 0.1% Triton-X-100. Samples were treated with the same antibodies and protocol as the frozen sections.

4.1.2 Human osteoclast cultures (II)

The protocol of human osteoclast culture is described by Heervä and coworkers (Heervä et al., 2010). Blood samples were obtained from healthy volunteers. Mononuclear monocytes were isolated using Ficoll centrifugation. The fraction of white blood cells was collected from each sample and washed with phosphate-buffered saline. Isolated monocytes were differentiated into osteoclasts in medium containing alpha-MEM (Gibco, Grand Island, NY), 10% heat-inactivated fetal bovine serum (Gibco, Grand Island, NY penicillin-streptomycin, RANKL (20 ng/ml, Peprotech, Rocky Hill, NJ) and M-CSF (10 ng/ml, R&D systems, Minneapolis, MN).

4.1.3 Macrophage cultures (II)

Macrophage cultures were established as previously described with some modifications (Tedesco et al., 2015). The initial steps of the procedure mainly follow the protocol of osteoclast cultures. Monocytes were isolated to form blood samples, which were obtained from healthy volunteers. Monocytes were seeded to petri dishes and allowed to adhere for 2 hours. Non-adherent cells were rinsed away, and adherent cells were differentiated into macrophages for 7 days in medium containing alpha-MEM, 10% heat-inactivated fetal bovine serum, penicillin-streptomycin and M-CSF.

4.1.4 Keratinocyte cultures (II)

Keratinocyte cultures were established as previously published (Siljamäki et al., 2014). Briefly, skin samples were obtained from mammoplastic operations of healthy women. Keratinocyte differentiation was induced in the presence of a high (1.4 mM) Ca^{2+} concentration, and cell cultures were then used for indirect immunofluorescence labeling.

4.1.5 Generation of the Nf1Ocl mouse strain (III)

Generation of the Nf1Ocl mouse strain is based on the cross breeding of two previously published mouse models being $Nf1^{flox/flox}$ (Zhu et al., 2001) and TRAP-Cre mice (Dossa et al., 2010). Specific Nf1 gene inactivation is processed with the Cre-LoxP system. Inactivation of the Nf1 gene is based on excision of exons 31 and 32, when the TRACPCre promoter is active. The principle of Cre-mediated recombination is schematically illustrated in **Figure 11**. Briefly, exons 31 and 32 are flanked with LoxP sequences in $Nf1^{flox/flox}$ mice. The sequence of the Cre enzyme is incorporated into the vicinity of TRACP promoter in TRAP-Cre mice. The

TRACPCre promoter regulates the expression of the Cre enzyme. The Cre enzyme recognizes LoxP sequences and induces the recombination. Consequently, excision of exons 31 and 32 results in a functionally inactive Nf1 gene.

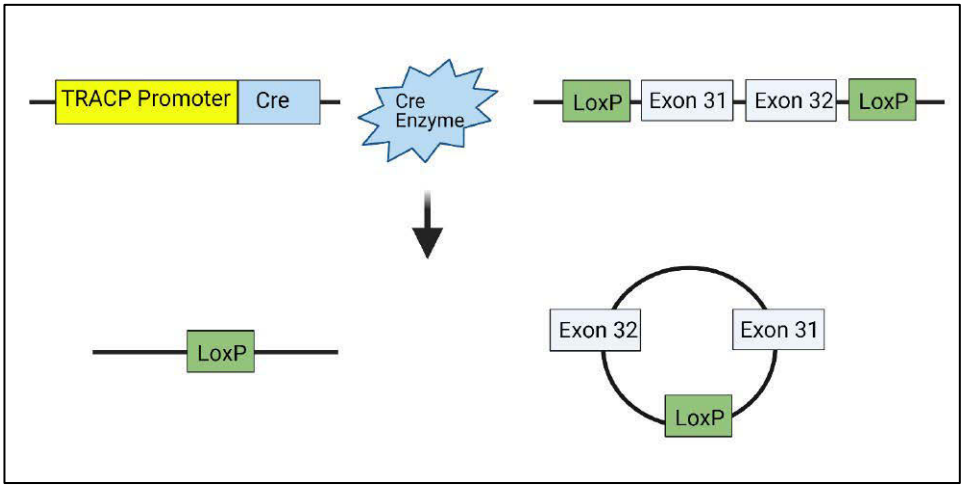

Figure 11. Schematic illustration of Cre-mediated recombination in Nf1 gene.

$Nf1^{flox/flox}$ mice were generated in the laboratory of Dr. Luis Parada (University of Texas Southwestern Medical Center) and the TRAP-Cre mouse strain has been generated by Dr Jolene Windle (Virginia Commonwealth University, Richmond, VA). $Nf1^{flox/flox}$ and TRAP-Cre were mated and produced the Nf1Ocl mouse strain. The Nf1Ocl mice were maintained in the modern animal housing facilities of the Central Animal Laboratory of the University of Turku under the guidelines of the University Ethics Committee.

4.1.6 Genotyping of Nf1Ocl mice and osteoclasts (II)

To genotype Nf1Ocl mice and osteoclasts, DNA was isolated from ear marks and osteoclast cultures (see below) with DNeasy® Blood & Tissue Kit (Qiagen, Hilden, Germany) by a protocol provided by the manufacturer. PCR for recognizing wild type, native and recombined Nf1flox alleles was carried out as previously described (Zhu et al. 2001). A primer pair P1–P4 detected the Nf1flox allele and LoxP produced a 350-bp band, a PCR with primer pair P1–P3 showed a band from the wt allele (480 bp) and a third primer pair P1–P2 detected completion of Cre-mediated recombination. The sequences for primers (5′ to 3′) were: P1, CTTCAGAC TGATTGTTGTACCTGA; P2, CATCTGCTGCTCTTAGAG GAACA; P3, ACCTCTCTAGCCTCAGGAATGA; P4, TGATT CCCACTTTGTGGTTCTAAG.

To genotype each bone cell type form in the bone tissue section, cells were isolated with laser microdissection to an adhesive cap of collection tubes. Collection tubes were vigorously vortexed and centrifuged to detach cell content from an adhesive cap. DNA was isolated by using QIAamp DNA FFPE Tissue Kit (Qiagen) according to the manufacturer. PCR was performed in two parts. DNA was pre-amplified using the P1–P2 primers, and pre-amplified DNA was treated as described for genomic DNA (see above).

4.1.7 Tissue samples from the Nf1Ocl mouse strain (III)

Mice were sacrificed at the age of 8 weeks. Body and spleen weights were measured. Tissue samples including liver, spleen, kidneys, heart, skeletal muscle, the central nervous system, reproductive organs, the digestive track, femur, tibia and the calvaria were collected and fixed with 10% formalin for 24–48 h. For the paraffin embedding, the tibias and femurs were decalcified with 10% EDTA incubation for 2 weeks. For μCT and three-point bending analysis, tibias were fixed with 10% formalin for 24–48% and stored in 70% ethanol.

4.1.8 Culturing of mouse osteoclasts (III)

Mouse osteoclast cultures were performed as previously described (Bradley and Oursler 2008). Cell cultures were established from spleens of homozygous $Nf1Ocl^{-/-}$ mice and control $Nf1Ocl^{+/+}$ mice. Cells were pressed out from spleen, and cell suspensions were seeded onto a petri dish. Mononuclear precursor cells were differentiated into mature osteoclasts in the presence of alpha-MEM (Gibco, Grand Island, NY), 10% heat-inactivated fetal bovine serum penicillin-streptomycin, RANKL (20 ng/ml, Peprotech, Rocky Hill, NJ) and M-CSF. Cultures were differentiated for 0, 2, 4, 7 or 10 days as previously described (Heervä et al., 2010).

4.1.9 Antibodies

Several commercial mono- and polyclonal preparations were used as primary antibodies. The antibodies, suppliers and product data are listed in **Table 1**. Information of the secondary antibodies, conjugated stains and nuclear stains used in this study can be found in **Table 2**.

Table 1. List of primary antibodies.

Antibody	Cat. no	Source	Used in
Rabbit Pab to human claudin-1	51-9000	Zymed Laboratories Inc, South San Francisco, CA	I
Rabbit Pab to human claudin-2	51-6100	Zymed Laboratories Inc, South San Francisco, CA	I
Rabbit Pab to humanclaudin-3	34-1700	Zymed Laboratories Inc, South San Francisco, CA	I
Rabbit Pab to human claudin-4	32-9400	Zymed Laboratories Inc, South San Francisco, CA	I
Rabbit Pab to human claudin-5	34-1600	Zymed Laboratories Inc, South San Francisco, CA	I
Rabbit Pab to human claudin-11	36-4500	Zymed Laboratories Inc, South San Francisco, CA	I
Rabbit Pab to human occludin	71-1500	Zymed Laboratories Inc, South San Francisco, CA	I
Rabbit Pab to cow S-100	18-0046	Zymed Laboratories Inc, South San Francisco, CA	I
Mouse Mab to human claudin-5	35-2500	Zymed Laboratories Inc, South San Francisco, CA	I
Mouse Mab to human type IV collagen	C1926	Sigma-Aldrich, St. Louis, MO	I
Mouse Mab to human E-cadherin	33-4000	Zymed Laboratories Inc, South San Francisco, CA	I
Mouse Mab to human ZO-1	33-9100	Zymed Laboratories Inc, South San Francisco, CA	I
Mouse Mab to human occludin	33-1500	Zymed Laboratories Inc, South San Francisco, CA	I
Mouse Mab to human pan Na1 channel	S8809	Sigma-Aldrich, St. Louis, MO	I
Mouse Mab to human Class III b-tubulin	MMS-435P	Nordic BioSite, Täby, Sweden	I
Rabbit Pab to human Phospho-p44/42 MAP Kinase(Thr202/Tyr204)	9101	Cell Signaling Technology, Beverly, MA	III
Mouse Mab to human p44/42 MAP Kinase	4696	Cell Signaling Technology, Beverly, MA	III
Rabbit Pab to human Phospho-AKT (ser473)	9271	Cell Signaling Technology, Beverly, MA	III
Rabbit pab to human pan-AKT(phosphoT308)	ab38449	Abcam, Cambridge, UK	III
Rabbit pab pan-AKT	ab8805	Abcam, Cambridge, UK	III
Rabbit pab to huma Akt1 (C-20)	sc-1618	Santa Cruz Biotechnology Inc, Santa Cruz, CA	III
Rabbit Mab to human c-Src	2109	Cell Signaling Technology, Beverly, MA	II
Mouse Mab to human Cortactin	55579	Santa Cruz Biotechnology Inc, Santa Cruz, CA	II
Rabbit Pab to human Arp2 antibody	ab47657	Abcam, Cambridge, UK	II
Mouse Mab to human cofilin	53934	Santa Cruz Biotechnology Inc, Santa Cruz, CA	II

Table 2. List of conjugated staining reagents, secondary antibodies and nuclear stains.

Antibody	Cat. no	Source	Used in
Alexa-Fluor 488-conjugated goat anti-mouse IgG	A11029	Molecular Probes, Eugene, OR	I
Alexa-Fluor 568-conjugated goat anti-mouse IgG	A11011	Molecular Probes, Eugene, OR	I, II
Alexa Fluor® 488 Phalloidin	A12379	Molecular Probes, Eugene, OR	I, II
ATTO 647-Phalloidin	65906	Sigma-Aldrich	II
DiI Stain: 1, 1'-Dioctadecyl-3, 3, 3', 3'-tetramethylindocarbocyanine perchlorate	D3911	Molecular Probes, Eugene, OR	II
Hoechst 33342	H3570	Molecular Probes, Eugene, OR	I, II, III
Phalloidin conjugation STAR635	2-0205-002	Abberior GmbH, Gottingen, Germany	II
Quant-iT™ PicoGreen® dsDNA Reagent	P7581	Molecular Probes, Eugene, OR	II
Rabbit Anti-Goat IgG, HRP-linked	P 0160	Dako, Glostrup, Denmark	III
Swine-Anti-Rabbit IgG, HRP-linked	P02170	Dako, Glostrup, Denmark	III

4.2 Methods

This thesis includes common and specific microscopy techniques, protein analyses and histological staining methods which are categorized according to publication**.** Microscopy equipment and softwares are listed in **Table 3.** Histological staining methods are listed in **Table 4** and protein analyses are seen in **Table 5**.

Table 3. Equipment used in cell and tissue imaging.

Microscope	Used in
Zeiss LSM 510 META confocal microscope equipped with argon-ion and helium-neon lasers (Zeiss; Jena, Germany) and LSM 3.0 software	I
Leica TCS SP5 STED microscope, equipped with MaiTai HP (Leica Microsystems GmbH, Mannheim, Germany and Spectra-Physics, US) and operated with LAS AF software (Leica Microsystems)	II
Olympus BX51TF Digital Virtual Microscope Olympus BX51TF Digital Virtual Microscope)	III
SkyScan 1072 microcomputer tomography reconstructed by NRecon 1.6.3.1 software, CTAn 1.9.3.0 and CTVol 2.1.1.0 softwares and DataViewer 1.4.2 software (Skyscan).	III
Zeiss AxioImager M1 microscope with AxioCam ICc3 cameran ane AxioVision Release 4.8 software	II-III
Zeiss P.A.L.M. laser microdissection	III

Table 4. Histological staining methods.

Method	Used in
Alizarin Red and Alcian Blue staining	III
Acid Phosphatase Leukocyte (Trap) staining	III
Hematoxylin and eosin (HE) staining	II-III
WGA-lectin staining	II-III

Table 5. Methods of protein analyses.

Method	Used in
Indirect immunofluoresence	I, II, III
Avidin-Biotin labeling	III
Western transfer analysis	III
Enzyme-linked immunosorbent assay (ELISA)	III

4.2.1 Confocal and STED microscopy (I, II)

Systematic confocal and STED imaging were used. Each sample was optically sectioned into multiple layers. The scanning process was extended to cover the entire subject including axial and lateral dimensions. Therefore, all the details of the sample were taken into account. Further, optically sectioned layers were processed to individual images or 3-dimensional reconstructions.

Imaging of all nervous tissue samples was carried out using a Zeiss LSM 510 META confocal microscope (**Table 3**). The objectives had a magnification of x40 (oil immersion, NA 1.3), x63 (oil immersion, NA 1.4) and x100 (oil immersion, NA1.4).

Sequential imaging of human osteoclasts was carried out with confocal mode and STED mode (**Table 3**). Phalloidin Atto647N or Star635 was excited by a 635 nm pulsed laser (LDH-P-C-640B, PicoQuant, Berlin, Germany), and fluorescence was collected with an avalanche photo diode detector at a 665–705 nm range.

For super-resolution STED imaging, Atto647N or Star635 was depleted at 760 nm. Images of cells stained with DiI were acquired with a water immersion objective lens (NA1.2 63x water, Leica) and the remainder was acquired with an oil immersion objective lens (NA1.4 100x oil, Leica). The confocal pinhole was set to one airy unit with a line-scan speed of 600 Hz with a line averaging of either 8 or 16. The pixel size (sampling) was set to 20 nm for STED imaging thus satisfying the Nyquist sampling requirement (Nyquist 1928).

4.2.2 Micro-computed tomography (III)

Structural details of bone architecture and bone content were evaluated with micro-computed tomography. Formaline-fixed tibias of Nf1Ocl$^{+/+}$, Nf1Ocl$^{+/-}$ Nf1Ocl$^{-/-}$ mice were scanned with a SkyScan 1072 (Skyscan, Aartselaar, Belgium) X-ray microtomograph with following settings: an X-ray tube of 72 kV and 138 µA, a pixel size of 5.32 µm, a 1.3 s exposure time, a 180° rotation in 0.45° rotation steps. Transmission X-ray images were recorded, and primary data were reconstructed by NRecon 1.6.3.1 software (Skyscan). Trabecular and cortical bone analysis and visualization and bone mineral density (BMD) analysis were carried out by CTAn 1.9.3.0 and CTVol 2.1.1.0 software (Skyscan) according to the manufacturer's guide. The thickness of growth plate was analyzed by DataViewer 1.4.2 software (Skyscan). Triplicate measurements were analyzed from the lateral, medial and central parts of the growth plate.

4.2.3 Laser microdissection (III)

Laser-capture microdissection was utilized in genotyping each bone cell type: osteoclasts, osteocytes and chondrocytes from the tissue section. Sections of tibia in Nf1Ocl$^{+/+}$ and Nf1Ocl$^{-/-}$ mice were processed with P.A.L.M. laser microdissection equipment (ZEISS, Jena, Germany). Each bone cell type was pooled from 10 histological sections on average. Briefly, paraffin-embedded sections of tibia were stained with Trap-kit according to the manufacturer. TRACP-positive osteoclasts, chondrocytes of the growth plate and diaphyseal osteocytes were identified with FLUAR 10x/0.50 objective and Zeiss Axiovert 200 microscopy. The region of interest was delineated from each tissue section using a PALM®Robo software. The catapulting pressure of the laser beam detached the cell content from the glass slide and lifted the cell content to an adhesive cap of a collection tube. DNA was isolated, and the concentration was analyzed with PicoGreen® to ensure sufficient DNA content. Genotyping was performed as described earlier.

4.2.4 Histomorphometric analysis of spleens and megakaryocytes (III)

Histological sections were imaged by an Olympus BX51TF Digital Virtual Microscope (Olympus, Tokyo, Japan), saved in .vsi file format, and analyzed by dotSlide software (Soft Imaging System GmbH, Münster, Germany). Four equal areas (1×106 µm^2) from each H&E-stained spleen sections were randomly selected for histomorphometric analysis with dotSlide software, and areas of white and red pulp were measured. The percentage of white pulp from the total tissue area was

calculated, and the number of megakaryocytes (MKs) and their total area were determined from the histological sections.

4.2.5 RNA analyses for claudin expression (I)

RNA was isolated from the sciatic nerves of 19- and 26-week-old fetuses and adult great auricular nerves. Nerve tissue samples were immediately submerged in RNAlater RNA Stabilization Reagent (76104; Qiagen, Valencia, CA). RNA was isolated using the RNeasy Mini Kit (74104; Qiagen) according to the protocol provided by the manufacturer. RNA was reverse transcribed into single-stranded cDNA and used as templates for PCR amplification. PCR reactions, to detect expression of claudins 1–11, and GAPDH, were performed using a MultiGene-12 RT-PCR profiling Kit (PH-083B; SuperArray Bioscience, Frederick, MD) according to the protocol provided by the manufacturer. PCR reactions for claudin-19 were performed as described (Lee et al. 2006) using claudin-19 primers (sense primer: 5′-AATTTGGCCCAGCCCTGTTCGTGG- 3′; anti-sense primer: 5′-GATTGGATGTGACCGTCCAGGGCG-3′). The PCR product size was 290 bp.

4.2.6 Bone resorption analyses (III)

Nf1Ocl$^{+/+}$ and Nf1Ocl$^{-/-}$ osteoclast cultures were performed as described earlier. For bone resorption assays and IIF, 1 million cells were plated to each bovine bone slice in 24-well plates. Five mice (n = 5) from each genotype were used, and five parallel cultures per mouse were established. Culture medium was collected on the 10th day, and concentrations of C-terminal telopeptides of type I collagen (CTX) were measured using a CrossLaps® for Culture (CTX-I) ELISA kit (Immunodiagnostic Systems Ltd., Boldon, Tyne and Wear, UK). Analysis was performed according to the manufacturer's protocol, and the results were correlated to the bone slice area. Resorption pits of the bone slice were visualized by wheat germ agglutinin (WGA)-lectin labeling as described previously (Heervä et al., 2010).

4.2.7 Three-point bending assay (III)

A three-point bending assay was carried out as previously described (Peng et al., 1994). Tibial bones were compressed at a constant rate of 0.155 mm/s until breakdown. Mechanical parameters, such as ultimate strength with a maximal load in N, and energy absorbed by the bone tissue representing structural toughness were analyzed using RatBone analyzer v1.2 software (Timo Rautiala, Oulu, Finland).

5 Results

5.1 Tight junctions in peripheral nerves

5.1.1 Tight junctions in human adult nerves (I)

To analyze the localization of autotypic tight junction expression patterns in human adult peripheral nerves, indirect immunolabeling was performed, and the nerves were analyzed using confocal microscopy. To assist in the localization of autotypic tight junction proteins, which seal adjacent membrane lamellae of the same cell, Schwann cell-specific structures such as nodal and paranodal regions, Schmidt-Lanterman incisures and the inner- and outer mesaxon, were first visualized in teased nerve fibers. Frozen sections of peripheral nerves were labeled with antibodies for type IV collagen, E-cadherin and Na^+ channels. A schematic illustration of Schwann cell summarizes these endoneurial structures in **Figure 12**. The results showed that the transmembrane protein, claudin-1, was the most prominent tight junction protein when analyzed with indirect immunofluorescence at the protein level and RT-PCR at the RNA level. Claudin-1 was localized to the paranodal area, to the Schmidt-Lanterman incisures and to mesaxons. Claudin-1 was co-localized with adherens junction protein E-cadherin in Schmidt-Lanterman incisures and outer mesaxons. In addition, claudin-1 co-localized with the intracellular tight junction protein ZO-1 in paranodal regions and partially co-localized in the inner mesaxon. At the RNA level, RT-PCR analysis showed robust claudin-1 expression in the human adult auricular nerve.

Claudin-2 was detected in the Schmidt-Lanterman incisures and in the paranodal areas thus co-localizing with E-cadherin. Claudin-2 expression was also seen in the inner mesaxon, while E-cadherin could not be detected in the inner mesaxon. Even though the expression pattern of claudin-2 was mainly similar to claudin-1, claudin-2 expression was sparser in the outer mesaxon. Claudin-3 expression was recognized in the Schmidt-Lanterman incisures and outer mesaxons. Claudin-5 was occasionally expressed in only the Schmidt-Lanterman incisures. Expression of claudin-4 and claudin-11 was not detected by indirect immunofluorescence.

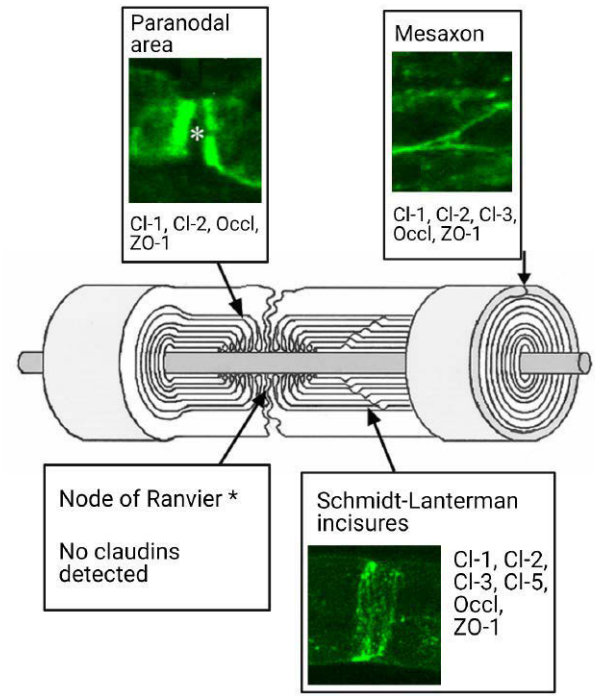

Figure 12. Schematic illustration and actual fluorescent labeling pattern of subcellular structures in myelinated Schwann cell such as paranodal area, mesaxons, Schmidt-Lanterman incisures and node of Ranvier. The expression of tight junction proteins and adherens junction proteins in human peripheral nerve is localized to each subcellular structure.

Localization of the transmembrane protein occludin was also characterized. Occludin expression was mapped to Schmidt-Lanterman incisures and the outer mesaxons, but the expression pattern was weak, punctate and sparse. Occludin also co-localized with claudin-2. None of the tight junction proteins analyzed could be mapped to the nodal region. The expression pattern of tight junction and adherens junction proteins is summarized in **Figure 12**.

Claudin expression was analyzed at the RNA level using RT-PCR. The results showed that mRNAs of claudins 1–4, 6–9, and 11 were expressed. However, expression of claudin-5 and claudin-10 mRNA were not observed. mRNA expression of claudin-19 could not be detected in samples of adult great auricular nerve and fetal sciatic nerves at 19 and 26 weeks of gestation.

5.1.2 Tight junctions in developing nerves (I)

The claudin expression pattern was characterized from a developmental aspect with confocal microscopy. Frozen sections of fetal sciatic nerves at 23 and 37 weeks of gestation were labeled for claudin-1, claudin-3, ZO-1 and occludin. The results

showed, in general, a linear punctate labeling pattern of all tight junction proteins at 23 and 37 weeks of gestation indicating mesaxonal localization. The claudin-1 labeling pattern was punctate at 23 weeks of gestation. In addition to a linear labeling pattern, occasionally claudin-1 was orientated in a circular shape suggesting localization in Schmidt-Lanterman incisures. Later at 37 weeks of gestation, the structure of the fetal sciatic nerve still remained somewhat immature. The result showed that claudin-1, claudin-3, occludin and ZO-1 featured a punctate labeling pattern. Certain structural details such as the inner- and outer mesaxons could not be distinguished from each other while Schmidt-Lanterman incisures, mesaxons and paranodal regions were distinguishable at this time point, although the labeling pattern of tight junction proteins was punctate.

5.2 The Nf1Ocl mouse strain

5.2.1 Creating a conditional knockout Nf1Ocl mouse strain (II)

The principles of a conditional knockout Nf1 mouse model are described in the Material and Methods on page 49. The $Nf1^{flox/flox}$ and Trap-Cre mice were mated to generate a new Nf1Ocl mouse strain. Mating yielded a Nf1Ocl mouse strain, where the Nf1 gene is inactivated in osteoclasts and precursors, while other cells contain a normally functional Nf1 gene. $Nf1Ocl^{+/+}$, $Nf1Ocl^{+/-}$ and $Nf1Ocl^{-/-}$ mice were apparently healthy by displaying a normal body and behavior. Body weight and stature were also normal in all mice. The skeleton was evaluated at the macroscopic level. Alizarin red/alcian blue staining did not show any macroscopic abnormalities in the skeleton or in cartilage. However, the spleen was obviously enlarged in $Nf1Ocl^{-/-}$ mice. Spleen weight of $Nf1Ocl^{-/-}$ mice was actually twofold compared to control mice or heterozygous $Nf1Ocl^{+/-}$ mice. Other macroscopic or microscopic abnormalities were not observed in internal organs such as the liver, the kidney, the heart, skeletal muscle, the central nervous system, bone marrow, reproductive organs and the digestive track.

5.2.2 Genotyping Nf1 gene inactivation in mouse bone (II)

To analyze inactivation of Nf1 gene in bone, TRACP-positive osteoclasts, osteocytes and chondrocytes were collected from formalin-fixed, paraffin-embedded bone tissue samples with laser-capture microdissection. Implementation of laser-capture microdissection was crucial in detection of the Nf1 gene inactivation directly from bone tissue in a cell-specific manner. The recombined DNA sequence was recognized by PCR as described earlier (Zhu et al., 2001). The 280-bp PCR product was detected only in osteoclast samples, which indicates inactivation of Nf1 gene. The 350-bp PCR product, which recognizes the intact Nf1 flox allele, was observed in osteoclast, osteocyte and

chondrocyte samples. The results clearly confirmed that the Nf1 gene was inactive specifically in osteoclasts *in vivo*. The results also demonstrated that the activity of the TRACP promoter is sufficient to induce the conditional Nf1 gene inactivation in a cell-specific manner as expected. Inactivation of the Nf1 gene was also confirmed from $Nf1Ocl^{+/-}$ and $Nf1Ocl^{-/-}$ spleen-derived cell cultures and from ear mark samples.

5.2.3 Alterations in Ras and PI3K signaling pathways in bone and cultured osteoclasts (II)

A NF1 gene mutation is related to accelerated activity of the Ras signaling pathway in osteoclasts (Yang et al., 2006). Phosphorylated p44/42 mitogen-activate protein kinase (MAPK) indicates accelerated activity in the Ras signaling pathway. Ras activity was analyzed by immunolabeling the bone tissue *in vivo* and differentiating osteoclast cultures *in vitro*. Tibial bone sections of $Nf1Ocl^{+/-}$ and $Nf1Ocl^{-/-}$ mice showed a positive immunoreaction for phosphorylated p44/42, which was localized to osteoclasts. The immunolabeling pattern for phosphorylated p44/42 is seen later in **Figure 14**. As expected, tibial bone sections of control mice remained negative.

Activity of Ras signaling pathway in differentiating osteoclasts was evaluated by western transfer analysis. Since the spleen is a reservoir of monocytes, spleen cell suspensions of $Nf1Ocl^{+/+}$ and $Nf1Ocl^{-/-}$ mice were differentiated to multinuclear osteoclasts, and cell cultures were analyzed on days 0, 2 and 4. The results showed that phosphorylated p44/42 was detected in osteoclast cell cultures isolated from $Nf1Ocl^{+/+}$ and $Nf1Ocl^{-/-}$ mice. However, the analysis revealed that Nf1-deficient ($Nf1Ocl^{-/-}$) osteoclast cultures displayed a twofold increase in Ras activity in general. Specifically, on day 4, Ras signaling pathway was markedly accelerated in $Nf1Ocl^{-/-}$ osteoclast cultures. The results suggest that deficiency of neurofibromin predisposes to the hyperactivation of Ras signaling pathway during the osteoclast differentiation.

Additionally, the role of neurofibromin in PI3K signaling pathway was evaluated with western transfer analysis. Akt, a downstream target of PI3K, accelerates PI3K signaling pathway in its phosphorylated state. The results showed that increased levels of phosphorylated Akt were detected in $Nf1Ocl^{-/-}$ osteoclasts. However, the expression prolife of phosphorylated Akt followed different timetables in different sample sets, and the results were not conclusive even though the experiments were carried out with two Akt and two p-Akt antibodies. To summarize, neurofibromin is involved in regulation of Ras signaling pathway in osteoclasts. Even haploinsufficient expression of neurofibromin predisposes to hyperactivation of Ras signaling. Neurofibromin may also have an influence on the PI3K signaling pathway.

5.2.4 Morphometric analysis of tibial bones of Nf1 knockout mice (II)

Sequential µCT was carried out to study structural details of tibial bone. Additional post-processing of raw data yielded parameters according to Parfitt's nomenclature (Parfitt et al., 1987). Tibial bones of Nf1Ocl$^{+/+}$, Nf1Ocl$^{+/-}$ and Nf1Ocl$^{-/-}$ mice were analyzed. Cortical and trabecular bone (**Figure 13**) were characterized separately. In general, alterations were slight but significant. Diaphyseal bone of tibia was used to cortical bone analysis. The results showed that the tissue volume and cross-sectional area of cortical bone and bone marrow cavity were smaller in Nf1Ocl$^{-/-}$ mice. These results were similar despite the gender. However, the bone volume was equal in each group. In fact, the relative content of cortical bone was increased in Nf1Ocl$^{-/-}$ mice compared to Nf1Ocl$^{+/+}$ mice. The thickness of cortical bone was evaluated from the anterior, lateral, medial and posterior parts. The results confirmed that thickness of cortical bone was equally distributed in the diaphyseal bone.

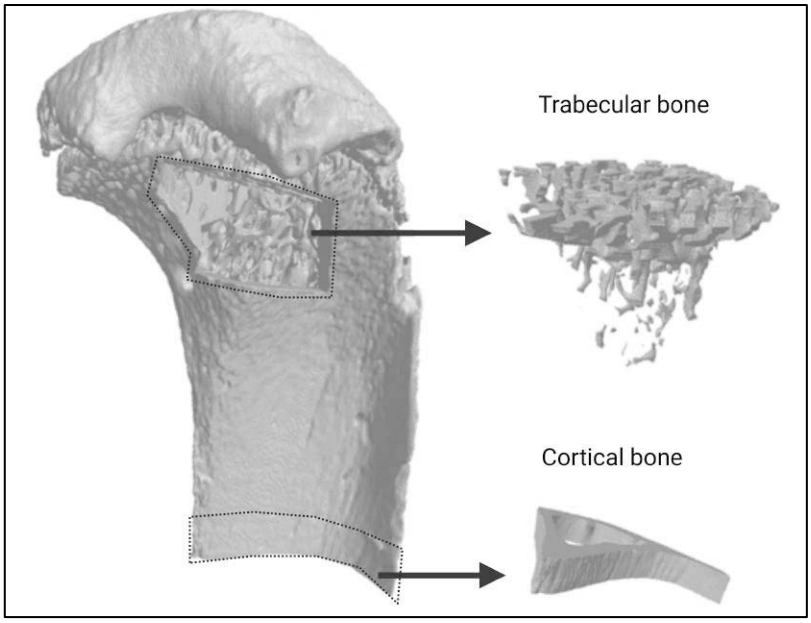

Figure 13. 3D reconstructed µCT image of tibial bone shows trabecular and cortical bone compartments which were included in the analysis.

The proximal metaphysis of tibia contains trabecular bone, which was analyzed similarly to cortical bone. Morphometric analysis showed that bone volume was smaller, and a smaller number of trabecles was detected in Nf1Ocl$^{-/-}$ mice. Bone characteristics in heterozygous Nf1Ocl$^{+/-}$ mice appeared to be of an intermediate

phenotype compared to that seen in Nf1Ocl$^{-/-}$ and Nf1Ocl$^{+/+}$ mice. In addition, statistical analysis revealed that the standard deviation particularly in heterozygous Nf1Ocl$^{-/-}$ females was variable. To conclude, the results of morphometric data suggested that tibial bones of knockout mice were smaller compared to control mice, although the results were not statistically significant.

Bone mineral density was evaluated from morphometric data. Equal bone mineral density was detected in trabecular and cortical bone in Nf1Ocl$^{+/+}$, Nf1Ocl$^{+/-}$ and Nf1Ocl$^{-/-}$ mice. In addition, three-point bending analysis did not show any abnormalities in mechanical strength in Nf1Ocl$^{+/-}$ and Nf1Ocl$^{-/-}$ mice compared to Nf1Ocl$^{+/+}$ mice. The results of bone mineral density and mechanical properties suggest that Nf1Ocl mice do not represent a fragile or osteoporotic bone phenotype.

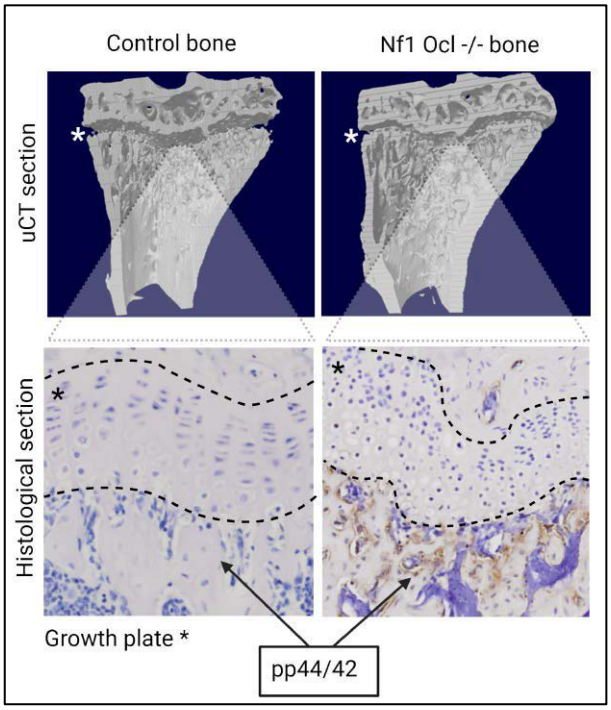

Figure 14. Conditional Nf1 gene inactivation in osteoclasts predispose alterations in bone: narrower growth plate, disorganized chondrocyte columns, and hyperactivation of Ras signaling pathway beneath the growth plate.

During the post-processing of the morphometric data, the morphology of the growth plate seemed to be variable. Thus, the thickness of growth plate was measured from three distinct points in reconstructed images. The growth plate was approximately 20% more narrow in Nf1Ocl$^{-/-}$ mice compared to control mice. In addition, histological alterations were seen particularly in the proliferative zone, where

chondrocytes in columns were disorganized. These alterations in growth plate are summarized in **Figure 14**. To conclude, in the morphometric analysis of cortical and trabecular bone, Nf1-deficient mice featured minor alterations in their bone volume and their growth plates.

5.2.5 Histomorphometric analysis of spleen (II)

Since Nf1Ocl$^{-/-}$ mice displayed an enlarged spleen, histological analysis was evaluated carefully. In general, the histology of enlarged spleens was apparently normal. The ratios of red and white pulp remained equal. White pulp covered 40.6% of the total area in spleens of knockout mice, and 42% of the total area in spleens of control mice. The number of megakaryocytes was calculated from histological sections of spleen. Enlarged spleens of Nf1Ocl$^{-/-}$ mice featured significantly increased number of megakaryocytes (8.5 MKs/mm^2) compared to control spleens (3.2 MKs/mm^2, $P < 0.001$). However, no evidence of increased myeloid cell proliferation was detected.

5.2.6 Differentiation of Nf1-deficient osteoclasts (II)

Features of osteoclasts, such as differentiation capacity, morphology of the cytoskeleton and the ability to resorb bone were further studied. Spleen-derived osteoclast cultures from Nf1Ocl$^{+/+}$ and Nf1Ocl$^{-/-}$ mice were established. Cells were seeded on the bovine bone slice, and cultures were differentiated to osteoclasts for 10 days. Cells containing more than three nuclei were considered as mature osteoclasts in these experiments. Equal numbers of osteoclasts differentiated to mature osteoclasts in Nf1$^{-/-}$ and Nf1$^{+/+}$ genotypes (ratio 1:1002, $P = 0.908$). Osteoclasts were labeled with phalloidin to evaluate the morphology of the actin cytoskeleton. Imaging was performed with wide-field fluorescent microscopy. Morphological alterations such as disorganized actin ring formation and variable cell size and irregular cell shape were distinguished in Nf1-deficient osteoclasts. Occasionally Nf1$^{-/-}$ osteoclasts contained several small actin rings.

5.2.7 Bone resorption capacity of Nf1-deficient mouse osteoclasts (II)

Bone resorption capacity was evaluated by measuring the concentration of the C-terminal telopeptide of type I collagen (CTX) from culture medium and visualizing the resorption pits in bovine bone slices with WGA-lectin staining method. Approximately a 30% higher secreted CTX concentration (0.096 ± 0.006 nM/mm^2 vs. 0.065 ± 0.007 nM/mm^2, $P < 0.002$) was detected in medium collected from

Nf1Ocl$^{-/-}$ cultures compared to control cells. In addition, bone resorption pits in bovine bone slice appeared larger in size and featured an irregular shape in Nf1Ocl$^{-/-}$ cultures compared to bovine bone slices in Nf1Ocl$^{+/+}$ and Nf1Ocl$^{-/-}$ osteoclast cultures. To summarize these results, Nf1-deficient osteoclasts displayed an abnormal actin cytoskeleton in addition to showing increased bone resorption capacity.

5.3 Cultured human osteoclasts

5.3.1 Bending and branching of actin (III)

The actin cytoskeleton of cultured human osteoclasts was investigated using STED super-resolution microscopy. Briefly, mononuclear monocytes were isolated from human blood samples and differentiated into osteoclasts. Actin was visualized with phalloidin labeling, and nuclei were stained with Hoechst nuclear stain. The actin ring and podosome belt are typical characteristics of osteoclasts, which are located in the basal side of cell. Therefore, systematic imaging was extended to cover the whole cell. The results revealed that the actin cytoskeleton featured unexpected morphology in osteoclasts. Curved and branched actin filaments fulfilled the intracellular space from the basal side of the cell to the top of the cell (**Figure 15**). At the basal side of the cells, actin displayed a common morphology, which was easily recognizable in scattered actin-rich adhesion complexes such as podosomes or podosome belts. Immediately above the podosomes, characteristics of actin changed into curved and branching filaments. Specifically, systematic imaging of each and all optical sections revealed that curved and branched actin filaments had loosely enclosed nuclei. Furthermore, the cell membrane was visualized with a DiI membrane stain solution to evaluate colocalization of membrane ruffles and curved actin. The results showed that the cell membrane was intimately in contact with curved actin filaments and cell membrane delineated actin containing structures in subcellular localization. Occasionally, actin filaments were accumulated in the vicinity of cell membrane. Curved actin filaments were observed also in human macrophages and keratinocytes. Thus, bending actin is not a specific feature of osteoclasts of multinucleated cells as such.

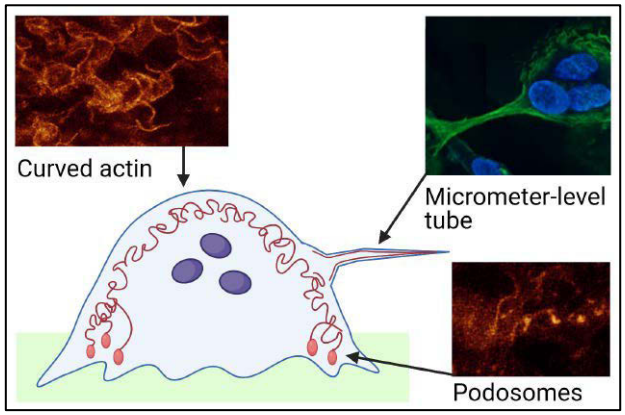

Figure 15. Scematic illustration of osteoclast. STED microscopy revealed actin filaments being curved and branched in intracellular space whereas cell protrusion, MLT, contained straight actin filaments.

5.3.2 Micrometer-level tubes associate closely to nuclei (III)

Systematic imaging with super-resolution microscopy revealed that osteoclasts displayed cell protrusions, which are named as the micrometer-level tube (MLT). MLTs were located between two osteoclasts as bridge-like structures significantly above the cell culture substratum. MLTs contained straight actin filaments which extended up to 40 µm, and diameter varied 1-5 µm. 3D-reconstructed images demonstrated more details of the morphology and location of MLTs. The membrane staining showed that MLTs were covered by a cell membrane, and that the cell membrane continued seamlessly between two cells. Actin filaments of MLT seemed to integrate into both osteoclasts. Main findings of MLT are summarized in **Figure 15.** Actually, labeling for actin or cell membranes could not to distinguish MLT and adjacent osteoclasts as separate individual structures. One crucial finding was that the nuclei of osteoclasts located in the vicinity of protrusive MLTs. Curved actin filaments surrounded nuclei and continued as straight actin filaments in the MLT. The results also showed that occasionally a single nucleus was located inside of MLT. Nuclei located in MLTs showed elongated morphology while the intracellular nuclei were rounded. These findings suggest that nuclei were transferred from one osteoclast to another via MLTs.

5.3.3 Arp2/3, cofilin, cortactin and c-Src expression pattern in osteoclasts (III)

Osteoclasts were labeled for Arp2/3, cofilin, cortactin and c-Src in order to evaluate the dynamics of actin. The results showed that Arp2/3 was expressed abundantly on the basal side of osteoclasts. A punctate labelling pattern of Arp2/3 was localized to

the branching site of actin as expected. Cofilin was accumulated in the middle part of osteoclasts near nuclei and did not co-localize with actin. Cortactin was also detected near nuclei. In addition, cortactin was occasionally co-localized in the vicinity of podosomes at the cell periphery. Labeling for c-Src was partially co-localized with curved actin filaments in the cell periphery and around the nuclei. The results showed evidence of active actin dynamics in osteoclasts.

6 Discussion

6.1 Developmental aspects of bioimaging

The ultimate goal and a dream of scientists developing and using bioimaging techniques would be to reach the point where whole-body imaging in single cell resolution is available (Susaki & Ueda, 2016). This type of imaging would help to unravel pathological mechanisms behind diseases and develop new and effective treatments.

Genetically modified mouse models have been a powerful and widely used tool in modeling diseases during the past 20–30 years, but the determining of the phenotypic consequences of gene modifications have been laborious. It is also possible that phenotypic data has been missed due to incomplete analyses. Whole-body imaging on single cell level would allow, for example, studying the whole transgenic animal and various tissues or tumor cells in their natural environment without time-consuming processes of histological staining. Imaging techniques used in the present study have aimed at a careful analysis of the mouse phenotype by combining information from various methods. For example, combining data of μCT images of mouse bones with histology, and combining protein and genotype analyses of selected cell types by utilizing laser-capture microdissection revealed the slight phenotypic differences of knockout mice in Study II.

Imaging at the nanoscale level has advanced bioimaging during the recent years. The laser-scanning microscope technique enables for the detection of more than one research objects simultaneously and can localize the target more accurately than fluorescence microscopy. When the first Study (I) of this thesis was carried out, confocal laser scanning microscopy had become widely available, and the technique was up to date. However, STED microscope would have been a much more powerful tool in the analyses of Schwann cell junctions but was not yet in routine use during those experiments. Luckily, STED microscope was available for the third Study (III) of this thesis and revealed previously unforeseen views of actin structures in cultured cells. With STED resolution, the previously fuzzy image of the actin “cloud” sharpened to filaments of bending and branching actin. Findings from these the new techniques may create a need for a new nomenclature of these structures.

Nowadays, a modern technology for imaging of several fluorescent labels simultaneously would probably be multiphoton microscopy. Live multiphoton microscopy would be the most up-to-date method for studying transgenic animals. Live multiphoton microscopy without need for labeling will probably be the next step in obtaining real-time molecular level information from single cells in live tissues.

6.2 Imaging challenges and some solutions in studying human peripheral nerves

The structure of peripheral nerve is challenging to study for three main reasons. First, the availability of fresh tissue samples that is very limited because human beings have few peripheral nerves which can even be biopsied for diagnostic purposes without causing functional damage. The great auricular nerve is a superficial branch of the cervical plexus and innervates parts of the skin in cheek, earlobes, and scalp behind the ear. This nerve must be sacrificed sometimes during operations for squamous cell cancer, which has metastasized into the parotic gland. The nerve excision causes little functional damage for the patient. Collection of the nerves from the cancer operations provided a unique opportunity to obtain fresh nerve tissue for the study. Developing nerves used in the study had been collected for the previous studies (Jaakkola et al., 1993; Pummi et al., 2004). The second challenge in studying peripheral nerves is the structure of the tissue. Preparation of the peripheral nerve for histology is easiest by cutting cross-sections. However, cross-sections of nerves provide a very limited view of longitudinal structures such as axons and Schwann cells. Cutting the tissue longitudinally is possible, but the Schwann cell axon units are embedded in the collagenous extracellular matrix of endoneurium and thus does not reveal long stretches of Schwann cells. Teasing is a technique in which the axon-Schwann cell units are separated from the endoneurial connective tissue material using thin needles. This technique used on fresh nerves provided an opportunity to image Schwann cells and their autotypic junctions in unforeseen detail. The third challenge in imaging through immunofluorescence labeling of Schwann cells is the absence of simple background staining. The commonly used nuclear stains do not serve as good landmarks for longitudinally stretched Schwann cells, or axons which do not have nuclei in peripheral nerve. Instead, antibodies for Na^+ channel were used to localize nodes of Ranvier, S-100 was chosen for Schwann cells, axons could be visualized using class III tubulin and antibodies for type IV collagen were used to delineate the basement membranes of Schwann cells.

It was somewhat surprising to find tight junction components only in autotypic junctions of Schwann cells, such as areas which the seal of the cell membrane contacts various layers of one myelin-forming cell, while adjacent Schwann cells did

not show junctional components in internodal areas. Autotypic tight junctions were demonstrated in areas of non-compact myelin being paranodal regions, mesaxons and Schmidt-Lanterman incisures. The protein composition of these areas showed slight differences. The junctions of paranodal regions contained E-cadherin, claudin-1, claudin-2 and ZO-1, while mesaxons additionally revealed that claudin-3 and Schmidt-Lanterman incisures also expressed claudin-5. Labeling for occludin was only present in mesaxons and was punctate. Mapping the junctions to developing nerves showed punctate labeling for claudin-1, claudin-3, ZO-1 and occludin, which corresponds to the immature myelin sheaths. It can be speculated that the formation of Schwann cell takes place simultaneously with myelination. The molecular composition of human autotypic junctions showed some differences compared to mice (Poliak et al., 2002), which again emphasizes the need for human studies prior to drawing general conclusions based on mouse models.

Although this study resulted in the knowledge of tight junction components present in Schwann cell autotypic junctions, the structure of the junctions and existing claudin combinations in junctions are not known. The selection of tight junction components in Schwann cells differ from those in epithelial tight junctions in which occludin is a crucial sealing protein. In fact, we do not know the exact function of these junctions in Schwann cells either. It can, however, be speculated that the autotypic junctions of Schwann cells differ from epithelial tight junctions, in their structure, and perhaps for their function because of the different requirements for diffusion barriers in peripheral nerve and epithelia, and because the autotypic junctions are located between the cell membranes of the same cell when Schwann cells wrap around axons.

It should also be noted that the expression of claudin-2, -3 and -5 differs between murine and human nerves (Poliak et al., 2002). Thus, conclusions of Schwann cell autotypic junctions cannot be drawn solely based on murine studies.

This study adds to the basic knowledge of the structure of peripheral nerves. The results have been cited in studies concerning, for example, the blood-nerve barrier, nerve damage and neuropathies.

6.3 Lessons learned in characterizing the Nf Ocl mouse model

Osteopenia and osteoporosis are common in adult patients with NF1 (Elefteriou et al., 2009; Heervä et al., 2010; Kuorilehto et al., 2005). In the current study, a conditional knockout mouse strain, Nf1Ocl, was generated to model osteoclast abnormalities seen in NF1 patients and to study the role of the neurofibromin-deficient osteoclasts in bone dynamics. A conditional knockout was generated using the TRACP promoter, which has previously been used in mouse models generated

to study osteoclasts (Dossa et al., 2010). The results showed that Nf1 inactivation was successfully targeted to osteoclasts. Specifically, a targeted analysis at the cellular level was carried out using LCM. After TRACP staining of osteoclasts, chondrocytes and diaphyseal osteocytes were microdissected using laser microdissection equipment. Samples of each cell type were pooled, and DNA analysis showed that the Nf1 gene is inactivated only in osteoclasts, while the other bone cell types remained wild type. Without this imaging application, it would not have been possible to ensure that the Nf1 knockout was successfully targeted to osteoclasts. Another possible method to study knockout effects in different cell types separately would have been to isolate cells from mouse bones and to differentiate them in culture. However, setting up pure cultures and using various growth factors in differentiation would not have been straightforward either and would potentially introduce other potential errors.

Contrary to our hypothesis, the Nf1Ocl mouse strain did not reveal apparent osteoporotic bone phenotype. The bones were macroscopically normal in size and shape and did not show abnormal fragility. Several reasons may explain the outcome. First, the mechanical load of mouse bones differs from human because of their different postures. Second, osteoporosis in individuals with NF1 takes place in tissues with a $NF1^{+/-}$ background, and all cells are haploinsufficient for NF1, while in the mouse model, the surrounding tissues had a $Nf1^{+/+}$ genotype. Third, various environmental and physiologic factors such as hormones play a role in osteoporosis, which cannot be taken into account in a mouse study. Several mouse models have been created to model bone alterations in NF1, and modeling the NF1-driven osteoporosis has proven to be challenging also in other studies (Kühnisch et al., 2014). It is apparent that the timing of the knockout during the differentiation of osteoclasts may be important in the phenotype, and the earlier timing may yield more apparent changes (Rhodes et al., 2015).

6.4 Imaging in the characterization of Nf1 genotype of bone cell types

Because the results did not show evidence of an altered phenotype, more modern imaging methods were applied to study the bones in more detail. Micro-computed tomography (μCT) provides three-dimensional data and has in part replaced older laborious histomorphometric methods, in which various measurements are carried out on histologic sections. And if needed, the tissue is still available for histology. Analysis of bones by μCT detected slight abnormalities in bone that would not have been evident without this technique. μCT revealed that the tibial bone marrow cavity, trabecular tissue volume and the perimeter of cortical bone were smaller in Nf1Ocl mice compared to control mice. Nf1 mice also demonstrated another unexpected

finding with their growth plate of long bones narrowed, and chondrocytes displayed abnormal morphology and seemed disorganized in Nf1Ocl mice.

The most apparent findings in the Nf1Ocl mouse strain were detected at the cellular level. Microscopic analysis of phalloidin fluorescence showed that actin structures were disorganized in neurofibromin-deficient osteoclasts. These results were similar to the $Nf1^{+/-}$ mouse models, where one NF1 gene is inactivated in osteoclasts, or the inactivation is programmed to an early phase of osteoclastogenesis (LysMCre;Nf1flox/+) or after completion of osteoclastogenesis (CtskCre ;Nf1flox/+) (Jacks et al., 1994; Rhodes et al., 2015; Yang et al., 2006). All the results together suggest that neurofibromin is necessary in proper osteoclastogenesis and bone homeostasis.

6.5 Correlation of the results of the mouse model with findings in NF1

The results of clinical and translational studies carried out during and after the initiation of the present study emphasize that the abnormalities in bone resorption caused by NF1 mutations is a clinically relevant study object. The skeletal phenotype of NF1 includes a variety of bone abnormalities including pseudarthrosis scoliosis and osteopenia, which tends to develop into osteoporosis (Heervä et al., 2014). Osteoporosis or osteopenia can be diagnosed at a rather young age and also in men with NF1 (Kuorilehto et al., 2005). Besides, increased risk for bone fractures and delayed bone healing has been recognized in NF1 patients (Heervä et al., 2012). These findings can be explained by the effects of NF1 in Ras signaling. Increased Ras signaling, abnormal cell differentiation and increased bone resorption capacity *in vitro* have been reported in osteoclasts cultured from NF1 patients (Heervä et al., 2010). In the present study, neurofibromin-deficient mouse osteoclasts also displayed enhanced bone resorption capacity and a hyperactivated Ras-signaling pathway *in vitro*.

A recent report demonstrated that, in addition to the Ras/MEK/Erk signaling pathway, human osteoclastogenesis is regulated by multiple interacting signaling pathways including also PI3K and mTOR. The results of the study by Pennanen et al. also emphasize the differences between human and murine osteoclasts with respect to the regulation of differentiation. Inhibition of MEK, PI3K and mTOR reduced markedly the number of NF1-deficient osteoclasts, but no effect was observed in control samples (Pennanen et al., 2021).

In normal bone, chondrocytes are aligned to columns in the growth plate, while in Nf1 knockout mice, chondrocytes in the growth plate were disorganized. However, Nf1 gene was confirmed to represent the wild type, and contrary to $Nf1^{-/-}$ osteoclasts, Ras signaling pathway was not hyperactivated. While cell-cell

communication between the osteoblast and osteoclast has been studied to some extent, the cell-cell communication between osteoclasts and chondrocytes remains unknown. The findings may suggest that osteoclast-chondrocyte, cell-to-cell communication may exist and contribute to the regulation of bone homeostasis. The slight abnormalities in the growth plate seen in Nf1Ocl mice may suggest one plausible pathoethiology explaining why NF1 patients are shorter than the general population. Another Rasopathy, namely Noonan syndrome, is also related to short stature (Hauer et al., 2018).

One of the unexpected findings in Nf1Ocl mice was splenomegaly. Histological analysis revealed that spleen contained a remarkable amount of megacaryocytes, which arise from a hematopoietic cell lineage. Juvenile myelomonocytic leukemia JMML is very rare form of leukemia characterized by an overproduction of immature monocytic and granulocytic cells that infiltrate various organs, including the spleen, the liver, the lung, the skin, and those in the gastrointestinal tract. JMML is rarely associated with NF1 in children (Niemeyer, 2018; Wang, Wei-Hao et al., 2021). A case report has been published, where chronic myeloid leukemia and splenomegaly were diagnosed in an adult NF1 patient (Gulhane & Kotwal, 2015). In addition, thrombocytosis has also been described in a patient with NF1 (Hasle et al., 1997). In general, a myeloidcell lineage-related abnormalities are not common features of the NF1 disease itself (Uusitalo et al., 2016). In the Nf1Ocl mouse model, both alleles of the Nf1 gene were inactivated, whereas other cell types remained as a healthy genotype. This may suggest that a sporadic and second inactivation of NF1 gene could promote abnormal behavior in a myeloid cell lineage, which may predispose to splenomegaly and myeloid cell lineage malignancies.

6.6 Novel insights into the actin cytoskeleton

Our understanding of cultured osteoclasts and the nomenclature of the cell structures are based on imaging studies using fluorescence microscopy and confocal laser scanning microscopy. During differentiation, the cell-matrix contacts of osteoclasts, the podosomes, are organized into a belt which is surrounded by a loose actin “cloud” at the cell periphery (Saltel et al., 2008). Comprehensive super-resolution imaging of cultured osteoclasts revealed new aspects of the cell structure. The actin “cloud” was in fact composed of curved actin filaments. Systematic whole-cell imaging from the basal aspect of the cells to the top visualized an extensive cone-like arrangement of curved actin, which constantly embedded the nuclei. Based on these findings, it could be speculated that the actin structure was called a “cloud,” because the resolution of conventional fluorescence microscopy or even laser-scanning microscopy could only reveal dizzy fluorescence instead of separate actin filaments.

Actin filaments themselves have been considered to be straight or in globular form. Most of the studies on actin structure have been carried out *in vitro* on purified actin filaments. These circumstances thus lack the natural intracellular environment. Actin is involved with various cellular functions such as cell migration, vesicle trafficking and cytokinesis, which are highly dynamic processes. The curved form of actin has been connected to properties such as restoring energy. Our results using a super-resolution microscope clearly showed that the actin filaments in osteoclasts are bending and branching. Similar bending actin filaments were also present in macrophages and keratinocytes that demonstrated that bending in the actin network is not specific to osteoclasts or multinucleate cells but is a more general component of cytoskeleton in cultured cells. The bending and branching actin cytoskeleton is a novel concept, which has not previously been reported. However, a single study showing that curved actin is present in nucleus has been published (Kokai et al., 2014).

Super-resolution microscopy imaging also revealed another feature that would have remained unseen with conventional confocal microscope. For example, osteoclasts formed intercellular protrusions that were not in contact with the cell substratum. Occasionally, these protrusions between the cells contained a single nucleus. When this study was carried out, literature about these structures was sparse. More studies have since emerged naming the structures as tunneling nanotubes, filopodia bridges, conduit, tubes or nanotubules (for review see Dupont et al., 2018). Tunneling nanotubes represent a dynamic structure that the cells can use to communicate with each other and exchange small molecular particles. It is also possible to exchange cell organelles such as lysosomes and mitochondria. Our study was the first to show transfer of nuclei. Nanotubes could be important means of translocation for nuclei during the formation of multinucleated osteoclasts. Research on tunneling nanotubes is expanding and seems to be a potentially important field that will develop in the future.

7 Conclusions

Bioimaging was a major part of this study. Advanced imaging methods, used alone or in combination, revealed findings in complex tissues bone and peripheral nerve that otherwise would not have been discovered.

Tight junctions of Schwann cells in human adult and peripheral nerves were localized to the specific cell membrane structures of non-compacted myelin compartments. These junctions were autotypic, i.e., they were formed between the adjacent cell membranes of the same cell. E-cadherin, claudin-1, claudin-2 and ZO-1 were detected in all locations, although slight differences in claudin composition were detected between junctions of paranodal regions, mesaxons and Schmidt Lanterman incisures. Developing nerves showed discontinuous labeling for tight junctions at 23 gestational weeks, which corresponds to the immature state of myelin and emphasizes that the nerve-tissue barrier of Schwann cells is not developed at this time point. Furthermore, these results together emphasize the importance of human data even if various mouse models have been invaluable tool for scientists. It is essential to comprehend the molecular differences between the species when data is translated from mouse to man. These results give us new insight about the structural, and perhaps, physiological properties of nerve-blood-barrier.

A mouse strain Nf1Ocl, in which the NF1 gene was conditionally knocked out in osteoclasts, was generated and analyzed in detail. The phenotype showed slight abnormalities of bone, as the tibial bone marrow cavity, trabecular tissue volume and the perimeter of cortical bone were smaller in Nf1Ocl mice compared to control mice. The growth plate of long bones was narrowed, and chondrocytes displayed abnormal morphology that seemed disorganized in Nf1Ocl mice. However, the osteoporotic phenotype could not be detected *ex vivo*, whereas *in vitro* analysis showed that bone resorption capacity is increased, and the actin cytoskeleton appeared abnormal in $Nf1^{-/-}$ osteoclasts. Taking into account the major alterations in chondrocytes and growth plate, slight alterations in bone microarchitecture and the results of *in vitro* analyses, these findings together suggest that neurofibromin is essential for proper bone homeostasis by influencing the microenvironment and bone cell communication. Nf1-deficient osteoclasts alone are insufficient to induce the

bone abnormalities seen in NF1 patients. The pathomechanisms of bone abnormalities remains unclear in NF1 disease to some extent.

Cultured osteoclasts were analyzed using indirect immunofluorescence and STED microscopy. Systematic whole-cell imaging from the basal aspect of the cells to the top showed an extensive cone-like arrangement of actin that constantly embedded the nuclei. Surprisingly, the actin filaments in osteoclasts were bending and branching. Corresponding curved actin was also demonstrated in cultured macrophages and keratinocytes. In addition, an intercellular protrusion, a micrometer-level tube was bridging between two osteoclasts and enclosed a single nucleus occasionally. In future, the superresolution microscopy may detect curved actin in other cell types which features rheological properties.

Acknowledgements

This thesis work was carried out at the Department of Cell Biology and Anatomy, Institute of Biomedicine, University of Turku. I wish to thank all the present and former heads of the Department and Institute: Professors Kalervo Väänänen, Pirkko Härkönen, Juha Peltonen and Sari Mäkelä for providing the facilities and supportive working environment for the current study. Thesis work was financially supported by Turku Doctoral Programme in Clinical Research (DPCR), National Graduate School of Clinical Investigations (VKTK), The Finnish Medical Foundation and Turku University Hospital EVO Funding.

I want to express my immense gratitude to my supervisors Professor Juha Peltonen and Professor Sirkku Peltonen for introducing me to the fascinating world of science. I deeply appreciate your expertise and talent to build bridge between the patients and basic science. Juha is warmly thanked for the deep scientific discussions which are inspired me for these years. I would like to thank Sirkku specially for the encouragement during the final steps of this work.

Professor Mikko Lammi and Docent Kirsi Rilla are gratefully acknowledged for carefully reviewing this thesis and providing valuable criticism. I would like to thank you my steering group Professor Matti Laato and Docent Outi Hirvonen for these years and for expertise.

All my co-authors Takahiro Deguchi, Reidan Grènman, Anthony Heape, Jorma Määttä, Tuomas Näreoja, Luis Parada, Kati Pummi, Elina Siljamäki and Jolene Windle are warmly thanked for their contribution and expertise to this project. I would like to thank Takahiro and Tuomas for showing me the vivid and joy of imaging. Jorma Määttä is thanked for the delightful discussions and expertise of mice.

I would acknowledge my sincere gratitude for the present and former NF1 team members: Eeva-Mari Jouhilahti, Paula Pennanen, Elina Uusitalo, Laura Raiko, Eetu Heervä, Roope Kallionpää, Jussi Leppävirta, Kati Pummi, Vivian Reinhold, Vesa Aaltonen, Heli Ylä-Outinen, Tommi Kuorilehto, Pekka Leinonen, Riina Myllylä and Miso Immonen. Eeva-Mari, Laura, Elina, Paula and Eetu are warmly thanked for their precious friendship and all the “happening” beyond the office and laboratory. Eeva-Mari has been a solid rock of science and fun for the very beginning and shared

joy and sorrow around a teacup. Vivacious mind of Paula has encouraged me during these years.

I would thank my research colleagues Teuvo Hentunen, Tiina Leinonen, Kaisa Ivaska-Papaioannou, Terhi Heino, Teresa Elo, Salla Laine, Jussi Mäkilä, Jonas Nyman, Jorma Paranko, Lauri Polari, Natalija Eigeliene and Niina Loponen. I would thank the all the people at the Department of Cell Biology and Anatomy for these valuable years.

Iris Dunder, Petra Heikkilä, Soili Huhta, Mirva Metsälä, Piia Tahvanainen and Elina Tammi are warmly appreciated for secretary help and assistance during these years. Technical help of Paula Pennanen, Pirkko Rauhamäki, Mari Erlin, Ludmilla Shumskaya, Krista Seppälä, Taina Malinen and Anneli Kurkela are greatly acknowledmed.

All the volunteers who donated samples for this study are warmly thanked for their contribution to science.

I would like to thank all my colleagues in TYKS AKUUTTI. Each of you has encouraged me in many ways during this journey.

Vilkkaat Martat has fulfilled my life with happiness, laugh and friendship and I thank them for the precious moments together. I would thank my colleague of bioscience and a good friend Etvi Juntunen for advices and encouragement.

I want to thank my dear parents Riitta and Esko Pekkanen for caring, encouraging and just being for me. I want to thank my sister Hanna Kuusisto for all the supporting. My family-in-law is warmly thanked for all the encouragement.

Lastly, I owe my deepest gratitude for my husband Tuomas Alanne for standing by me, for endless love and supporting attitude during these years. You have reminded the life beyond the science and hospital. Our son Anton has brought the joy and sense of humour in his own way to our life. You are the most crucial persons in my heart.

Turku, April 2021

Maria Alanne

References

Abbe, E. (1873). Beiträge zur Theorie des Mikroskops und der mikroskopischen Wahrnehmung. *Archiv Für Mikroskopische Anatomie, 9*, 413–468.

Abella, J. V. G., Galloni, C., Pernier, J., Barry, D. J., Kjær, S., Carlier, M., & Way, M. (2016). Isoform diversity in the Arp2/3 complex determines actin filament dynamics. *Nature Cell Biology, 18*(1), 76-86. 10.1038/ncb3286

Abercrombie, M., Heaysman, J. E., & Pegrum, S. M. (1970). The locomotion of fibroblasts in culture. 3. Movements of particles on the dorsal surface of the leading lamella. *Experimental Cell Research, 62*(2), 389-398. 10.1016/0014-4827(70)90570-7

Abramowicz, A., & Gos, M. (2014). Neurofibromin in neurofibromatosis type 1 - mutations in NF1gene as a cause of disease. *Developmental Period Medicine, 18*(3), 297-306.

Adil, M. S., Narayanan, S. P., & Somanath, P. R. (2020). Cell-cell junctions: structure and regulation in physiology and pathology. *Tissue Barriers,* , 1848212. 10.1080/21688370.2020.1848212

Alok, A., Lei, Z., Jagannathan, N. S., Kaur, S., Harmston, N., Rozen, S. G., Tucker-Kellogg, L., & Virshup, D. M. (2017). Wnt proteins synergize to activate β-catenin signaling. *Journal of Cell Science, 130*(9), 1532-1544. 10.1242/jcs.198093

Anderson, J. L., & Gutmann, D. H. (2015). Neurofibromatosis type 1. *Handbook of Clinical Neurology, 132*, 75-86. 10.1016/B978-0-444-62702-5.00004-4

Andrianantoandro, E., & Pollard, T. D. (2006). Mechanism of actin filament turnover by severing and nucleation at different concentrations of ADF/cofilin. *Molecular Cell, 24*(1), 13-23. 10.1016/j.molcel.2006.08.006

Arana-Chavez, V. E., & Castro-Filice, L. S. (2019). Transmission Electron Microscopy (TEM) and Scanning Electron Microscopy (SEM) for the Examination of Dental Hard Tissues. *Methods in Molecular Biology (Clifton, N.J.), 1922*, 325-332. 10.1007/978-1-4939-9012-2_29

Arroyo, E. J., & Scherer, S. S. (2000). On the molecular architecture of myelinated fibers. *Histochemistry and Cell Biology, 113*(1), 1-18. 10.1007/s004180050001

Baldelli, E., Haura, E. B., Crinò, L., Cress, D. W., Ludovini, V., Schabath, M. B., Liotta, L. A., Petricoin, E. F., & Pierobon, M. (2015). Impact of upfront cellular enrichment by laser capture microdissection on protein and phosphoprotein drug target signaling activation measurements in human lung cancer: Implications for personalized medicine. *Proteomics. Clinical Applications, 9*(9-10), 928-937. 10.1002/prca.201400056

Bayguinov, P. O., Oakley, D. M., Shih, C., Geanon, D. J., Joens, M. S., & Fitzpatrick, J. A. J. (2018). Modern Laser Scanning Confocal Microscopy. *Current Protocols in Cytometry, 85*(1), e39. 10.1002/cpcy.39

Becker, K., Kremmer, E., Eulitz, M., Schulz, S., Mages, J., Handschuh, G., Wheelock, M. J., Cleton-Jansen, A., Höfler, H., & Becker, I. (2002). Functional allelic loss detected at the protein level in archival human tumours using allele-specific E-cadherin monoclonal antibodies. *The Journal of Pathology, 197*(5), 567-574. 10.1002/path.1149

Bergoug, M., Doudeau, M., Godin, F., Mosrin, C., Vallée, B., & Bénédetti, H. (2020). Neurofibromin Structure, Functions and Regulation. *Cells, 9*(11)10.3390/cells9112365

Bernards, A., Snijders, A. J., Hannigan, G. E., Murthy, A. E., & Gusella, J. F. (1993). Mouse neurofibromatosis type 1 cDNA sequence reveals high degree of conservation of both coding and non-coding mRNA segments. *Human Molecular Genetics, 2*(6), 645-650. 10.1093/hmg/2.6.645

Bezniakow, N., Gos, M., & Obersztyn, E. (2014). The RASopathies as an example of RAS/MAPK pathway disturbances - clinical presentation and molecular pathogenesis of selected syndromes. *Developmental Period Medicine, 18*(3), 285-296.

Blanchoin, L., Boujemaa-Paterski, R., Sykes, C., & Plastino, J. (2014). Actin dynamics, architecture, and mechanics in cell motility. *Physiol Rev, 94*(1), 235-263. 10.1152/physrev.00018.2013

Boerckel, J. D., Mason, D. E., McDermott, A. M., & Alsberg, E. (2014). Microcomputed tomography: approaches and applications in bioengineering. *Stem Cell Research & Therapy, 5*(6), 144. 10.1186/scrt534

Borisy, G. G., & Taylor, E. W. (1967). The mechanism of action of colchicine. Binding of colchincine-3H to cellular protein. *The Journal of Cell Biology, 34*(2), 525-533. 10.1083/jcb.34.2.525

Bouxsein, M. L., Boyd, S. K., Christiansen, B. A., Guldberg, R. E., Jepsen, K. J., & Müller, R. (2010). Guidelines for assessment of bone microstructure in rodents using micro-computed tomography. *Journal of Bone and Mineral Research: The Official Journal of the American Society for Bone and Mineral Research, 25*(7), 1468-1486. 10.1002/jbmr.141

Boyce, B. F., Yao, Z., & Xing, L. (2009). PMC2856465; Osteoclasts have multiple roles in bone in addition to bone resorption. *Crit Rev Eukaryot Gene Expr, 19*(3), 171-180. 12b6e91c2627fc7a,03210611080ec17a [pii]

Brannan, C. I., Perkins, A. S., Vogel, K. S., Ratner, N., Nordlund, M. L., Reid, S. W., Buchberg, A. M., Jenkins, N. A., Parada, L. F., & Copeland, N. G. (1994). Targeted disruption of the neurofibromatosis type-1 gene leads to developmental abnormalities in heart and various neural crest-derived tissues. *Genes Dev, 8*(9), 1019-1029. http://www.ncbi.nlm.nih.gov/entrez/query.fcgi?cmd=Retrieve&db=PubMed&dopt=Citation&list_uids=7926784

Brasko, C., Smith, K., Molnar, C., Farago, N., Hegedus, L., Balind, A., Balassa, T., Szkalisity, A., Sukosd, F., Kocsis, K., Balint, B., Paavolainen, L., Enyedi, M. Z., Nagy, I., Puskas, L. G., Haracska, L., Tamas, G., & Horvath, P. (2018). Intelligent image-based in situ single-cell isolation. *Nature Communications, 9*(1), 226. 10.1038/s41467-017-02628-4

Calderón, J. F., & Retamal, M. A. (2016). Regulation of Connexins Expression Levels by MicroRNAs, an Update. *Frontiers in Physiology, 7*, 558. 10.3389/fphys.2016.00558

Campbell, H. K., Maiers, J. L., & DeMali, K. A. (2017). Interplay between tight junctions & adherens junctions. *Experimental Cell Research, 358*(1), 39-44. 10.1016/j.yexcr.2017.03.061

Castellanos-Martínez, R., Jiménez-Camacho, K. E., & Schnoor, M. (2020). Cortactin Expression in Hematopoietic Cells: Implications for Hematological Malignancies. *The American Journal of Pathology, 190*(5), 958-967. 10.1016/j.ajpath.2019.12.011

Cawthon, R. M., Andersen, L. B., Buchberg, A. M., Xu, G. F., O'Connell, P., Viskochil, D., Weiss, R. B., Wallace, M. R., Marchuk, D. A., & Culver, M. (1991). cDNA sequence and genomic structure of EV12B, a gene lying within an intron of the neurofibromatosis type 1 gene. *Genomics, 9*(3), 446-460. 10.1016/0888-7543(91)90410-g

Cawthon, R. M., Weiss, R., Xu, G. F., Viskochil, D., Culver, M., Stevens, J., Robertson, M., Dunn, D., Gesteland, R., & O'Connell, P. (1990). A major segment of the neurofibromatosis type 1 gene: cDNA sequence, genomic structure, and point mutations. *Cell, 62*(1), 193-201. 10.1016/0092-8674(90)90253-b

Celentano, A., Mignogna, M. D., McCullough, M., & Cirillo, N. (2017). Pathophysiology of the Desmo-Adhesome. *Journal of Cellular Physiology, 232*(3), 496-505. 10.1002/jcp.25515

Čermák, V., Dostál, V., Jelínek, M., Libusová, L., Kovář, J., Rösel, D., & Brábek, J. (2020). Microtubule-targeting agents and their impact on cancer treatment. *European Journal of Cell Biology, 99*(4), 151075. 10.1016/j.ejcb.2020.151075

Chabadel, A., Bañon-Rodríguez, I., Cluet, D., Rudkin, B. B., Wehrle-Haller, B., Genot, E., Jurdic, P., Anton, I. M., & Saltel, F. (2007). PMC2096584; CD44 and beta3 integrin organize two functionally distinct actin-based domains in osteoclasts. *Mol Biol Cell, 18*(12), 4899-4910. 10.1091/mbc.E07-04-0378

Chang, C., Leu, J., & Lee, Y. (2015). The actin depolymerizing factor (ADF)/cofilin signaling pathway and DNA damage responses in cancer. *International Journal of Molecular Sciences, 16*(2), 4095-4120. 10.3390/ijms16024095

Chellaiah, M. A., & Hruska, K. A. (2003). The integrin alpha(v)beta(3) and CD44 regulate the actions of osteopontin on osteoclast motility. *Calcif Tissue Int, 72*(3), 197-205. 10.1007/s00223-002-1025-6

Cheng, L., Zhang, S., MacLennan, G. T., Williamson, S. R., Davidson, D. D., Wang, M., Jones, T. D., Lopez-Beltran, A., & Montironi, R. (2013). Laser-assisted microdissection in translational research: theory, technical considerations, and future applications. *Applied Immunohistochemistry & Molecular Morphology: AIMM, 21*(1), 31-47. 10.1097/PAI.0b013e31824d0519

Chu, L., Chang, S., Tang, W., Tseng, Y., Chen, P., & Chen, B. (2020). 5D superresolution imaging for a live cell nucleus. *Current Opinion in Genetics & Development, 67*, 77-83. 10.1016/j.gde.2020.11.005

Clarke, B. (2008). Normal Bone Anatomy and Physiology. *Clinical Journal of the American Society of Nephrology : CJASN, 3*(Suppl 3), S131-S139. 10.2215/CJN.04151206

Coopman, P., & Djiane, A. (2016). Adherens Junction and E-Cadherin complex regulation by epithelial polarity. *Cellular and Molecular Life Sciences: CMLS, 73*(18), 3535-3553. 10.1007/s00018-016-2260-8

Costa, S., Correia-de-Sá, P., Porto, M. J., & Cainé, L. (2017). The Use of Laser Microdissection in Forensic Sexual Assault Casework: Pros and Cons Compared to Standard Methods. *Journal of Forensic Sciences, 62*(4), 998-1006. 10.1111/1556-4029.13348

Coutts, A. S., & La Thangue, N. B. (2016). Regulation of actin nucleation and autophagosome formation. *Cellular and Molecular Life Sciences: CMLS, 73*(17), 3249-3263. 10.1007/s00018-016-2224-z

Cummings, M., Mappa, G., & Orsi, N. M. (2018). Laser Capture Microdissection and Isolation of High-Quality RNA from Frozen Endometrial Tissue. *Methods in Molecular Biology (Clifton, N.J.), 1723*, 155-166. 10.1007/978-1-4939-7558-7_8

Danglot, G., Régnier, V., Fauvet, D., Vassal, G., Kujas, M., & Bernheim, A. (1995). Neurofibromatosis 1 (NF1) mRNAs expressed in the central nervous system are differentially spliced in the 5' part of the gene. *Human Molecular Genetics, 4*(5), 915-920. 10.1093/hmg/4.5.915

Daston, M. M., & Ratner, N. (1992). Neurofibromin, a predominantly neuronal GTPase activating protein in the adult, is ubiquitously expressed during development. *Developmental Dynamics: An Official Publication of the American Association of Anatomists, 195*(3), 216-226. 10.1002/aja.1001950307

Daston, M. M., Scrable, H., Nordlund, M., Sturbaum, A. K., Nissen, L. M., & Ratner, N. (1992). The protein product of the neurofibromatosis type 1 gene is expressed at highest abundance in neurons, Schwann cells, and oligodendrocytes. *Neuron, 8*(3), 415-428. 10.1016/0896-6273(92)90270-n

Denninger, A. R., Breglio, A., Maheras, K. J., LeDuc, G., Cristiglio, V., Demé, B., Gow, A., & Kirschner, D. A. (2015). Claudin-11 Tight Junctions in Myelin Are a Barrier to Diffusion and Lack Strong Adhesive Properties. *Biophysical Journal, 109*(7), 1387-1397. 10.1016/j.bpj.2015.08.012

Destaing, O., Saltel, F., Géminard, J. C., Jurdic, P., & Bard, F. (2003). PMC149981; Podosomes display actin turnover and dynamic self-organization in osteoclasts expressing actin-green fluorescent protein. *Mol Biol Cell, 14*(2), 407-416. 10.1091/mbc.E02-07-0389

Dewey, M. M., & Barr, L. (1962). Intercellular Connection between Smooth Muscle Cells: the Nexus. *Science (New York, N.Y.), 137*(3531), 670-672. 10.1126/science.137.3531.670-a

Dogterom, M., & Koenderink, G. H. (2019). Actin-microtubule crosstalk in cell biology. *Nature Reviews. Molecular Cell Biology, 20*(1), 38-54. 10.1038/s41580-018-0067-1

Dossa, T., Arabian, A., Windle, J. J., Dedhar, S., Teitelbaum, S. L., Ross, F. P., Roodman, G. D., & St-Arnaud, R. (2010). Osteoclast-specific inactivation of the integrin-linked kinase (ILK) inhibits bone resorption. *J Cell Biochem, 110*(4), 960-967. 10.1002/jcb.22609

du Plessis, A., Broeckhoven, C., Guelpa, A., & le Roux, S. G. (2017). Laboratory x-ray micro-computed tomography: a user guideline for biological samples. *GigaScience, 6*(6), 1-11. 10.1093/gigascience/gix027

Dupont, M., Souriant, S., Lugo-Villarino, G., Maridonneau-Parini, I., & Vérollet, C. (2018). Tunneling Nanotubes: Intimate Communication between Myeloid Cells. *Frontiers in Immunology, 9*, 43. 10.3389/fimmu.2018.00043

Eisenberg, K. A., & Vuillermin, C. B. (2019). Management of Congenital Pseudoarthrosis of the Tibia and Fibula. *Current Reviews in Musculoskeletal Medicine,* , 356-368. 10.1007/s12178-019-09566-2

Elefteriou, F., Benson, M. D., Sowa, H., Starbuck, M., Liu, X., Ron, D., Parada, L. F., & Karsenty, G. (2006). PMC2756713; ATF4 mediation of NF1 functions in osteoblast reveals a nutritional basis for congenital skeletal dysplasiae. *Cell Metab, 4*(6), 441-451. S1550-4131(06)00339-1 [pii] 10.1016/j.cmet.2006.10.010

Elefteriou, F., Kolanczyk, M., Schindeler, A., Viskochil, D. H., Hock, J. M., Schorry, E. K., Crawford, A. H., Friedman, J. M., Little, D., Peltonen, J., Carey, J. C., Feldman, D., Yu, X., Armstrong, L., Birch, P., Kendler, D. L., Mundlos, S., Yang, F. C., Agiostratidou, G., . . . Stevenson, D. A. (2009). Skeletal abnormalities in neurofibromatosis type 1: approaches to therapeutic options. *Am J Med Genet A, 149A*(10), 2327-2338. 10.1002/ajmg.a.33045

Elliott, J. C., & Dover, S. D. (1982). X-ray microtomography. *Journal of Microscopy, 126*(Pt 2), 211-213. 10.1111/j.1365-2818.1982.tb00376.x

Etienne-Manneville, S. (2013). Microtubules in cell migration. *Annual Review of Cell and Developmental Biology, 29*, 471-499. 10.1146/annurev-cellbio-101011-155711

Evans, D. G. R., Baser, M. E., McGaughran, J., Sharif, S., Howard, E., & Moran, A. (2002). Malignant peripheral nerve sheath tumours in neurofibromatosis 1. *Journal of Medical Genetics, 39*(5), 311-314. 10.1136/jmg.39.5.311

Fang, Y., Elahi, A., Denley, R. C., Rao, P. H., Brennan, M. F., & Jhanwar, S. C. (2009). Molecular characterization of permanent cell lines from primary, metastatic and recurrent malignant peripheral nerve sheath tumors (MPNST) with underlying neurofibromatosis-1. *Anticancer Research, 29*(4), 1255-1262.

Fannon, A. M., Sherman, D. L., Ilyina-Gragerova, G., Brophy, P. J., Friedrich, V. L., & Colman, D. R. (1995). PMC2120363; Novel E-cadherin-mediated adhesion in peripheral nerve: Schwann cell architecture is stabilized by autotypic adherens junctions. *J Cell Biol, 129*(1), 189-202. http://www.ncbi.nlm.nih.gov/pubmed/7698985

Farquhar, M. G., & Palade, G. E. (1963). Junctional complexes in various epithelia. *The Journal of Cell Biology, 17*, 375-412. 10.1083/jcb.17.2.375

Federico, L. B., Silva, G. M., de Fraga Dias, A., Figueiró, F., Battastini, A. M. O., Dos Santos, Cleydson Breno Rodrigues, Costa, L. T., Rosa, J. M. C., & de Paula da Silva, Carlos Henrique Tomich. (2020). Identification of novel αβ-tubulin modulators with antiproliferative activity directed to cancer therapy using ligand and structure-based virtual screening. *International Journal of Biological Macromolecules, 165*(Pt B), 3040-3050. 10.1016/j.ijbiomac.2020.10.136

Feng, H., Wang, X., Xu, Z., Zhang, X., & Gao, Y. (2018). Super-Resolution Fluorescence Microscopy for Single Cell Imaging. *Advances in Experimental Medicine and Biology, 1068*, 59-71. 10.1007/978-981-13-0502-3_6

Feng, X. (2009). Chemical and Biochemical Basis of Cell-Bone Matrix Interaction in Health and Disease. *Current Chemical Biology, 3*(2), 189-196. 10.2174/187231309788166398

Fiore, M., Goulas, C., & Pillois, X. (2017). A new mutation in TUBB1 associated with thrombocytopenia confirms that C-terminal part of β1-tubulin plays a role in microtubule assembly. *Clinical Genetics, 91*(6), 924-926. 10.1111/cge.12879

Freedman, J. C., Shrestha, A., & McClane, B. A. (2016). Clostridium perfringens Enterotoxin: Action, Genetics, and Translational Applications. *Toxins, 8*(3)10.3390/toxins8030073

Furuse, M., Fujita, K., Hiiragi, T., Fujimoto, K., & Tsukita, S. (1998). PMC2132999; Claudin-1 and -2: novel integral membrane proteins localizing at tight junctions with no sequence similarity to occludin. *J Cell Biol, 141*(7), 1539-1550. http://www.ncbi.nlm.nih.gov/pubmed/9647647

Gadadhar, S., Bodakuntla, S., Natarajan, K., & Janke, C. (2017). The tubulin code at a glance. *Journal of Cell Science, 130*(8), 1347-1353. 10.1242/jcs.199471

Galbraith, C. G., & Galbraith, J. A. (2011). Super-resolution microscopy at a glance. *Journal of Cell Science, 124*(Pt 10), 1607-1611. 10.1242/jcs.080085

Gallagher, R. I., Blakely, S. R., Liotta, L. A., & Espina, V. (2012). Laser capture microdissection: Arcturus(XT) infrared capture and UV cutting methods. *Methods in Molecular Biology (Clifton, N.J.), 823*, 157-178. 10.1007/978-1-60327-216-2_11

Gamble, H. J., & Eames, R. A. (1964). PMC1261349; AN ELECTRON MICROSCOPE STUDY OF THE CONNECTIVE TISSUES OF HUMAN PERIPHERAL NERVE. *J Anat, 98*, 655-663. http://www.ncbi.nlm.nih.gov/pubmed/14229996

Geisse, N. A. (2009). AFM and combined optical techniques. *Materials Today (Kidlington, England), 12*(7-8), 40-45. 10.1016/S1369-7021(09)70201-9

Geissinger, H. D., & Abandowitz, H. M. (1976). Correlated transmission electron microscopy (TEM) and scanning electron microscopy (SEM) of single cells. *Mikroskopie, 32*(1-2), 17-25.

Georgess, D., Machuca-Gayet, I., Blangy, A., & Jurdic, P. (2014). Podosome organization drives osteoclast-mediated bone resorption. *Cell Adhesion & Migration, 8*(3), 191-204. 10.4161/cam.27840

Ghadakzadeh, S., Kannu, P., Whetstone, H., Howard, A., & Alman, B. A. (2016). β-Catenin modulation in neurofibromatosis type 1 bone repair: therapeutic implications. *FASEB Journal: Official Publication of the Federation of American Societies for Experimental Biology, 30*(9), 3227-3237. 10.1096/fj.201500190RR

Gong, D., Zhang, Z., Shi, Q., van den Hengel, A., Shen, C., & Zhang, Y. (2020). Learning Deep Gradient Descent Optimization for Image Deconvolution. *IEEE Transactions on Neural Networks and Learning Systems, 31*(12), 5468-5482. 10.1109/TNNLS.2020.2968289

González-Mariscal, L., Tapia, R., & Chamorro, D. (2008). Crosstalk of tight junction components with signaling pathways. *Biochimica Et Biophysica Acta, 1778*(3), 729-756. 10.1016/j.bbamem.2007.08.018

Goodenough, D. A., & Paul, D. L. (2009). Gap junctions. *Cold Spring Harbor Perspectives in Biology, 1*(1), a002576. 10.1101/cshperspect.a002576

Goodwin, M., & Yap, A. S. (2004). Classical cadherin adhesion molecules: coordinating cell adhesion, signaling and the cytoskeleton. *Journal of Molecular Histology, 35*(8-9), 839-844. 10.1007/s10735-004-1833-2

Goodwin, P. C. (2015). A primer on the fundamental principles of light microscopy: Optimizing magnification, resolution, and contrast. *Molecular Reproduction and Development, 82*(7-8), 502-507. 10.1002/mrd.22385

Gordan, G. S. (1951). Metabolic bones diseases in practice. Osteoporosis, Paget's disease, von Recklinghausen's disease, and Albright's syndrome. *American Practitioner and Digest of Treatment, 2*(2), 113-119.

Gulhane, S. R., & Kotwal, M. N. (2015). Chronic Myeloid Leukemia Arising in a Patient of Neurofibromatosis Type 1. *Indian Journal of Dermatology, 60*(5), 523. 10.4103/0019-5154.164443

Guo, M., Li, Y., Su, Y., Lambert, T., Nogare, D. D., Moyle, M. W., Duncan, L. H., Ikegami, R., Santella, A., Rey-Suarez, I., Green, D., Beiriger, A., Chen, J., Vishwasrao, H., Ganesan, S., Prince, V., Waters, J. C., Annunziata, C. M., Hafner, M., . . . Shroff, H. (2020). Rapid image deconvolution and multiview fusion for optical microscopy. *Nature Biotechnology, 38*(11), 1337-1346. 10.1038/s41587-020-0560-x

Gutman, D. H., Andersen, L. B., Cole, J. L., Swaroop, M., & Collins, F. S. (1993). An alternatively-spliced mRNA in the carboxy terminus of the neurofibromatosis type 1 (NF1) gene is expressed in muscle. *Human Molecular Genetics, 2*(7), 989-992. 10.1093/hmg/2.7.989

Harris, J. R. (2015). Transmission electron microscopy in molecular structural biology: A historical survey. *Archives of Biochemistry and Biophysics, 581*, 3-18. 10.1016/j.abb.2014.11.011

Hartsock, A., & Nelson, W. J. (2008). Adherens and tight junctions: structure, function and connections to the actin cytoskeleton. *Biochimica Et Biophysica Acta, 1778*(3), 660-669. 10.1016/j.bbamem.2007.07.012

Hasle, H., Nir, M., & Tommerup, N. (1997). Prolonged extreme thrombocytosis associated with neurofibromatosis type 1. *The Journal of Pediatrics, 130*(2), 317-319. 10.1016/s0022-3476(97)70363-9

Hassanzadeh, G., Hosseini Quchani, S., Sahraian, M. A., Abolhassani, F., Sadighi Gilani, M. A., Dehghan Tarzjani, M., & Atoof, F. (2016). Leukocyte Gene Expression and Plasma Concentration in Multiple Sclerosis: Alteration of Transforming Growth Factor-βs, Claudin-11, and Matrix Metalloproteinase-2. *Cellular and Molecular Neurobiology, 36*(6), 865-872. 10.1007/s10571-015-0270-y

Hauer, N. N., Popp, B., Schoeller, E., Schuhmann, S., Heath, K. E., Hisado-Oliva, A., Klinger, P., Kraus, C., Trautmann, U., Zenker, M., Zweier, C., Wiesener, A., Abou Jamra, R., Kunstmann, E., Wieczorek, D., Uebe, S., Ferrazzi, F., Büttner, C., Ekici, A. B., . . . Thiel, C. T. (2018). Clinical relevance of systematic phenotyping and exome sequencing in patients with short stature. *Genetics in Medicine: Official Journal of the American College of Medical Genetics, 20*(6), 630-638. 10.1038/gim.2017.159

Hawi, Z., Tong, J., Dark, C., Yates, H., Johnson, B., & Bellgrove, M. A. (2018). The role of cadherin genes in five major psychiatric disorders: A literature update. *American Journal of Medical Genetics. Part B, Neuropsychiatric Genetics: The Official Publication of the International Society of Psychiatric Genetics, 177*(2), 168-180. 10.1002/ajmg.b.32592

Hayashida, C., Ito, J., Nakayachi, M., Okayasu, M., Ohyama, Y., Hakeda, Y., & Sato, T. (2014). Osteocytes produce interferon-β as a negative regulator of osteoclastogenesis. *The Journal of Biological Chemistry, 289*(16), 11545-11555. 10.1074/jbc.M113.523811

He, Y., Rhodes, S. D., Chen, S., Wu, X., Yuan, J., Yang, X., Jiang, L., Li, X., Takahashi, N., Xu, M., Mohammad, K. S., Guise, T. A., & Yang, F. (2012). c-Fms signaling mediates neurofibromatosis Type-1 osteoclast gain-in-functions. *PloS One, 7*(11), e46900. 10.1371/journal.pone.0046900

Heervä, E., Koffert, A., Jokinen, E., Kuorilehto, T., Peltonen, S., Aro, H. T., & Peltonen, J. (2012). A controlled register-based study of 460 neurofibromatosis 1 patients: increased fracture risk in children and adults over 41 years of age. *J Bone Miner Res, 27*(11), 2333-2337. 10.1002/jbmr.1685

Heervä, E., Leinonen, P., Kuorilehto, T., Peltonen, S., Pöyhönen, M., Väänänen, K., & Peltonen, J. (2013). Neurofibromatosis 1-related osteopenia often progresses to osteoporosis in 12 years. *Calcif Tissue Int, 92*(1), 23-27. 10.1007/s00223-012-9661-y

Heervä, E., Alanne, M. H., Peltonen, S., Kuorilehto, T., Hentunen, T., Väänänen, K., & Peltonen, J. (2010). Osteoclasts in neurofibromatosis type 1 display enhanced resorption capacity, aberrant morphology, and resistance to serum deprivation. *Bone, 47*(3), 583-590. 10.1016/j.bone.2010.06.001

Heervä, E., Huilaja, L., Leinonen, P., Peltonen, S., & Peltonen, J. (2014). Follow-up of six patients with neurofibromatosis 1-related osteoporosis treated with alendronate for 23 months. *Calcified Tissue International, 94*(6), 608-612. 10.1007/s00223-013-9835-2

Hell, S. W., & Wichmann, J. (1994). Breaking the diffraction resolution limit by stimulated emission: stimulated-emission-depletion fluorescence microscopy. *Optics Letters, 19*(11)10.1364/ol.19.000780

Hodge, J. M., Kirkland, M. A., & Nicholson, G. C. (2007). Multiple roles of M-CSF in human osteoclastogenesis. *Journal of Cellular Biochemistry, 102*(3), 759-768. 10.1002/jcb.21331

Hooke, R. (1665). *Micrographia, or some physiological descriptions of minute bodies made by magnifying glasses, with observations and inquiries thereupon. By R. Hooke.* The British Library.

Hookway, C., Ding, L., Davidson, M. W., Rappoport, J. Z., Danuser, G., & Gelfand, V. I. (2015). Microtubule-dependent transport and dynamics of vimentin intermediate filaments. *Molecular Biology of the Cell, 26*(9), 1675-1686. 10.1091/mbc.E14-09-1398

Hou, J., Renigunta, A., Gomes, A. S., Hou, M., Paul, D. L., Waldegger, S., & Goodenough, D. A. (2009). PMC2741254; Claudin-16 and claudin-19 interaction is required for their assembly into tight junctions and for renal reabsorption of magnesium. *Proc Natl Acad Sci U S A, 106*(36), 15350-15355. 10.1073/pnas.0907724106

Hu, N., Kadota, M., Liu, H., Abnet, C. C., Su, H., Wu, H., Freedman, N. D., Yang, H. H., Wang, C., Yan, C., Wang, L., Gere, S., Hutchinson, A., Song, G., Wang, Y., Ding, T., Qiao, Y., Koshiol, J., Dawsey, S. M., . . . Lee, M. P. (2016). Genomic Landscape of Somatic Alterations in Esophageal Squamous Cell Carcinoma and Gastric Cancer. *Cancer Research, 76*(7), 1714-1723. 10.1158/0008-5472.CAN-15-0338

Hunt, A. L., Pierobon, M., Baldelli, E., Oliver, J., Mitchell, D., Gist, G., Bateman, N. W., Larry Maxwell, G., Petricoin, E. F., & Conrads, T. P. (2020). The impact of ultraviolet- and infrared-based laser microdissection technology on phosphoprotein detection in the laser microdissection-reverse phase protein array workflow. *Clinical Proteomics, 17*, 9. 10.1186/s12014-020-09272-z

Huson, S. M., Compston, D. A., Clark, P., & Harper, P. S. (1989). A genetic study of von Recklinghausen neurofibromatosis in south east Wales. I. Prevalence, fitness, mutation rate, and effect of parental transmission on severity. *Journal of Medical Genetics, 26*(11), 704-711. 10.1136/jmg.26.11.704

Huson, S. M., Harper, P. S., & Compston, D. A. (1988). Von Recklinghausen neurofibromatosis. A clinical and population study in south-east Wales. *Brain: A Journal of Neurology, 111 (Pt 6)*, 1355-1381. 10.1093/brain/111.6.1355

Huttner, A. J., Kieran, M. W., Yao, X., Cruz, L., Ladner, J., Quayle, K., Goumnerova, L. C., Irons, M. B., & Ullrich, N. J. (2010). Clinicopathologic study of glioblastoma in children with neurofibromatosis type 1. *Pediatric Blood & Cancer, 54*(7), 890-896. 10.1002/pbc.22462

Hwang, I., An, B. S., Yang, H., Kang, H. S., Jung, E. M., & Jeung, E. B. (2013). Tissue-specific expression of occludin, zona occludens-1, and junction adhesion molecule A in the duodenum, ileum, colon, kidney, liver, lung, brain, and skeletal muscle of C57BL mice. *Journal of Physiology and Pharmacology: An Official Journal of the Polish Physiological Society, 64*(1), 11-18.

Ikenouchi, J., Sasaki, H., Tsukita, S., Furuse, M., & Tsukita, S. (2008). Loss of occludin affects tricellular localization of tricellulin. *Molecular Biology of the Cell, 19*(11), 4687-4693. 10.1091/mbc.e08-05-0530

Illés, T., Halmai, V., de Jonge, T., & Dubousset, J. (2001). Decreased bone mineral density in neurofibromatosis-1 patients with spinal deformities. *Osteoporos Int, 12*(10), 823-827. http://www.ncbi.nlm.nih.gov/entrez/query.fcgi?cmd=Retrieve&db=PubMed&dopt=Citation&list_uids=11716184

Ishikawa, H., Bischoff, R., & Holtzer, H. (1968). Mitosis and intermediate-sized filaments in developing skeletal muscle. *The Journal of Cell Biology, 38*(3), 538-555. 10.1083/jcb.38.3.538

Ishimoto, H., Oshima, T., Sei, H., Yamasaki, T., Kondo, T., Tozawa, K., Tomita, T., Ohda, Y., Fukui, H., Watari, J., & Miwa, H. (2017). Claudin-2 expression is upregulated in the ileum of diarrhea predominant irritable bowel syndrome patients. *Journal of Clinical Biochemistry and Nutrition, 60*(2), 146-150. 10.3164/jcbn.16-92

Isogai, T., & Innocenti, M. (2016). New nuclear and perinuclear functions of formins. *Biochemical Society Transactions, 44*(6), 1701-1708. 10.1042/BST20160187

Jaakkola, S., Savunen, O., Halme, T., Uitto, J., & Peltonen, J. (1993). Basement membranes during development of human nerve: Schwann cells and perineurial cells display marked changes in their expression profiles for laminin subunits and beta 1 and beta 4 integrins. *J Neurocytol, 22*(3), 215-230. http://www.ncbi.nlm.nih.gov/pubmed/8478643

Jacks, T., Shih, T. S., Schmitt, E. M., Bronson, R. T., Bernards, A., & Weinberg, R. A. (1994). Tumour predisposition in mice heterozygous for a targeted mutation in Nf1. *Nat Genet, 7*(3), 353-361. 10.1038/ng0794-353

James, A. W., Shurell, E., Singh, A., Dry, S. M., & Eilber, F. C. (2016). Malignant Peripheral Nerve Sheath Tumor. *Surgical Oncology Clinics of North America, 25*(4), 789-802. 10.1016/j.soc.2016.05.009

Jouhilahti, E. M., Peltonen, S., Heape, A. M., & Peltonen, J. (2011). PMC3081157; The pathoetiology of neurofibromatosis 1. *Am J Pathol, 178*(5), 1932-1939. S0002-9440(11)00172-6 [pii] 10.1016/j.ajpath.2010.12.056

Jouhilahti, E., Peltonen, S., & Peltonen, J. (2008). Class III beta-tubulin is a component of the mitotic spindle in multiple cell types. *The Journal of Histochemistry and Cytochemistry: Official Journal of the Histochemistry Society, 56*(12), 1113-1119. 10.1369/jhc.2008.952002

Karakus, O. O., Godugu, K., Rajabi, M., & Mousa, S. A. (2020). Dual Targeting of Norepinephrine Transporter (NET) Function and Thyrointegrin αvβ3 Receptors in the Treatment of Neuroblastoma. *Journal of Medicinal Chemistry, 63*(14), 7653-7662. 10.1021/acs.jmedchem.0c00537

Kaszak, I., Witkowska-Piłaszewicz, O., Niewiadomska, Z., Dworecka-Kaszak, B., Ngosa Toka, F., & Jurka, P. (2020). Role of Cadherins in Cancer-A Review. *International Journal of Molecular Sciences, 21*(20)10.3390/ijms21207624

Katsetos, C. D., Herman, M. M., & Mörk, S. J. (2003). Class III beta-tubulin in human development and cancer. *Cell Motility and the Cytoskeleton, 55*(2), 77-96. 10.1002/cm.10116

Kaufmann, D., Müller, R., Kenner, O., Leistner, W., Hein, C., Vogel, W., & Bartelt, B. (2002). The N-terminal splice product NF1-10a-2 of the NF1 gene codes for a transmembrane segment. *Biochemical and Biophysical Research Communications, 294*(2), 496-503. 10.1016/S0006-291X(02)00501-6

Kehrer-Sawatzki, H., Mautner, V., & Cooper, D. N. (2017). Emerging genotype-phenotype relationships in patients with large NF1 deletions. *Human Genetics, 136*(4), 349-376. 10.1007/s00439-017-1766-y

Kelley, L. C., Hayes, K. E., Ammer, A. G., Martin, K. H., & Weed, S. A. (2010). Cortactin phosphorylated by ERK1/2 localizes to sites of dynamic actin regulation and is required for carcinoma lamellipodia persistence. *PloS One, 5*(11), e13847. 10.1371/journal.pone.0013847

Kikuchi, S., Ninomiya, T., Tatsumi, H., Sawada, N., & Kojima, T. (2010). PMC2989243; Tricellulin is expressed in autotypic tight junctions of peripheral myelinating Schwann cells. *J Histochem Cytochem, 58*(12), 1067-1073. 10.1369/jhc.2010.956326

Kiuru, M., & Busam, K. J. (2017). The NF1 gene in tumor syndromes and melanoma. *Laboratory Investigation; a Journal of Technical Methods and Pathology, 97*(2), 146-157. 10.1038/labinvest.2016.142

Klar, T. A., Jakobs, S., Dyba, M., Egner, A., & Hell, S. W. (2000). Fluorescence microscopy with diffraction resolution barrier broken by stimulated emission. *Proceedings of the National Academy of Sciences of the United States of America, 97*(15), 8206-8210. 10.1073/pnas.97.15.8206

Kokai, E., Beck, H., Weissbach, J., Arnold, F., Sinske, D., Sebert, U., Gaiselmann, G., Schmidt, V., Walther, P., Münch, J., Posern, G., & Knöll, B. (2014). Analysis of nuclear actin by overexpression of wild-type and actin mutant proteins. *Histochemistry and Cell Biology, 141*(2), 123-135. 10.1007/s00418-013-1151-4

Kolanczyk, M., Kossler, N., Kühnisch, J., Lavitas, L., Stricker, S., Wilkening, U., Manjubala, I., Fratzl, P., Spörle, R., Herrmann, B. G., Parada, L. F., Kornak, U., & Mundlos, S. (2007). Multiple roles for neurofibromin in skeletal development and growth. *Hum Mol Genet, 16*(8), 874-886. m032 [pii] 10.1093/hmg/ddm032

Kolanczyk, M., Kühnisch, J., Kossler, N., Osswald, M., Stumpp, S., Thurisch, B., Kornak, U., & Mundlos, S. (2008). PMC2516519; Modelling neurofibromatosis type 1 tibial dysplasia and its treatment with lovastatin. *BMC Med, 6*, 21. 1741-7015-6-21 [pii] 10.1186/1741-7015-6-21

Kong, L., Schäfer, G., Bu, H., Zhang, Y., Zhang, Y., & Klocker, H. (2012). Lamin A/C protein is overexpressed in tissue-invading prostate cancer and promotes prostate cancer cell growth, migration and invasion through the PI3K/AKT/PTEN pathway. *Carcinogenesis, 33*(4), 751-759. 10.1093/carcin/bgs022

Kühnisch, J., Seto, J., Lange, C., Schrof, S., Stumpp, S., Kobus, K., Grohmann, J., Kossler, N., Varga, P., Osswald, M., Emmerich, D., Tinschert, S., Thielemann, F., Duda, G., Seifert, W., El Khassawna, T., Stevenson, D. A., Elefteriou, F., Kornak, U., . . . Kolanczyk, M. (2014). Multiscale, converging defects of macro-porosity, microstructure and matrix mineralization impact long bone fragility in NF1. *PloS One, 9*(1), e86115. 10.1371/journal.pone.0086115

Kuorilehto, T., Ekholm, E., Nissinen, M., Hietaniemi, K., Hiltunen, A., Paavolainen, P., Penttinen, R., & Peltonen, J. (2006). NF1 gene expression in mouse fracture healing and in experimental rat pseudarthrosis. *J Histochem Cytochem, 54*(3), 363-370. jhc.5A6784.2005 [pii] 10.1369/jhc.5A6784.2005

Kuorilehto, T., Nissinen, M., Koivunen, J., Benson, M. D., & Peltonen, J. (2004). NF1 tumor suppressor protein and mRNA in skeletal tissues of developing and adult normal mouse and NF1-deficient embryos. *J Bone Miner Res, 19*(6), 983-989. 10.1359/JBMR.040130

Kuorilehto, T., Pöyhönen, M., Bloigu, R., Heikkinen, J., Väänänen, K., & Peltonen, J. (2005). Decreased bone mineral density and content in neurofibromatosis type 1: lowest local values are located in the load-carrying parts of the body. *Osteoporos Int, 16*(8), 928-936. 10.1007/s00198-004-1801-4

Laasmaa, M., Vendelin, M., & Peterson, P. (2011). Application of regularized Richardson-Lucy algorithm for deconvolution of confocal microscopy images. *Journal of Microscopy, 243*(2), 124-140. 10.1111/j.1365-2818.2011.03486.x

Lacey, D. L., Timms, E., Tan, H. L., Kelley, M. J., Dunstan, C. R., Burgess, T., Elliott, R., Colombero, A., Elliott, G., Scully, S., Hsu, H., Sullivan, J., Hawkins, N., Davy, E., Capparelli, C., Eli, A., Qian, Y. X., Kaufman, S., Sarosi, I., . . . Boyle, W. J. (1998). Osteoprotegerin ligand is a cytokine that regulates osteoclast differentiation and activation. *Cell, 93*(2), 165-176. S0092-8674(00)81569-X [pii]

Langdahl, B., Ferrari, S., & Dempster, D. W. (2016). Bone modeling and remodeling: potential as therapeutic targets for the treatment of osteoporosis. *Therapeutic Advances in Musculoskeletal Disease, 8*(6), 225-235. 10.1177/1759720X16670154

Lee, S. M., Choi, I. H., Lee, D. Y., Lee, H. R., Park, M. S., Yoo, W. J., Chung, C. Y., & Cho, T. (2012). Is double inactivation of the Nf1 gene responsible for the development of congenital pseudarthrosis of the tibia associated with NF1? *Journal of Orthopaedic Research: Official Publication of the Orthopaedic Research Society, 30*(10), 1535-1540. 10.1002/jor.22121

Leskelä, H. V., Kuorilehto, T., Risteli, J., Koivunen, J., Nissinen, M., Peltonen, S., Kinnunen, P., Messiaen, L., Lehenkari, P., & Peltonen, J. (2009). Congenital pseudarthrosis of neurofibromatosis type 1: impaired osteoblast differentiation and function and altered NF1 gene expression. *Bone, 44*(2), 243-250. S8756-3282(08)00864-8 [pii] 10.1016/j.bone.2008.10.050

Li, Z., Yin, S., Zhang, L., Liu, W., & Chen, B. (2017). Prognostic value of reduced E-cadherin expression in breast cancer: a meta-analysis. *Oncotarget, 8*(10), 16445-16455. 10.18632/oncotarget.14860

Liang, G. H., & Weber, C. R. (2014). Molecular aspects of tight junction barrier function. *Current Opinion in Pharmacology, 19*, 84-89. 10.1016/j.coph.2014.07.017

Lilly, E., Sellitto, C., Milstone, L. M., & White, T. W. (2016). Connexin channels in congenital skin disorders. *Seminars in Cell & Developmental Biology, 50*, 4-12. 10.1016/j.semcdb.2015.11.018

Lin, T., Neuner, A., & Schiebel, E. (2015). Targeting of γ-tubulin complexes to microtubule organizing centers: conservation and divergence. *Trends in Cell Biology, 25*(5), 296-307. 10.1016/j.tcb.2014.12.002

Liu, Y., Jordan, J. T., Bredella, M. A., Erdin, S., Walker, J. A., Vangel, M., Harris, G. J., Plotkin, S. R., & Cai, W. (2020). Correlation between NF1 genotype and imaging phenotype on whole-body MRI: NF1 radiogenomics. *Neurology, 94*(24), e2521-e2531. 10.1212/WNL.0000000000009490

Lowndes, M., Rakshit, S., Shafraz, O., Borghi, N., Harmon, R. M., Green, K. J., Sivasankar, S., & Nelson, W. J. (2014). Different roles of cadherins in the assembly and structural integrity of the desmosome complex. *Journal of Cell Science, 127*(Pt 10), 2339-2350. 10.1242/jcs.146316

Lutz, B. M., & Peng, J. (2018). Deep Profiling of the Aggregated Proteome in Alzheimer's Disease: From Pathology to Disease Mechanisms. *Proteomes, 6*(4)10.3390/proteomes6040046

Luxenburg, C., Geblinger, D., Klein, E., Anderson, K., Hanein, D., Geiger, B., & Addadi, L. (2007). PMC1779809; The architecture of the adhesive apparatus of cultured osteoclasts: from podosome formation to sealing zone assembly. *PLoS One, 2*(1), e179. 10.1371/journal.pone.0000179

Ma, J., Li, M., Hock, J., & Yu, X. (2012). Hyperactivation of mTOR critically regulates abnormal osteoclastogenesis in neurofibromatosis Type 1. *Journal of Orthopaedic Research: Official Publication of the Orthopaedic Research Society, 30*(1), 144-152. 10.1002/jor.21497

MacDonald, M. L., Favo, D., Garver, M., Sun, Z., Arion, D., Ding, Y., Yates, N., Sweet, R. A., & Lewis, D. A. (2019). Laser capture microdissection-targeted mass spectrometry: a method for multiplexed protein quantification within individual layers of the cerebral cortex. *Neuropsychopharmacology: Official Publication of the American College of Neuropsychopharmacology, 44*(4), 743-748. 10.1038/s41386-018-0260-0

MacGrath, S. M., & Koleske, A. J. (2012). Cortactin in cell migration and cancer at a glance. *Journal of Cell Science, 125*(Pt 7), 1621-1626. 10.1242/jcs.093781

Mahalingam, M. (2018). Laser Capture Microdissection: Insights into Methods and Applications. *Methods in Molecular Biology (Clifton, N.J.), 1723*, 1-17. 10.1007/978-1-4939-7558-7_1

Maounis, N. F., Dráberová, E., Trakas, N., Chorti, M., Riga, D., Tzannis, K., Kanakis, M., Voralu, K., Ellina, E., Mahera, E., Demonakou, M., Lioulias, A., Dráber, P., & Katsetos, C. D. (2019). Expression of γ-tubulin in non-small cell lung cancer and effect on patient survival. *Histology and Histopathology, 34*(1), 81-90. 10.14670/HH-18-027

Margraf, R. L., VanSant-Webb, C., Mao, R., Viskochil, D. H., Carey, J., Hanson, H., D'Astous, J., Grossmann, A., & Stevenson, D. A. (2019). NF1 Somatic Mutation in Dystrophic Scoliosis. *Journal of Molecular Neuroscience: MN, 68*(1), 11-18. 10.1007/s12031-019-01277-0

Martin, G. A., Viskochil, D., Bollag, G., McCabe, P. C., Crosier, W. J., Haubruck, H., Conroy, L., Clark, R., O'Connell, P., & Cawthon, R. M. (1990). The GAP-related domain of the neurofibromatosis type 1 gene product interacts with ras p21. *Cell, 63*(4), 843-849. 0092-8674(90)90150-D [pii]

Martincorena, I., & Campbell, P. J. (2015). Somatic mutation in cancer and normal cells. *Science (New York, N.Y.), 349*(6255), 1483-1489. 10.1126/science.aab4082

Mazaud-Guittot, S., Meugnier, E., Pesenti, S., Wu, X., Vidal, H., Gow, A., & Le Magueresse-Battistoni, B. (2010). Claudin 11 deficiency in mice results in loss of the Sertoli cell epithelial phenotype in the testis. *Biology of Reproduction, 82*(1), 202-213. 10.1095/biolreprod.109.078907

Meşe, G., Richard, G., & White, T. W. (2007). Gap junctions: basic structure and function. *The Journal of Investigative Dermatology, 127*(11), 2516-2524. 10.1038/sj.jid.5700770

Mineta, K., Yamamoto, Y., Yamazaki, Y., Tanaka, H., Tada, Y., Saito, K., Tamura, A., Igarashi, M., Endo, T., Takeuchi, K., & Tsukita, S. (2011). Predicted expansion of the claudin multigene family. *FEBS Lett, 585*(4), 606-612. 10.1016/j.febslet.2011.01.028

Miron, R. J., Zohdi, H., Fujioka-Kobayashi, M., & Bosshardt, D. D. (2016). Giant cells around bone biomaterials: Osteoclasts or multi-nucleated giant cells? *Acta Biomaterialia, 46*, 15-28. 10.1016/j.actbio.2016.09.029

Niemeyer, C. M. (2018). JMML genomics and decisions. *Hematology, 2018*(1), 307-312. 10.1182/asheducation-2018.1.307

Novack, D. V., & Mbalaviele, G. (2016). Osteoclasts-Key Players in Skeletal Health and Disease. *Microbiology Spectrum, 4*(3)10.1128/microbiolspec.MCHD-0011-2015

Oh, S., Kim, J., Kim, Y., Lee, M. N., Kook, M., Choi, E. Y., Im, S., & Koh, J. (2017). The extracellular matrix protein Edil3 stimulates osteoblast differentiation through the integrin α5β1/ERK/Runx2 pathway. *PloS One, 12*(11), e0188749. 10.1371/journal.pone.0188749

Ong, C. J., Tan, Q. X., Lim, H. J., Shannon, N. B., Lim, W. K., Hendrikson, J., Ng, W. H., Tan, J. W. S., Koh, K. K. N., Wasudevan, S. D., Ng, C. C. Y., Rajasegaran, V., Lim, T. K. H., Ong, C. K., Kon, O. L., Teh, B. T., Tan, G. H. C., Chia, C. S., Soo, K. C., & Teo, M. C. C. (2020). An Optimised Protocol Harnessing Laser Capture Microdissection for Transcriptomic Analysis on Matched Primary and Metastatic Colorectal Tumours. *Scientific Reports, 10*(1), 682. 10.1038/s41598-019-55146-2

Ortuzar, R., Atria, P., & Mena, I. (1956). Clinical aspects of 20 cases of fibrous dysplasia of the bones, von Recklinghausen's neurofibromatosis, osteomalacia, osteoporosis and hyperparathyroidism. *Revista Medica De Chile, 84*(8), 417-429.

Overgaard, C. E., Daugherty, B. L., Mitchell, L. A., & Koval, M. (2011). Claudins: control of barrier function and regulation in response to oxidant stress. *Antioxidants & Redox Signaling, 15*(5), 1179-1193. 10.1089/ars.2011.3893

Parfitt, A. M., Drezner, M. K., Glorieux, F. H., Kanis, J. A., Malluche, H., Meunier, P. J., Ott, S. M., & Recker, R. R. (1987). Bone histomorphometry: standardization of nomenclature, symbols, and units. Report of the ASBMR Histomorphometry Nomenclature Committee. *J Bone Miner Res, 2*(6), 595-610. 10.1002/jbmr.5650020617

Peltonen, J., Jaakkola, S., Lebwohl, M., Renvall, S., Risteli, L., Virtanen, I., & Uitto, J. (1988). Cellular differentiation and expression of matrix genes in type 1 neurofibromatosis. *Lab Invest, 59*(6), 760-771. http://www.ncbi.nlm.nih.gov/pubmed/2462129

Peltonen, S., Alanne, M., & Peltonen, J. (2013). PMC3867511; Barriers of the peripheral nerve. *Tissue Barriers, 1*(3), e24956. 10.4161/tisb.24956

Peltonen, S., Kallionpää, R. A., & Peltonen, J. (2017). Neurofibromatosis type 1 (NF1) gene: Beyond café au lait spots and dermal neurofibromas. *Experimental Dermatology, 26*(7), 645-648. 10.1111/exd.13212

Peng, Z., Tuukkanen, J., Zhang, H., Jämsä, T., & Väänänen, H. K. (1994). The mechanical strength of bone in different rat models of experimental osteoporosis. *Bone, 15*(5), 523-532. http://www.ncbi.nlm.nih.gov/pubmed/7980963

Pennanen, P., Kallionpää, R. A., Peltonen, S., Nissinen, L., Kähäri, V., Heervä, E., & Peltonen, J. (2021). Signaling pathways in human osteoclasts differentiation: ERK1/2 as a key player. *Molecular Biology Reports,* 10.1007/s11033-020-06128-5

Pereira, M., Petretto, E., Gordon, S., Bassett, J. H. D., Williams, G. R., & Behmoaras, J. (2018). Common signalling pathways in macrophage and osteoclast multinucleation. *Journal of Cell Science, 131*(11)10.1242/jcs.216267

Petramala, L., Giustini, S., Zinnamosca, L., Marinelli, C., Colangelo, L., Cilenti, G., Formicuccia, M. C., D'Erasmo, E., Calvieri, S., & Letizia, C. (2012). Bone mineral metabolism in patients with neurofibromatosis type 1 (von Recklingausen disease). *Archives of Dermatological Research, 304*(4), 325-331. 10.1007/s00403-011-1191-3

Plotkin, S. R., Bredella, M. A., Cai, W., Kassarjian, A., Harris, G. J., Esparza, S., Merker, V. L., Munn, L. L., Muzikansky, A., Askenazi, M., Nguyen, R., Wenzel, R., & Mautner, V. F. (2012). Quantitative assessment of whole-body tumor burden in adult patients with neurofibromatosis. *PloS One, 7*(4), e35711. 10.1371/journal.pone.0035711

Poliak, S., Matlis, S., Ullmer, C., Scherer, S. S., & Peles, E. (2002). PMC2173042; Distinct claudins and associated PDZ proteins form different autotypic tight junctions in myelinating Schwann cells. *J Cell Biol, 159*(2), 361-372. 10.1083/jcb.200207050

Pollard, T. D. (2016). Theory from the Oster Laboratory Leaps Ahead of Experiment in Understanding Actin-Based Cellular Motility. *Biophysical Journal, 111*(8), 1589-1592. 10.1016/j.bpj.2016.08.044

Pummi, K. P., Heape, A. M., Grénman, R. A., Peltonen, J. T., & Peltonen, S. A. (2004). Tight junction proteins ZO-1, occludin, and claudins in developing and adult human perineurium. *J Histochem Cytochem, 52*(8), 1037-1046. 10.1369/jhc.3A6217.2004

Rayleigh, L. (1903). On the Theory of Optical Images, with special reference to the Microscope. *Journal of the Royal Microscopical Society, 23*(4), 474-482. https://doi.org/10.1111/j.1365-2818.1903.tb04831.x

Reale, E., Luciano, L., & Spitznas, M. (1975). Freeze-fracture faces of the perineurial sheath of the rabbit sciatic nerve. *J Neurocytol, 4*(3), 261-270. http://www.ncbi.nlm.nih.gov/pubmed/1133587

Renner, G., Noulet, F., Mercier, M., Choulier, L., Etienne-Selloum, N., Gies, J., Lehmann, M., Lelong-Rebel, I., Martin, S., & Dontenwill, M. (2016). Expression/activation of α5β1 integrin is linked to the β-catenin signaling pathway to drive migration in glioma cells. *Oncotarget, 7*(38), 62194-62207. 10.18632/oncotarget.11552

Revel, J. P., & Karnovsky, M. J. (1967). Hexagonal array of subunits in intercellular junctions of the mouse heart and liver. *The Journal of Cell Biology, 33*(3), C7-C12. 10.1083/jcb.33.3.c7

Rhodes, S. D., & Yang, F. (2016). Aberrant Myeloid Differentiation Contributes to the Development of Osteoporosis in Neurofibromatosis Type 1. *Current Osteoporosis Reports, 14*(1), 10-15. 10.1007/s11914-016-0298-z

Rhodes, S. D., Yang, H., Dong, R., Menon, K., He, Y., Li, Z., Chen, S., Staser, K. W., Jiang, L., Wu, X., Yang, X., Peng, X., Mohammad, K. S., Guise, T. A., Xu, M., & Yang, F. (2015). Nf1 Haploinsufficiency Alters Myeloid Lineage Commitment and Function, Leading to Deranged Skeletal Homeostasis. *Journal of Bone and Mineral Research: The Official Journal of the American Society for Bone and Mineral Research, 30*(10), 1840-1851. 10.1002/jbmr.2538

Riccardi, C., Perrone, L., Napolitano, F., Sampaolo, S., & Melone, M. A. B. (2020). Understanding the Biological Activities of Vitamin D in Type 1 Neurofibromatosis: New Insights into Disease Pathogenesis and Therapeutic Design. *Cancers, 12*(10)10.3390/cancers12102965

Risal, D., Gourinath, S., Himmel, D. M., Szent-Györgyi, A. G., & Cohen, C. (2004). Myosin subfragment 1 structures reveal a partially bound nucleotide and a complex salt bridge that helps couple nucleotide and actin binding. *Proceedings of the National Academy of Sciences of the United States of America, 101*(24), 8930-8935. 10.1073/pnas.0403002101

Rogowski, K., van Dijk, J., Magiera, M. M., Bosc, C., Deloulme, J., Bosson, A., Peris, L., Gold, N. D., Lacroix, B., Bosch Grau, M., Bec, N., Larroque, C., Desagher, S., Holzer, M., Andrieux, A., Moutin, M., & Janke, C. (2010). A family of protein-deglutamylating enzymes associated with neurodegeneration. *Cell, 143*(4), 564-578. 10.1016/j.cell.2010.10.014

Rüegsegger, P., Koller, B., & Müller, R. (1996). A microtomographic system for the nondestructive evaluation of bone architecture. *Calcified Tissue International, 58*(1), 24-29. 10.1007/BF02509542

Ruska, E., & Knoll, M. (1931). Die magnetische Sammelspule für schnelle Elektronenstrahlen (The magnetic concentrating coil for fast electron beams.). *Z. techn. Physik, 12*, 389-400. Retrieved from https://www.zvab.com/magnetische-Sammelspule-schnelle-Elektronenstrahlen-pp.389-399-Abb/1239520011/bd

Ryan, J., Gerhold, A. R., Boudreau, V., Smith, L., & Maddox, P. S. (2017). Introduction to Modern Methods in Light Microscopy. *Methods in Molecular Biology (Clifton, N.J.), 1563*, 1-15. 10.1007/978-1-4939-6810-7_1

Sage, D., Donati, L., Soulez, F., Fortun, D., Schmit, G., Seitz, A., Guiet, R., Vonesch, C., & Unser, M. (2017). DeconvolutionLab2: An open-source software for deconvolution microscopy. *Methods (San Diego, Calif.), 115*, 28-41. 10.1016/j.ymeth.2016.12.015

Saitou, M., Ando-Akatsuka, Y., Itoh, M., Furuse, M., Inazawa, J., Fujimoto, K., & Tsukita, S. (1997). Mammalian occludin in epithelial cells: its expression and subcellular distribution. *European Journal of Cell Biology, 73*(3), 222-231.

Saitou, M., Furuse, M., Sasaki, H., Schulzke, J. D., Fromm, M., Takano, H., Noda, T., & Tsukita, S. (2000). Complex phenotype of mice lacking occludin, a component of tight junction strands. *Molecular Biology of the Cell, 11*(12), 4131-4142. 10.1091/mbc.11.12.4131

Sakamoto, A., Yoshida, T., Yamamoto, H., Oda, Y., Tsuneyoshi, M., & Iwamoto, Y. (2007). Congenital pseudarthrosis of the tibia: analysis of the histology and the NF1 gene. *Journal of Orthopaedic Science: Official Journal of the Japanese Orthopaedic Association, 12*(4), 361-365. 10.1007/s00776-007-1142-1

Saltel, F., Chabadel, A., Bonnelye, E., & Jurdic, P. (2008). Actin cytoskeletal organisation in osteoclasts: a model to decipher transmigration and matrix degradation. *European Journal of Cell Biology, 87*(8-9), 459-468. 10.1016/j.ejcb.2008.01.001

Sant, D. W., Margraf, R. L., Stevenson, D. A., Grossmann, A. H., Viskochil, D. H., Hanson, H., Everitt, M. D., Rios, J. J., Elefteriou, F., Hennessey, T., & Mao, R. (2015). Evaluation of somatic mutations in tibial pseudarthrosis samples in neurofibromatosis type 1. *Journal of Medical Genetics, 52*(4), 256-261. 10.1136/jmedgenet-2014-102815

Schackmann, R. C. J., Tenhagen, M., van de Ven, Robert A. H., & Derksen, P. W. B. (2013). p120-catenin in cancer - mechanisms, models and opportunities for intervention. *Journal of Cell Science, 126*(Pt 16), 3515-3525. 10.1242/jcs.134411

Schoenenberger, C., Mannherz, H. G., & Jockusch, B. M. (2011). Actin: from structural plasticity to functional diversity. *European Journal of Cell Biology, 90*(10), 797-804. 10.1016/j.ejcb.2011.05.002

Schulzke, J. D., Gitter, A. H., Mankertz, J., Spiegel, S., Seidler, U., Amasheh, S., Saitou, M., Tsukita, S., & Fromm, M. (2005). Epithelial transport and barrier function in occludin-deficient mice. *Biochimica Et Biophysica Acta, 1669*(1), 34-42. 10.1016/j.bbamem.2005.01.008

Shekhar, S., Pernier, J., & Carlier, M. (2016). Regulators of actin filament barbed ends at a glance. *Journal of Cell Science, 129*(6), 1085-1091. 10.1242/jcs.179994

Shi, J., Hua, X., Zhu, B., Ravichandran, S., Wang, M., Nguyen, C., Brodie, S. A., Palleschi, A., Alloisio, M., Pariscenti, G., Jones, K., Zhou, W., Bouk, A. J., Boland, J., Hicks, B., Risch, A., Bennett, H., Luke, B. T., Song, L., . . . Landi, M. T. (2016). Somatic Genomics and Clinical Features of Lung Adenocarcinoma: A Retrospective Study. *PLoS Medicine, 13*(12), e1002162. 10.1371/journal.pmed.1002162

Siljamäki, E., Raiko, L., Toriseva, M., Nissinen, L., Näreoja, T., Peltonen, J., Kähäri, V., & Peltonen, S. (2014). p38δ mitogen-activated protein kinase regulates the expression of tight junction protein ZO-1 in differentiating human epidermal keratinocytes. *Archives of Dermatological Research, 306*(2), 131-141. 10.1007/s00403-013-1391-0

Simonet, W. S., Lacey, D. L., Dunstan, C. R., Kelley, M., Chang, M. S., Lüthy, R., Nguyen, H. Q., Wooden, S., Bennett, L., Boone, T., Shimamoto, G., DeRose, M., Elliott, R., Colombero, A., Tan, H. L., Trail, G., Sullivan, J., Davy, E., Bucay, N., . . . Boyle, W. J. (1997). Osteoprotegerin: a novel secreted protein involved in the regulation of bone density. *Cell, 89*(2), 309-319. S0092-8674(00)80209-3 [pii]

Siton-Mendelson, O., & Bernheim-Groswasser, A. (2017). Functional Actin Networks under Construction: The Cooperative Action of Actin Nucleation and Elongation Factors. *Trends in Biochemical Sciences, 42*(6), 414-430. 10.1016/j.tibs.2017.03.002

Skerrett, I. M., & Williams, J. B. (2017). A structural and functional comparison of gap junction channels composed of connexins and innexins. *Developmental Neurobiology, 77*(5), 522-547. 10.1002/dneu.22447

Skuse, G. R., Kosciolek, B. A., & Rowley, P. T. (1989). Molecular genetic analysis of tumors in von Recklinghausen neurofibromatosis: loss of heterozygosity for chromosome 17. *Genes, Chromosomes & Cancer, 1*(1), 36-41. 10.1002/gcc.2870010107

Söhl, G., Maxeiner, S., & Willecke, K. (2005). Expression and functions of neuronal gap junctions. *Nature Reviews. Neuroscience, 6*(3), 191-200. 10.1038/nrn1627

Spiegel, I., & Peles, E. (2002). Cellular junctions of myelinated nerves (Review). *Molecular Membrane Biology, 19*(2), 95-101. 10.1080/09687680210130009

Spiering, D., & Hodgson, L. (2011). Dynamics of the Rho-family small GTPases in actin regulation and motility. *Cell Adhesion & Migration, 5*(2), 170-180. 10.4161/cam.5.2.14403

Stahley, S. N., Bartle, E. I., Atkinson, C. E., Kowalczyk, A. P., & Mattheyses, A. L. (2016). Molecular organization of the desmosome as revealed by direct stochastic optical reconstruction microscopy. *Journal of Cell Science, 129*(15), 2897-2904. 10.1242/jcs.185785

Steed, E., Balda, M. S., & Matter, K. (2010). Dynamics and functions of tight junctions. *Trends in Cell Biology, 20*(3), 142-149. 10.1016/j.tcb.2009.12.002

Stevenson, D. A., Zhou, H., Ashrafi, S., Messiaen, L. M., Carey, J. C., D'Astous, J. L., Santora, S. D., & Viskochil, D. H. (2006). PMC1474128; Double inactivation of NF1 in tibial pseudarthrosis. *Am J Hum Genet, 79*(1), 143-148. S0002-9297(07)60020-2 [pii] 10.1086/504441

Stevenson, D. A., Little, D., Armstrong, L., Crawford, A. H., Eastwood, D., Friedman, J. M., Greggi, T., Gutierrez, G., Hunter-Schaedle, K., Kendler, D. L., Kolanczyk, M., Monsell, F., Oetgen, M., Richards, B. S., Schindeler, A., Schorry, E. K., Wilkes, D., Viskochil, D. H., Yang, F., & Elefteriou, F. (2013). Approaches to treating NF1 tibial pseudarthrosis: consensus from the Children's Tumor Foundation NF1 Bone Abnormalities Consortium. *Journal of Pediatric Orthopedics, 33*(3), 269-275. 10.1097/BPO.0b013e31828121b8

Stevenson, D. A., Yan, J., He, Y., Li, H., Liu, Y., Zhang, Q., Jing, Y., Guo, Z., Zhang, W., Yang, D., Wu, X., Hanson, H., Li, X., Staser, K., Viskochil, D. H., Carey, J. C., Chen, S., Miller, L., Roberson, K., . . . Yang, F. (2011). Multiple increased osteoclast functions in individuals with neurofibromatosis type 1. *American Journal of Medical Genetics. Part A, 155A*(5), 1050-1059. 10.1002/ajmg.a.33965

Susaki, E. A., & Ueda, H. R. (2016). Whole-body and Whole-Organ Clearing and Imaging Techniques with Single-Cell Resolution: Toward Organism-Level Systems Biology in Mammals. *Cell Chemical Biology, 23*(1), 137-157. 10.1016/j.chembiol.2015.11.009

Sweeney, M. D., Zhao, Z., Montagne, A., Nelson, A. R., & Zlokovic, B. V. (2019). Blood-Brain Barrier: From Physiology to Disease and Back. *Physiological Reviews, 99*(1), 21-78. 10.1152/physrev.00050.2017

Szudek, J., Joe, H., & Friedman, J. M. (2002). Analysis of intrafamilial phenotypic variation in neurofibromatosis 1 (NF1). *Genetic Epidemiology, 23*(2), 150-164. 10.1002/gepi.1129

Tabata, M. M., Li, S., Knight, P., Bakker, A., & Sarin, K. Y. (2020). Phenotypic heterogeneity of neurofibromatosis type 1 in a large international registry. *JCI Insight, 5*(16)10.1172/jci.insight.136262

Tang, D. D., & Gerlach, B. D. (2017). The roles and regulation of the actin cytoskeleton, intermediate filaments and microtubules in smooth muscle cell migration. *Respiratory Research, 18*(1), 54. 10.1186/s12931-017-0544-7

Tang, L., Xu, M., Zhang, L., Qu, L., & Liu, X. (2020). Role of αVβ3 in Prostate Cancer: Metastasis Initiator and Important Therapeutic Target. *OncoTargets and Therapy, 13*, 7411-7422. 10.2147/OTT.S258252

Tauchi, R., Kawakami, N., Castro, M. A., Ohara, T., Saito, T., Morishita, K., & Yamauchi, I. (2020). Long-term Surgical Outcomes After Early Definitive Spinal Fusion for Early-onset Scoliosis With Neurofibromatosis Type 1 at Mean Follow-up of 14 Years. *Journal of Pediatric Orthopedics, 40*(1), 42-47. 10.1097/BPO.0000000000001090

Tedesco, S., Bolego, C., Toniolo, A., Nassi, A., Fadini, G. P., Locati, M., & Cignarella, A. (2015). Phenotypic activation and pharmacological outcomes of spontaneously differentiated human monocyte-derived macrophages. *Immunobiology, 220*(5), 545-554. 10.1016/j.imbio.2014.12.008

Teitelbaum, S. L. (2011). The osteoclast and its unique cytoskeleton. *Ann N Y Acad Sci, 1240*, 14-17. 10.1111/j.1749-6632.2011.06283.x

Thomas, P. K. (1963). PMC1244253; The connective tissue of peripheral nerve: an electron microscope study. *J Anat, 97*, 35-44. http://www.ncbi.nlm.nih.gov/pubmed/13981107

Tikkanen, J., Leskelä, H. V., Lehtonen, S. T., Vähäsarja, V., Melkko, J., Ahvenjärvi, L., Pääkkö, E., Väänänen, K., & Lehenkari, P. (2010). Attempt to treat congenital pseudarthrosis of the tibia with mesenchymal stromal cell transplantation. *Cytotherapy, 12*(5), 593-604. 10.3109/14653249.2010.487898

Touihri-Barakati, I., Kallech-Ziri, O., Ayadi, W., Kovacic, H., Hanchi, B., Hosni, K., & Luis, J. (2017). Cucurbitacin B purified from Ecballium elaterium (L.) A. Rich from Tunisia inhibits α5β1 integrin-mediated adhesion, migration, proliferation of human glioblastoma cell line and angiogenesis. *European Journal of Pharmacology, 797*, 153-161. 10.1016/j.ejphar.2017.01.006

Trovó-Marqui, A. B., & Tajara, E. H. (2006). Neurofibromin: a general outlook. *Clinical Genetics, 70*(1), 1-13. 10.1111/j.1399-0004.2006.00639.x

Tucker, T., Schnabel, C., Hartmann, M., Friedrich, R. E., Frieling, I., Kruse, H. P., Mautner, V. F., & Friedman, J. M. (2009). Bone health and fracture rate in individuals with neurofibromatosis 1 (NF1). *J Med Genet, 46*(4), 259-265. 10.1136/jmg.2008.061895

Tunik, B., & Holtzer, H. (1961). The distribution of muscle antigens in contracted myofibrils determined by fluorescein-labeled antibodies. *The Journal of Biophysical and Biochemical Cytology, 11*, 67-75. 10.1083/jcb.11.1.67

Upadhyaya, M., Huson, S. M., Davies, M., Thomas, N., Chuzhanova, N., Giovannini, S., Evans, D. G., Howard, E., Kerr, B., Griffiths, S., Consoli, C., Side, L., Adams, D., Pierpont, M., Hachen, R., Barnicoat, A., Li, H., Wallace, P., Van Biervliet, J. P., . . . Messiaen, L. (2007). An absence of cutaneous neurofibromas associated with a 3-bp inframe deletion in exon 17 of the NF1 gene (c.2970-2972 delAAT): evidence of a clinically significant NF1 genotype-phenotype correlation. *American Journal of Human Genetics, 80*(1), 140-151. 10.1086/510781

Upadhyaya, M., Kluwe, L., Spurlock, G., Monem, B., Majounie, E., Mantripragada, K., Ruggieri, M., Chuzhanova, N., Evans, D. G., Ferner, R., Thomas, N., Guha, A., & Mautner, V. (2008). Germline and somatic NF1 gene mutation spectrum in NF1-associated malignant peripheral nerve sheath tumors (MPNSTs). *Human Mutation, 29*(1), 74-82. 10.1002/humu.20601

Upadhyaya, M., Ruggieri, M., Maynard, J., Osborn, M., Hartog, C., Mudd, S., Penttinen, M., Cordeiro, I., Ponder, M., Ponder, B. A., Krawczak, M., & Cooper, D. N. (1998). Gross deletions of the neurofibromatosis type 1 (NF1) gene are predominantly of maternal origin and commonly associated with a learning disability, dysmorphic features and developmental delay. *Human Genetics, 102*(5), 591-597. 10.1007/s004390050746

Uusitalo, E., Kallionpää, R. A., Kurki, S., Rantanen, M., Pitkäniemi, J., Kronqvist, P., Härkönen, P., Huovinen, R., Carpen, O., Pöyhönen, M., Peltonen, S., & Peltonen, J. (2017). Breast cancer in neurofibromatosis type 1: overrepresentation of unfavourable prognostic factors. *British Journal of Cancer, 116*(2), 211-217. 10.1038/bjc.2016.403

Uusitalo, E., Leppävirta, J., Koffert, A., Suominen, S., Vahtera, J., Vahlberg, T., Pöyhönen, M., Peltonen, J., & Peltonen, S. (2015). Incidence and mortality of neurofibromatosis: a total population study in Finland. *The Journal of Investigative Dermatology, 135*(3), 904-906. 10.1038/jid.2014.465

Uusitalo, E., Rantanen, M., Kallionpää, R. A., Pöyhönen, M., Leppävirta, J., Ylä-Outinen, H., Riccardi, V. M., Pukkala, E., Pitkäniemi, J., Peltonen, S., & Peltonen, J. (2016). Distinctive Cancer Associations in Patients With Neurofibromatosis Type 1. *Journal of Clinical Oncology: Official Journal of the American Society of Clinical Oncology, 34*(17), 1978-1986. 10.1200/JCO.2015.65.3576

van Rossum, Agnes G. S. H., Gibcus, J., van der Wal, J., & Schuuring, E. (2005). Cortactin overexpression results in sustained epidermal growth factor receptor signaling by preventing ligand-induced receptor degradation in human carcinoma cells. *Breast Cancer Research: BCR, 7*(6), 235-237. 10.1186/bcr1316

Vandewoestyne, M., Goossens, K., Burvenich, C., Van Soom, A., Peelman, L., & Deforce, D. (2013). Laser capture microdissection: should an ultraviolet or infrared laser be used? *Analytical Biochemistry, 439*(2), 88-98. 10.1016/j.ab.2013.04.023

Viskochil, D., Cawthon, R., O'Connell, P., Xu, G. F., Stevens, J., Culver, M., Carey, J., & White, R. (1991). The gene encoding the oligodendrocyte-myelin glycoprotein is embedded within the neurofibromatosis type 1 gene. *Molecular and Cellular Biology, 11*(2), 906-912. 10.1128/mcb.11.2.906

Visnapuu, V., Peltonen, S., Alivuotila, L., Happonen, R., & Peltonen, J. (2018). Craniofacial and oral alterations in patients with Neurofibromatosis 1. *Orphanet Journal of Rare Diseases, 13*(1), 131. 10.1186/s13023-018-0881-8

Vite, A., & Radice, G. L. (2014). N-cadherin/catenin complex as a master regulator of intercalated disc function. *Cell Communication & Adhesion, 21*(3), 169-179. 10.3109/15419061.2014.908853

Volksdorf, T., Heilmann, J., Eming, S. A., Schawjinski, K., Zorn-Kruppa, M., Ueck, C., Vidal-Y-Sy, S., Windhorst, S., Jücker, M., Moll, I., & Brandner, J. M. (2017). Tight Junction Proteins Claudin-1 and Occludin Are Important for Cutaneous Wound Healing. *The American Journal of Pathology, 187*(6), 1301-1312. 10.1016/j.ajpath.2017.02.006

Wallace, M. R., Marchuk, D. A., Andersen, L. B., Letcher, R., Odeh, H. M., Saulino, A. M., Fountain, J. W., Brereton, A., Nicholson, J., & Mitchell, A. L. (1990). Type 1 neurofibromatosis gene: identification of a large transcript disrupted in three NF1 patients. *Science, 249*(4965), 181-186. http://www.ncbi.nlm.nih.gov/pubmed/2134734

Wang, H., Rivenson, Y., Jin, Y., Wei, Z., Gao, R., Günaydın, H., Bentolila, L. A., Kural, C., & Ozcan, A. (2019). Deep learning enables cross-modality super-resolution in fluorescence microscopy. *Nature Methods, 16*(1), 103-110. 10.1038/s41592-018-0239-0

Wang, W., Nyman, J. S., Ono, K., Stevenson, D. A., Yang, X., & Elefteriou, F. (2011). Mice lacking Nf1 in osteochondroprogenitor cells display skeletal dysplasia similar to patients with neurofibromatosis type I. *Hum Mol Genet,* r310 [pii] 10.1093/hmg/ddr310

Wang, W., Lu, M., Tsai, C., Wang, S., Chou, S., & Jou, S. (2021). A child with juvenile myelomonocytic leukemia possessing a concurrent germline CBL mutation and a NF1 variant of uncertain significance: A rare case with a common problem in the era of high-throughput sequencing. *Journal of the Formosan Medical Association = Taiwan Yi Zhi, 120*(4), 1148-1152. 10.1016/j.jfma.2020.08.034

Wang, W., Zhang, H., Wang, X., Patterson, J., Winter, P., Graham, K., Ghosh, S., Lee, J. C., Katsetos, C. D., Mackey, J. R., Tuszynski, J. A., Wong, G. K., & Ludueña, R. F. (2017). Novel mutations involving βI-, βIIA-, or βIVB-tubulin isotypes with functional resemblance to βIII-tubulin in breast cancer. *Protoplasma, 254*(3), 1163-1173. 10.1007/s00709-016-1060-1

Wehrle-Haller, B. (2012). Structure and function of focal adhesions. *Current Opinion in Cell Biology, 24*(1), 116-124. 10.1016/j.ceb.2011.11.001

Wong, P., Laxton, V., Srivastava, S., Chan, Y. W. F., & Tse, G. (2017). The role of gap junctions in inflammatory and neoplastic disorders (Review). *International Journal of Molecular Medicine, 39*(3), 498-506. 10.3892/ijmm.2017.2859

Wozniak, M. A., Modzelewska, K., Kwong, L., & Keely, P. J. (2004). Focal adhesion regulation of cell behavior. *Biochimica Et Biophysica Acta, 1692*(2-3), 103-119. 10.1016/j.bbamcr.2004.04.007

Wu, C. (2007). Focal adhesion: a focal point in current cell biology and molecular medicine. *Cell Adhesion & Migration, 1*(1), 13-18. 10.4161/cam.1.1.4081

Wu, R. L., Vazquez-Roque, M. I., Carlson, P., Burton, D., Grover, M., Camilleri, M., & Turner, J. R. (2017). Gluten-induced symptoms in diarrhea-predominant irritable bowel syndrome are associated with increased myosin light chain kinase activity and claudin-15 expression. *Laboratory Investigation; a Journal of Technical Methods and Pathology, 97*(1), 14-23. 10.1038/labinvest.2016.118

Xing, L., & Boyce, B. F. (2014). RANKL-based osteoclastogenic assays from murine bone marrow cells. *Methods in Molecular Biology (Clifton, N.J.), 1130*, 307-313. 10.1007/978-1-62703-989-5_23

Yang, F. C., Chen, S., Robling, A. G., Yu, X., Nebesio, T. D., Yan, J., Morgan, T., Li, X., Yuan, J., Hock, J., Ingram, D. A., & Clapp, D. W. (2006). PMC1616197; Hyperactivation of p21ras and

PI3K cooperate to alter murine and human neurofibromatosis type 1-haploinsufficient osteoclast functions. *J Clin Invest, 116*(11), 2880-2891. 10.1172/JCI29092

Yao, Z., Guo, D., Li, H., Bai, Y., Sun, B., Zhang, X., Li, C., & Qi, X. (2019). Surgical Treatment of Dystrophic Scoliosis in Neurofibromatosis Type 1: Outcomes and Complications. *Clinical Spine Surgery, 32*(1), E50-E55. 10.1097/BSD.0000000000000716

Yapijakis, C., Pachis, N., Natsis, S., & Voumvourakis, C. (2016). Is Neurofibromatosis Type 1-Noonan Syndrome a Phenotypic Result of Combined Genetic and Epigenetic Factors? *In Vivo (Athens, Greece), 30*(3), 315-320.

Yasuda, H., Shima, N., Nakagawa, N., Yamaguchi, K., Kinosaki, M., Mochizuki, S., Tomoyasu, A., Yano, K., Goto, M., Murakami, A., Tsuda, E., Morinaga, T., Higashio, K., Udagawa, N., Takahashi, N., & Suda, T. (1998). PMC19881; Osteoclast differentiation factor is a ligand for osteoprotegerin/osteoclastogenesis-inhibitory factor and is identical to TRANCE/RANKL. *Proc Natl Acad Sci U S A, 95*(7), 3597-3602. http://www.ncbi.nlm.nih.gov/pubmed/9520411

Zhao, M., Ding, J., Mao, Q., Zhang, Y., Gao, Y., Ye, S., Qin, H., & Shi, H. (2020). A novel αvβ3 integrin-targeted NIR-II nanoprobe for multimodal imaging-guided photothermal therapy of tumors in vivo. *Nanoscale, 12*(13), 6953-6958. 10.1039/c9nr10720g

Zhu, L., Plow, E. F., & Qin, J. (2020). Initiation of focal adhesion assembly by talin and kindlin: A dynamic view. *Protein Science: A Publication of the Protein Society,* 10.1002/pro.4014

Zhu, Y., Romero, M. I., Ghosh, P., Ye, Z., Charnay, P., Rushing, E. J., Marth, J. D., & Parada, L. F. (2001). PMC312666; Ablation of NF1 function in neurons induces abnormal development of cerebral cortex and reactive gliosis in the brain. *Genes Dev, 15*(7), 859-876. 10.1101/gad.862101

TURUN
YLIOPISTO
UNIVERSITY
OF TURKU

Painosalama Oy, Turku, Finland 2021

ISBN 978-951-29-8461-9 (PRINT)
ISBN 978-951-29-8462-6 (PDF)
ISSN 0355-9483 (Print)
ISSN 2343-3213 (Online)